

**Università degli Studi di Pavia**

---

FACOLTÀ DI INGEGNERIA  
Corso di Laurea Magistrale in Ingegneria Civile

TESI DI LAUREA

**Lightweight structures:  
topology optimization and 3D printing.**

Strutture leggere:  
ottimizzazione topologica e stampa 3D.

Candidato:  
**Nicolò Manfredi**  
Matricola 420806

Relatore:  
**Prof. Ferdinando Auricchio**  
Correlatore:  
**Dott. Gianluca Alaimo**



*“Everything should be made as simple as possible, but not simpler.”*

A. Einstein



# Acknowledgments

I have always thought it is necessary to look ahead and run headlong into the new without ever looking back, you could define it my rule of life! But what is a rule without an exception? Well, this is one of the few cases where I want to turn around and look at the road taken. During my university years I have met many people and some of them have profoundly marked my career as a student. This is why, firstly, I want to thank my fellow students, who gave me (even without noticing it) the strength to pursue my education in engineering which, sometimes, may look like a real test of will. Of course, I want to thank as well the professors for allowing me to gain the solid knowledge that will be indispensable to start in the best way my future career.

I thank my advisor, Professor Ferdinando Auricchio, who has led me to face issues apparently different from those of civil engineering and has opened to me new worlds. I thank Dr. Gianluca Alaimo, who supported me in identifying important aspects of my thesis and taught me not to be discouraged by the difficulties I encountered. I thank my family without whom I could not dedicate myself full time to my university education and without whom I would not have the moral values that distinguish me. And, although unconventional in a section dedicated to acknowledgments, thank myself for the abnegation (and perhaps Stakhanovism!) in dealing with the work undertaken.



# Abstract

Engineering practice often highlights the necessity to decrease the mass of a structure preserving an adequate stiffness and resistance. The traditional solution resolves the problem by adopting a different material with superior properties. However, this option is often not viable mainly because of the cost of materials with better features. The question, then, is whether there is another way to maintain the performance of the structures (in terms of strength and stiffness) while reducing the mass. The answer lies in the *optimization* processes. What do we mean with optimization? The term “optimization” is connected to the need to maximize or minimize certain quantities. Structural engineering is a clear example, since it underlines the need to reduce costs, to reduce weight, to limit the stress or to increase the stiffness of the structure. The process of minimization or maximization of certain quantities can be done as long as we do not come across any constraints. To clarify problem of the optimization, simply imagine you want to minimize the mass of a beam. A solution could be the reduction of section size, but this would cause an increase in stresses and displacements, which consequently become the constraining quantities. Hence, the heart of the optimization is the improvement of the quantities studied as much as possible within the constraints imposed.

For a long time the concept of optimization was regarded as marginal and associated mostly to high tech. Today, however, several companies related to construction and transportation have been active in the implementation of optimized elements.

While we are aware of the number of opportunities offered by our theme, we will focus on a specific branch of the optimization, the so-called *topology optimization* in its two variants: *truss-based approach* and *density-based approach*. At the base of topology optimization there is the necessity to distribute the material in the design space in the best way possible, where the design space and the meaning of “best” are previously individuated.

A relatively new use topology optimization is in the field of materials, and more specifically in the study of the so-called *cellular materials*. The latter are an aggregation of cells that form a homogeneous agglomeration, which is identified as a real material. As we will see later, you can distinguish between *foams* and *lattice materials*. Foams are not suitable to be optimized as they are characterized by strong stochasticity in distribution, size and shape of the cells (consider the foam generated by the common soap). By contrast, cells

that constitute lattice materials are regular and periodic, thereby allowing a convenient mathematical modeling. Generally, lattice materials, as they are known today, are not obtained through a rigorous procedure of optimization, but through experimental trials. We will demonstrate that it is possible to obtain lattice materials with the same or even improved characteristics of lightness and stiffness once topology optimization is applied.

For an engineer, to realize what was first developed theoretically is a vital concept. This requirement is embodied in the will to realize physically what so far has remained on paper. The easiest and fastest way to manufacture optimized objects is through *3D printing*. This technique, although well-known, is still in its early stages, but it is widely used not only in academic research but also for industry-related purposes.

In writing this thesis, we were strongly inspired by what the sequence of events leading to the creation of a product should be: *theoretical study, design, manufacturing*.

The first chapter is devoted to topology optimization with a significant excursus on the meaning of mathematical optimization process. The second chapter focuses on cellular materials; we provide a brief classification for the main types and present lattice materials with respect to their mechanical properties and methods of production, both traditional and innovative. The third chapter deals with the theme of 3D printing while focusing on the various printing techniques, the use of this new technology in various sectors of industry and its impact on the society. In the last chapter we propose two codes of topology optimization through which objects are modeled:

- The first code is related to topology optimization of a beam through density-based approach.
- The second is related to the topology optimization of a lattice materials cell through truss-based approach.

This two codes have been made with the help of Matlab software. Later we will demonstrate how it is possible to use 3D printing for the creation of previously optimized objects.

# Sommario

Nella pratica ingegneristica, sovente, si evidenzia la necessità di diminuire la massa di una struttura mantenendo un'adeguata rigidità e resistenza. La soluzione tradizionale per risolvere il problema consiste nell'adottare un materiale con proprietà superiori. Tuttavia, questa opzione è spesso interdetta a causa dei costi dei materiali con caratteristiche migliori. La domanda da porsi, allora, è se esista un modo per mantenere le prestazioni delle strutture (in termini di resistenza e di rigidità) riducendo la massa. La risposta si trova nei processi di *ottimizzazione*. Che cosa si intende per ottimizzazione?

Il termine “ottimizzazione” è legato al bisogno di massimizzare o minimizzare determinate quantità. Una dimostrazione lampante nella progettazione strutturale si evidenzia con la necessità di ridurre la massa, ma anche di ridurre i costi, di limitare le sollecitazioni o di incrementare la rigidità della struttura. Il processo di *minimizzazione* o *massimizzazione* delle quantità può essere fatto fintantoché non sopraggiungano dei vincoli. Per chiarire il problema è sufficiente ipotizzare di voler ridurre al massimo la massa di una trave sollecitata. Una soluzione potrebbe essere ridurre le dimensioni della sezione, ma ciò causerebbe l'aumento di sforzi e spostamenti che, pertanto, diventerebbero quantità vincolanti. Dunque, l'essenza del processo ottimizzativo consiste nel migliorare tanto più la quantità studiata nel rispetto dei vincoli imposti.

A sostegno delle opportunità che offre il tema dell'ottimizzazione ci concentreremo su di un ramo specifico della suddetta, la cosiddetta *ottimizzazione topologica*, nelle due varianti: *truss-based approach* e *density-based approach*. Il fondamento su cui si basa l'ottimizzazione topologica è la redistribuzione del materiale all'interno dello spazio di progetto nella maniera più conveniente possibile, dove spazio di progetto e convenienza sono stati precedentemente individuati.

Un utilizzo recente dell'ottimizzazione topologica è nell'ambito dello studio dei materiali, ed in particolare nello studio dei cosiddetti *cellular materials*. Questi ultimi sono costituiti dall'aggregazione di celle a formare un agglomerato omogeneo che viene identificato come un vero e proprio materiale. Come si vedrà in seguito è possibile distinguere tra le *foams* e i *lattice materials*. Le foams non sono adatte al processo ottimizzativo, in quanto sono caratterizzate da forte stocasticità nella distribuzione, nelle dimensioni e nella forma delle celle (si pensi alla schiuma generata dal sapone). Al contrario le celle che costituiscono i lattice materials sono regolari e periodiche, permettendo una più agevole

modellazione matematica.

Spesso i lattice materials, oggi noti, non sono stati ottenuti tramite un procedimento rigoroso di ottimizzazione, ma sono stati progettati in maniera empirica. Applicheremo, quindi, l'ottimizzazione topologica al fine di ottenere lattice materials leggeri, ma nel contempo con opportune caratteristiche di rigidità, confrontandoli poi con quelli già esistenti. Un concetto fondamentale per un ingegnere è quello di concretizzare quello che è stato sviluppato in via teorica. Questa necessità si sostanzia nella volontà di produrre materialmente ciò che fino a questo momento è rimasto sulla carta. Vedremo come il modo più conveniente e veloce di realizzare oggetti ottimizzati sia tramite la *stampa 3D*. Questa tecnica, benché oggi sia molto conosciuta, è ancora nelle sue fasi iniziali, infatti è molto utilizzata in ambiti di ricerca non solo accademica, ma anche industriale. Nell'impostazione della presente tesi ci siamo fortemente ispirati a quella che dovrebbe essere la successione di eventi che portano alla creazione di un prodotto finito: *studio teorico, progettazione, realizzazione*.

Il primo capitolo è dedicato all'ottimizzazione topologica con un excursus sul significato matematico di processo ottimizzativo. Il secondo capitolo è incentrato sui cellular materials; viene fatta una breve classificazione delle tipologie principali di cellular material e vengono presentati i lattice materials con riferimento alle loro caratteristiche meccaniche e alle modalità di produzione, sia tradizionali che innovative. Nel terzo capitolo viene trattato il tema della stampa 3D ponendo l'attenzione alle varie tecniche di stampa, all'utilizzo di questa nuova tecnologia in vari settori dell'industria e al suo impatto sulla società. Nell'ultimo capitolo sono proposti due codici scritti con l'ausilio del software *Matlab*:

- Il primo legato all'ottimizzazione topologica di una trave tramite il density-based approach.
- Il secondo legato all'ottimizzazione topologica di una cella di lattice materials tramite il truss-based approach.

In seguito si dimostrerà come sia possibile utilizzare la stampa 3D per la realizzazione di oggetti in precedenza ottimizzati.

# Contents

<b>Abstract</b>	<b>vii</b>
<b>Sommario</b>	<b>ix</b>
<b>1 Topology Optimization</b>	<b>1</b>
1.1 Introduction . . . . .	1
1.1.1 Structural optimization . . . . .	1
1.1.2 Historical view . . . . .	1
1.1.3 Steps of optimization process . . . . .	2
1.1.4 Mathematical definition of structural optimization problem . . . . .	3
1.1.5 Types of structural optimization . . . . .	4
1.1.6 Discrete or continuum problem? . . . . .	4
1.2 Mathematical background . . . . .	5
1.2.1 Local or global optimum? . . . . .	5
1.2.2 A positive feature: convexity . . . . .	6
1.2.3 Research of local minimum for convex problems . . . . .	8
1.2.4 Research of local minimum for non-convex problems . . . . .	9
1.3 On topology optimization . . . . .	15
1.3.1 Truss-based approach . . . . .	16
1.3.2 Density-based approach . . . . .	28
<b>2 Cellular materials</b>	<b>37</b>
2.1 Introduction . . . . .	37
2.2 Initial considerations . . . . .	42
2.3 Mechanical overview . . . . .	47
2.3.1 Relative density . . . . .	47
2.3.2 Stretching-dominated and bending-dominated . . . . .	49
2.3.3 Stretching- or bending-dominated? . . . . .	53
2.4 Effective material properties of lattice material . . . . .	55
2.4.1 Homogenization method . . . . .	57
2.5 Manufacturing of cellular materials . . . . .	62

2.5.1	Stochastic cellular structures . . . . .	62
2.5.2	Ordered cellular structures . . . . .	64
2.5.3	Problem of the current cellular material manufacturing . . . . .	65
2.5.4	3D printing for lattice materials . . . . .	66
<b>3</b>	<b>3D printing</b>	<b>79</b>
3.1	Introduction . . . . .	79
3.2	Overview . . . . .	80
3.2.1	Definition . . . . .	80
3.2.2	Printing process in 8 steps . . . . .	80
3.2.3	Techniques of printing . . . . .	81
3.2.4	Types of printable materials . . . . .	88
3.3	Current applications . . . . .	90
3.4	Ten reasons for choosing 3D printing . . . . .	93
<b>4</b>	<b>Lightweight structure: design and production</b>	<b>97</b>
4.1	Realization of a beam . . . . .	97
4.1.1	Approach to the problem . . . . .	97
4.1.2	Finite Element Analysis . . . . .	99
4.1.3	Sensitivity analysis . . . . .	101
4.1.4	Functioning of the algorithm . . . . .	102
4.1.5	Matlab optimization . . . . .	102
4.1.6	Use of the code . . . . .	104
4.2	Realization of 2D lattice material . . . . .	110
4.2.1	Approach to the problem . . . . .	110
4.2.2	Finite Element Analysis . . . . .	113
4.2.3	Calculation of the compliance . . . . .	114
4.2.4	Sensitivity analysis . . . . .	117
4.2.5	Functioning of the algorithm . . . . .	118
4.2.6	Comparison . . . . .	119
4.2.7	Use of the code . . . . .	120
4.3	Use of 3D printing . . . . .	125
	<b>Concluding Remarks</b>	<b>130</b>
	<b>Appendix</b>	<b>133</b>
	<b>Bibliography</b>	<b>139</b>
	<b>Sitography</b>	<b>147</b>

# List of Figures

1.1	Cantilever optimized by Galileo Galilei. . . . .	2
1.2	Size, shape and continuum topology optimization. . . . .	5
1.3	Example of function with more local minima and maxima. . . . .	6
1.4	Convex and non-convex set. . . . .	7
1.5	(Strictly) convex function and (strictly) concave function. . . . .	7
1.6	Discrete topology optimization for a cantilever. . . . .	16
1.7	Continuum topology optimization for a cantilever. . . . .	17
1.8	Schematization of the bar to be studied. . . . .	18
1.9	Example of optimizing cantilever. . . . .	19
1.10	Cantilever and the cross section. . . . .	23
1.11	Cantilever when only A is elastic. . . . .	24
1.12	Example of density-based approach. . . . .	29
1.13	No relaxation, $\epsilon = 0$ . . . . .	33
1.14	$\epsilon = 0.15$ . . . . .	33
1.15	$\epsilon = 0.05$ . . . . .	34
1.16	$\epsilon = 0.01$ . . . . .	34
2.1	Materials time-line. . . . .	38
2.2	Progressive filling of the charts in time. . . . .	39
2.3	Stiffness–density chart and strength-density chart. . . . .	41
2.4	Some of the best known architected materials. . . . .	42
2.5	Microscopic vision of wood. . . . .	43
2.6	Microscopic vision of bone. . . . .	43
2.7	Microscopic vision of sponge. . . . .	43
2.8	2D extruded honeycomb. . . . .	44
2.9	3D lattice. . . . .	44
2.10	Example of cell distribution in a foam. . . . .	45
2.11	Example of cell distribution in a lattice. . . . .	45
2.12	Comparison between energy absorption in an elastic solid material and in a foam made of the same material. . . . .	47
2.13	Pentamode lattice. . . . .	48

2.14	Lattice with negative Poisson's ratio. . . . .	48
2.15	Cell to the left collapses due to mechanism. . . . .	49
2.16	Bending-dominated foam. . . . .	51
2.17	Cell collapses. . . . .	52
2.18	Stress-strain curve for a bending-dominated structure. . . . .	53
2.19	Stress-strain curve for a stretching-dominated structure. . . . .	54
2.20	Z=4, presence of mechanisms. . . . .	55
2.21	Z=4, absence of mechanisms. . . . .	56
2.22	Example of representative unit cell. . . . .	58
2.23	Foam made by sinterization. . . . .	63
2.24	Foam made by direct foaming. . . . .	63
2.25	Process of crimping and stamping. . . . .	65
2.26	Manufacturing process for creating cellular castings - from digital mold to resultant casting. . . . .	67
2.27	Example of printed lattice material made of Ti6Al4 V. . . . .	69
2.28	Surface sintering seen under the microscope. . . . .	69
2.29	Problem linked to effective length of the strut. . . . .	70
2.30	Overheating problem. . . . .	71
2.31	3D Printed lattice material as structure woodpile. . . . .	72
2.32	Optical image of 3D printing of a triangular honeycomb. . . . .	72
2.33	A PLA cellular lattice structure fabricated by FDM. . . . .	73
2.34	Truss thickness measured via microscope. . . . .	74
2.35	Samples on the building platform. . . . .	75
2.36	Schematic representation of the process used to form micro-lattice struc- ture from a self-propagating polymer waveguides. . . . .	76
2.37	Example structure formed by this process. . . . .	76
2.38	Demonstration of a significantly reduced size that can be achieved. . . . .	77
2.39	Example of a micro-lattice structure with anticlastic curvature. . . . .	78
3.1	Vat photopolymerization schematics. . . . .	83
3.2	Material Jetting schematics. . . . .	83
3.3	Binder Jetting schematics. . . . .	84
3.4	FDM schematics. . . . .	85
3.5	SLS schematics. . . . .	86
3.6	Sheet Lamination schematics. . . . .	87
3.7	Directed Energy Deposition schematics. . . . .	88
3.8	Example of accuracy of 3D printing. . . . .	89
3.9	3D printed wall. . . . .	90
3.10	Local Motor car 3D printed during the International Manufacturing Tech- nology Show (2014). . . . .	91
3.11	3D printed heart. . . . .	93

3.12	Example of architectural 3D model depicting a stadium. . . . .	94
4.1	Natural coordinates. . . . .	100
4.2	Structure to be analyzed [1]. . . . .	105
4.3	MBB beam: geometry and loading. . . . .	106
4.4	Progressive optimization. . . . .	107
4.5	Final result [1]. . . . .	108
4.6	Von Mises stress [1]. . . . .	108
4.7	Structure to be analyzed [2]. . . . .	109
4.8	Final result [2]. . . . .	109
4.9	Von Mises stress [2]. . . . .	110
4.10	Final result [3]. . . . .	111
4.11	Von Mises stress [3]. . . . .	111
4.12	Square packing with further reflectional symmetries. . . . .	115
4.13	Constraints of a quarter of a unit cell used for the calculation of the axial compliance. . . . .	116
4.14	Constraints of a quarter of a unit cell used for the calculation of the shear compliance. . . . .	117
4.15	Initial meshes used to model a square unit cell. . . . .	120
4.16	3D printer used. . . . .	126
4.17	Main steps in 3D printing. . . . .	126
4.18	First 3D printed object. . . . .	126
4.19	Solutions penalized (already seen) and solutions not penalized. . . . .	127
4.20	Example of percentage increase of infill. . . . .	128
4.21	Relative density map. . . . .	128
4.22	Second 3D printed object. . . . .	129



# List of Tables

2.1	Some properties for Ashby charts. . . . .	40
2.2	Designer freedom offered by various cellular material production techniques.	66
2.3	Designer freedom offered by various cellular material production techniques.	68
4.1	Square element with node numbering conventions. . . . .	100
4.2	Combinations of $\alpha_E$ and $\alpha_G$ . . . . .	121
4.3	Results for locally connected mesh. . . . .	123
4.4	Results for fully connected mesh. . . . .	124
4.5	Percentage increase for locally connected mesh and fully connected mesh.	125



# Chapter 1

## Topology Optimization

### 1.1 Introduction

#### 1.1.1 Structural optimization

“A *structure* can be defined as any assemblage of materials which is intended to sustain loads” [1]. Therefore, *structural optimization* can be defined as the discipline that studies how to make an assemblage of materials sustain loads in the best way possible. But what do we mean with the word “best”? The first meaning which comes to mind may be to make the structure as light as possible. Another idea could be to make the structure as stiff as possible or insensitive to buckling. Obviously, such maximizations or minimizations cannot be performed without constraints. For instance, if there is no limitation on the amount of material that can be employed, the structure can be made limitlessly stiff and we have an optimization problem without a well-defined solution. Constrained quantities in structural optimization problems are often displacements, stresses and the geometric dimensions. Notice that most quantities which can be thought of as constraints could be also used as objective functions.

#### 1.1.2 Historical view

Galileo Galilei (1564-1642) formulated the first concepts of seeking optimal shapes of structural elements between the 16th and 17th century. In his book “Discorsi e dimostrazioni matematiche intorno a due nuove scienze attinenti alla meccanica e ai moti locali”, he investigated the fracture process of brittle bodies, where the shape of bodies was considered with regard to strength as well [Fig. 1.1].

The work of Gottfried Wilhelm Leibniz (1646-1716) in the fields of mathematics and natural sciences can be seen as the basis of any analytic procedure, whereas the work of Leonard Euler (1707-1783) on the theory of extremes provided the basis for the development of the calculus of variations. In addition, Joseph-Louis Lagrange (1736-1813) and later William Rowan Hamilton (1805-1865) contributed in completing the variation

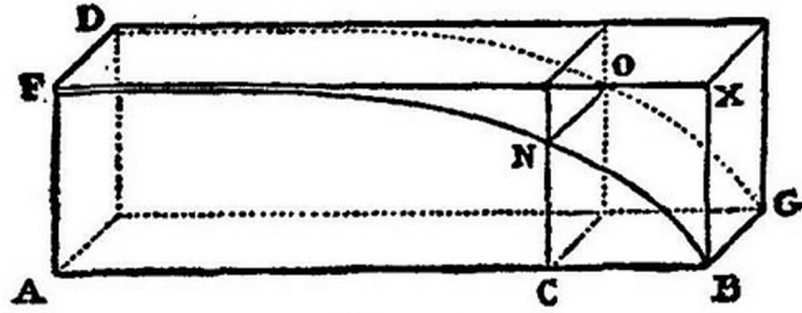


Figure 1.1: Cantilever optimized by Galileo Galilei. Figure taken from [79].

calculus.

Galileo, Leibniz and a few significant others also made initial investigations on finding the optimal shape of one dimensional load bearing structures under arbitrary load. Using variation calculus, they derived optimal cross-sections for columns, torsion bars and cantilever beams.

In the latest decades, with ever increasing computational capabilities, a new area of *Computer Aided Engineering* has emerged, often referred to as structural optimization, that has merged mechanical and mathematical knowledge with the computing capacity of the computers.

### 1.1.3 Steps of optimization process

The main questions in the process of product design [2] are:

- What is the use of the product?
- Which quantities are important for the product?
- What is the goal I want to accomplish? And the constraints to be respected?
- How do I optimize?

The traditional way of realizing the fourth step is via *iterative-intuitive* method:

1. a specific design is suggested,
2. investigation phase (does the chosen design meet the imposed demands?),
3. if demands are not satisfied, a new design must be suggested,

4. the suggested new design is brought back to the second step.

So an iterative process is formed, where a series of designs are created, which hopefully converges to an acceptable final design. Nowadays step 2 is performed through computer-based methods like *Finite Element Method (FEM)*. These methods imply that every design iteration can be analyzed with greater confidence and probably every step can be made more effective.

How to avoid relying on an intuitive process? Using the *mathematical design optimization method* which is very different from the iterative-intuitive one. When employing this method, we formulate a mathematical optimization problem where the concept “as good as possible” is given precise mathematical form.

#### 1.1.4 Mathematical definition of structural optimization problem

The mathematical definition of the problem requires:

*Design variable*( $\mathbf{x}$ ): A parameter or a vector of parameters that describes the design, which can change during optimization. It may represent geometry, type of material, distribution of material etc.

*Objective function*( $\mathbf{f}$ ): A function or many functions that return values, which indicate the goodness of the design.  $\mathbf{f}$  may represent weight, displacements in a given direction, stress or even cost of production.

Usually we choose a minimization problem, that is the minimization of  $\mathbf{f}$ . Therefore, a general (and simplified) structural optimization problem looks like this:

$$\begin{cases} \min_{\mathbf{x}} \mathbf{f}(\mathbf{x}) \\ \text{s.t.} \quad \mathbf{g}(\mathbf{x}) \leq 0 \\ \mathbf{x}_{min} \leq \mathbf{x} \leq \mathbf{x}_{max} \\ \mathbf{K}(\mathbf{x})\mathbf{u} = \mathbf{F}(\mathbf{x}) \end{cases} \quad (1.1)$$

where

- $\mathbf{g}(\mathbf{x}) \leq 0$  represents the constraint functions,
- $\mathbf{K}(\mathbf{x})\mathbf{u} = \mathbf{F}(\mathbf{x})$  represents the equilibrium equations,
- the matrix  $\mathbf{K}(\mathbf{x})$  is the stiffness matrix of the structure,
- $\mathbf{u}$  is the displacement vector,
- $\mathbf{F}(\mathbf{x})$  is the force vector.

In the formulation (1.1),  $\mathbf{x}$  is the vector of independent variables. This formulation is called *simultaneous formulation*, since equilibrium is solved simultaneously with the

optimization problem. In many situations  $\mathbf{u}$  depends on  $\mathbf{x}$ , i.e., if  $\mathbf{K}(\mathbf{x})$  is invertible for  $\mathbf{x}$ , we have  $\mathbf{u}(\mathbf{x}) = \mathbf{K}(\mathbf{x})^{-1}\mathbf{F}(\mathbf{x})$ . By treating  $\mathbf{u}(\mathbf{x})$  as a given function, the equilibrium constraint can be left out of (1.1), so we can reformulate the problem as:

$$\begin{cases} \min_{\mathbf{x}} f(\mathbf{x}) \\ \text{s.t.} \quad \mathbf{g}(\mathbf{x}) \leq 0 \\ \mathbf{x}_{min} \leq \mathbf{x} \leq \mathbf{x}_{max}. \end{cases} \quad (1.2)$$

This formulation is called *nested formulation*. In this thesis, we consider problems with only one scalar objective function, i.e. we do not consider the so-called *multicriteria optimization* [3].

### 1.1.5 Types of structural optimization

Optimization of structures can be divided into:

- size optimization
- shape optimization
- topology optimization

Size optimization is commonly employed to find the optimal cross-sectional area of the beam in a frame or to find the optimal thickness of plate elements while satisfying design criteria. Shape optimization is characterized by a redefinition of the shape in order to obtain an optimal solution. This kind of optimization can reshape the material inside the domain keeping its topological properties. Topology optimization is the most general form of structural optimization. In discrete cases (see truss-based approach in 1.3.1), it is achieved by taking cross-sectional areas of bars as design variables, and hence allowing the resizing and also the removal of bars in the frame. In continuum cases (see density-based approach in 1.3.2), topology optimization allows the best distribution of material inside the domain.

### 1.1.6 Discrete or continuum problem?

We talk of discrete problems if the design variables are finite. Typical examples are optimization problems for frames where the design variables  $\mathbf{x}$  represent the cross-sectional areas of bars. Conversely, if the design variables consist in a field we talk of continuum problem. Significant examples are shape optimization problems or the topology optimization problems in the continuum case. Frequently, in order to resolve continuum problems, it is common to use computer implementations performing discretization, which produce a discrete problems. To distinguish between derived discrete problems and original discrete problems, we talk of *naturally discrete problems* in the latter case. The solution

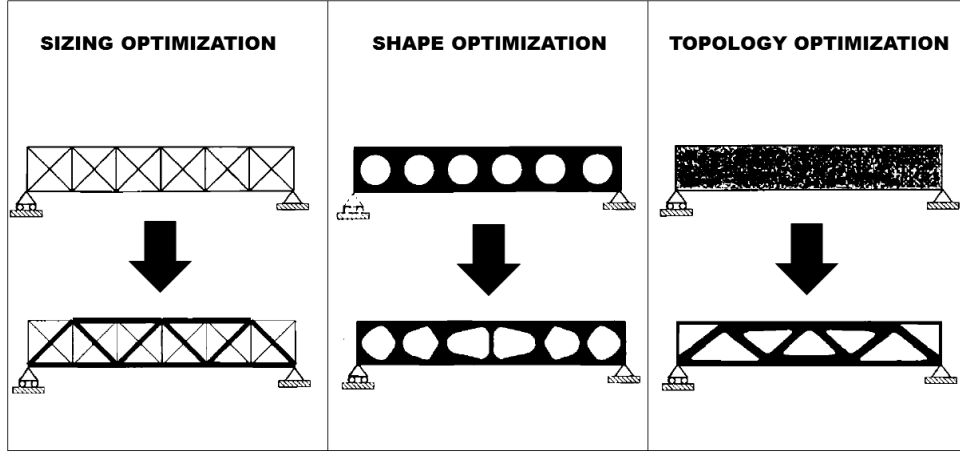


Figure 1.2: Size, shape and continuum topology optimization. Figure taken from [25]

of continuum discretized converges to the solution of the real continuum when the discretization is made finer and finer. However, sometimes such results are mathematically difficult to obtain, and convergence results are not always available. So it is fundamental the interpretation of the optimization data by the engineer.

## 1.2 Mathematical background

In this section we take [24] as reference. If not otherwise specified, theorems and definitions are borrowed from the the above-mentioned reference.

### 1.2.1 Local or global optimum?

Consider a general minimization problem under inequality constraints:

$$\begin{cases} \min_{\mathbf{x}} g_0(\mathbf{x}) \\ \text{s.t.} & g_i(\mathbf{x}) \leq 0, \quad i = 1, \dots, l \\ & \mathbf{x} \in X \end{cases} \quad (1.3)$$

where  $g_i : \mathbb{R}^n \rightarrow \mathbb{R}$ ,  $i = 0, \dots, l$  are assumed to be continuously differentiable functions and

$$X = \{\mathbf{x} \in \mathbb{R}^n : x_j^{\min} \leq x_j \leq x_j^{\max}, j = 1, \dots, n\} \quad (1.4)$$

Fortunately every maximization problem may be reformulated as a minimization problem by observing that  $\max g_0(\mathbf{x}) = -\min -g_0(\mathbf{x})$ . A *feasible point* of (1.3) is any point which satisfies all the constraints  $g_i(\bar{\mathbf{x}}) \leq 0, i = 1, \dots, l$  and  $\bar{\mathbf{x}} \in X$ . The problem (1.3) is related to the search of a feasible point  $\mathbf{x}^*$  such that  $g_0(\mathbf{x}^*) \leq g_0(\bar{\mathbf{x}})$  for all feasible points  $\bar{\mathbf{x}}$  of (1.3). This point is called *global minimum* of  $g_0$ . It is fundamental

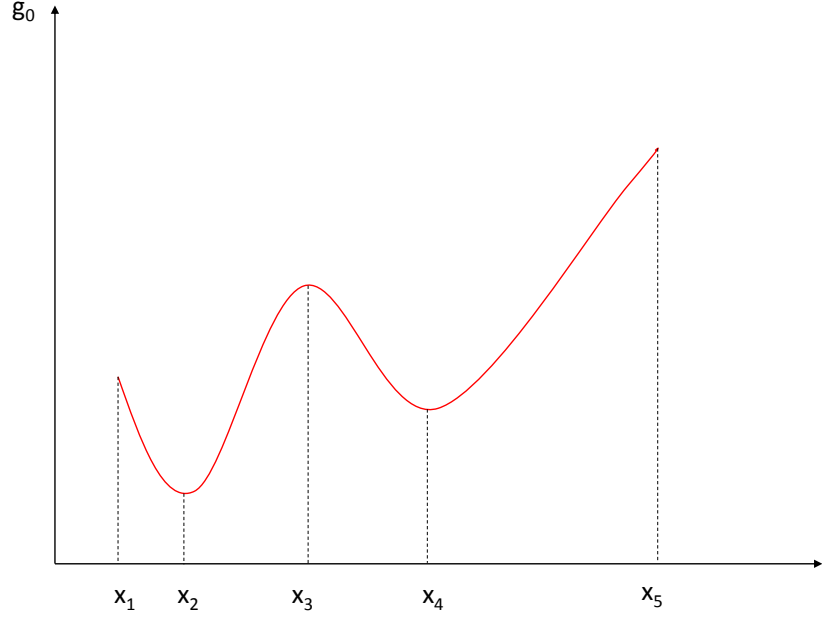


Figure 1.3: Example of function with more local minima and maxima.

to note that neither feasible points nor optimal solution need exist.

It is extremely hard to determine a global minimum, so we are satisfied to obtain a local minimum. A point  $\mathbf{x}^*$  is a local minimum if the objective function only assumes greater or equal values in the neighborhood of  $\mathbf{x}^*$ . Certainly outside of the neighborhood is possible a value smaller than  $\mathbf{x}^*$ . For unconstrained optimization problems (only  $\min g_0(\mathbf{x})$ ) local minima are located at stationary points where the gradient of  $g_0$  is null.

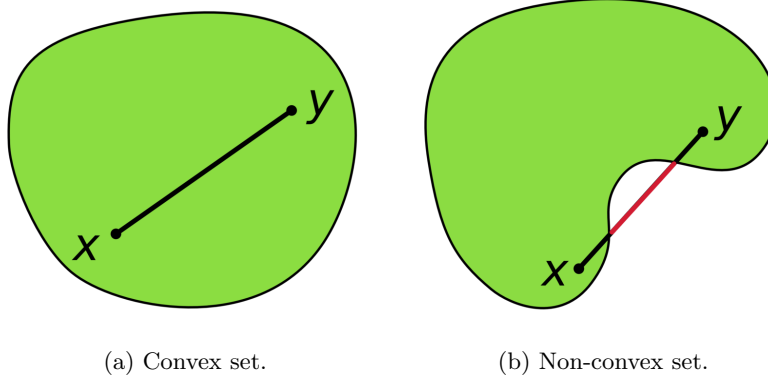
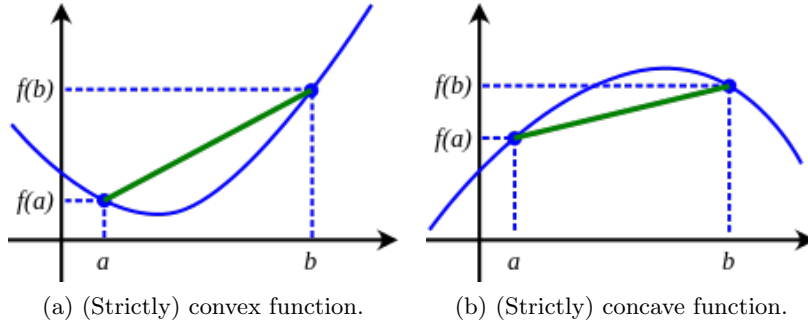
A problem arises: a stationary point may not be a local minimum, in fact it may be a local maximum. For constrained problems, local minima are not even necessarily located at stationary points, they may be located on the boundary of the feasible set [Fig. 1.3].

### 1.2.2 A positive feature: convexity

We recall briefly the definition of convex set and convex function:

**Definition 1** Let  $S$  be a vector space over the real numbers. A set  $C$  in  $S$  is said to be convex if, for all  $\mathbf{x}$  and  $\mathbf{y}$  in  $C$  and all  $t$  in the interval  $[0, 1]$ , the point  $(1 - t)\mathbf{x} + t\mathbf{y}$  also belongs to  $C$ .

**Definition 2** Let  $C$  be a convex set in a real vector space and let  $f : C \rightarrow \mathbb{R}$  be a function.  $f$  is called convex if:

Figure 1.4: Convex and non-convex set. Figures taken from *Wikipedia*.Figure 1.5: (Strictly) convex function and (strictly) concave function. Figures taken from *Wikipedia*.

$$\forall x_1, x_2 \in X, \forall t \in [0, 1] : \quad f(tx_1 + (1-t)x_2) \leq tf(x_1) + (1-t)f(x_2).$$

$f$  is called *strictly convex* if:

$$\forall x_1 \neq x_2 \in X, \forall t \in (0, 1) : \quad f(tx_1 + (1-t)x_2) < tf(x_1) + (1-t)f(x_2).$$

A function  $f$  is said to be *(strictly) concave* if  $-f$  is *(strictly) convex*.

These definitions are common in many books of math and algebra, but these just mentioned derive from *Wikipedia*. In [Fig. 1.4] and [Fig. 1.5] we show an example of convex/non-convex set and convex/concave function, respectively.

By applying the definitions of convex sets and convex functions we can say that if the objective function and the feasible set of (1.3) are convex, the problem (1.3) is convex. It is trivial that, for convex problems, local minima are also global minima, anyway they may not have a solution. But if the feasible set is compact, that is bounded and closed, a solution always exists (this is true for any continuous objective function). If the objective function is strictly convex and the feasible set is convex, there exists at most one solution. But how to determine whether a continuously differentiable function is

(strictly) convex in a convex set? Two main ways exist, and they are expressed through the following definitions:

**Definition 3** Let  $f : C \rightarrow \mathbb{R}$ , where  $C$  is convex and  $f$  is continuously differentiable. Then  $f$  is (strictly) convex if and only if the gradient  $\nabla f$  is (strictly) monotone.

**Definition 4** Let  $f : C \rightarrow \mathbb{R}$ , where  $C$  is convex and  $f$  is twice continuously differentiable. Then:

- (i)  $f$  is convex if and only if the Hessian  $\nabla^2 f$  is positive semidefinite,
- (ii)  $f$  is strictly convex if  $\nabla^2 f$  is positive definite.

These definitions derives from [31].

### 1.2.3 Research of local minimum for convex problems

#### Karush-Kuhn-Tucker conditions

First, we define the Lagrangian function for the general problem (1.3):

$$\mathcal{L}(\mathbf{x}, \lambda) = g_0(\mathbf{x}) + \sum_{i=1}^l \lambda_i g_i(\mathbf{x}) \quad (1.5)$$

where  $\lambda_i$  are called *Lagrangian multipliers*. We introduce the Karush-Kuhn-Tucker conditions (KKT) for (1.3):

$$\frac{\partial \mathcal{L}(\mathbf{x}, \lambda)}{\partial x_j} \leq 0, \quad \text{if } x_j = x_j^{max} \quad (1.6)$$

$$\frac{\partial \mathcal{L}(\mathbf{x}, \lambda)}{\partial x_j} = 0, \quad \text{if } x_j^{min} < x_j < x_j^{max} \quad (1.7)$$

$$\frac{\partial \mathcal{L}(\mathbf{x}, \lambda)}{\partial x_j} \geq 0, \quad \text{if } x_j = x_j^{min} \quad (1.8)$$

$$\lambda_i g_i(\mathbf{x}) = 0 \quad (1.9)$$

$$g_i(\mathbf{x}) = 0 \quad (1.10)$$

$$\lambda_i \geq 0 \quad (1.11)$$

$$\mathbf{x} \in X. \quad (1.12)$$

Each point  $(\mathbf{x}^*, \lambda^*)$  satisfying the above equations is called a *KKT point*.

The KKT conditions for regular non-convex problems are necessary (but not sufficient!) optimality conditions for (1.3). It is true that local optima are found among the KKT points, but there may exist KKT points which are not local optima. This is evident when studying the case of an unconstrained optimization problem, where the KKT

points are equivalent to stationary points. Numerical algorithms try to find KKT points, and thus one may conclude with finding a point that is not a local minimum, but a local maximum. Here's the convexity lets say that for convex problems a KKT point is always an optimal point.

**Theorem 1** *Let the problem (1.3) be convex and satisfy constraint qualification, i.e. there exists a point  $\tilde{\mathbf{x}} \in X$  such that  $g_i(\tilde{\mathbf{x}}) < 0$ ,  $i = 1, \dots, l$ . Let  $\mathbf{x}^*$  be a local (global) minimum of (1.3). Then there exists a  $\lambda^*$  such that  $(\mathbf{x}^*, \lambda^*)$  is a KKT point of (1.3).*

**Theorem 2** *Let (1.3) be a convex problem and let  $(\mathbf{x}^*, \lambda^*)$  be a KKT point of (1.3). Then  $\mathbf{x}^*$  is a local (global) minimum of (1.3).*

### Lagrangian duality

We can rewrite (1.3) in an equivalent formulation as min-max problem:

$$\min_{\mathbf{x} \in X} \max_{\lambda \geq 0} \mathcal{L}(\mathbf{x}, \lambda) = \min_{\mathbf{x} \in X} \max_{\lambda \geq 0} \left( g_0(\mathbf{x}) + \sum_{i=1}^l \lambda_i g_i(\mathbf{x}) \right). \quad (1.13)$$

More simply:

$$\begin{cases} \max_{\lambda} \phi(\lambda) \\ \text{s.t. } \lambda \geq 0 \end{cases} \quad (1.14)$$

where the dual objective function  $\phi$  is defined as

$$\begin{cases} \phi(\lambda) = \min_{\mathbf{x} \in X} \mathcal{L}(\mathbf{x}, \lambda). \end{cases} \quad (1.15)$$

But what do we gain from this duality?

It is easy to note that the constraints in these optimizations are very simple:  $\mathbf{x} \in X$  and  $\lambda \geq 0$ , respectively. This is the major advantage of duality theory. The following theorem stated that, under defined conditions, the resolution of (1.13) is equivalent to resolve (1.3).

**Theorem 3** *Let (1.3) be a convex problem with the set  $X$  compact, satisfying constraints qualification. Then there exist a  $\lambda^*$  which solves (1.14), and a  $\mathbf{x}^* \in \underset{\mathbf{x} \in X}{\operatorname{argmin}} \mathcal{L}(\mathbf{x}, \lambda^*)$  that solves (1.3), where  $g_0(\mathbf{x}^*) = \phi(\lambda^*)$ .*

#### 1.2.4 Research of local minimum for non-convex problems

Aspects to be considered in the structural optimization:

- Often, for large-scale problems, it is not possible obtain objective function and constraints as explicit functions of design variables. How may we resolve this issue? Generating a sequence of explicit sub-problems which are approximations of the original problem and, hence, solving these sub-problems;

- Many problems in structural optimization are non-convex. Because of the intrinsic difficulties with solving non-convex problems, we will choose approximations which are convex. The main focus will be on approximations that take into account specific characteristics of certain structural optimization problems.

The main procedures used to solve non-convex and large-scale problems are:

- Sequential Linear Programming (SLP)
- Sequential Quadratic Programming (SQP)
- Convex Linearization (CONLIN)
- Method of Moving Asymptotes (MMA)

### General problem

Consider a structural optimization problem of a system with a finite number of degrees of freedom (discrete problem!). If we assume linear elasticity, we can express the problem using a simultaneous formulation:

$$\begin{cases} \min_{\mathbf{x}} g_0(\mathbf{x}) \\ \text{s.t.} & g_i(\mathbf{x}) \leq 0, i = 1, \dots, l \\ & \mathbf{K}(\mathbf{x})\mathbf{u} = \mathbf{F}(\mathbf{x}) \\ & \mathbf{x} \in X = \{\mathbf{x} \in \mathbb{R}^n : x_j^{\min} \leq x_j \leq x_j^{\max}, j = 1, \dots, n\} \end{cases} \quad (1.16)$$

where:

- $\mathbf{K}(\mathbf{x})$  is the global stiffness matrix of the structure,
- $\mathbf{u}$  is the global displacement vector,
- $\mathbf{F}(\mathbf{x})$  is the global external force vector.

For small problems, the direct resolution is simple. We can write  $\mathbf{u}(\mathbf{x})$  as function of design variables,  $\mathbf{u}(\mathbf{x}) = \mathbf{K}(\mathbf{x})^{-1}\mathbf{F}(\mathbf{x})$ . When the number of design variables is great, this operation frequently produces a significant increase in the time to resolution. Then, the equilibrium equations will be employed to implicitly define  $\mathbf{u}(\mathbf{x})$ . Indeed, it is always possible to solve the equilibrium equations numerically for  $\mathbf{u}(\bar{\mathbf{x}})$  for any given design  $\bar{\mathbf{x}}$ . Recalling the definition of *nested problem* in paragraph 1.1.4 we can write:

$$\begin{cases} \min_{\mathbf{x}} \hat{g}_0(\mathbf{x}) \\ \text{s.t.} & \hat{g}_i(\mathbf{x}) \leq 0, i = 1, \dots, l \\ & \mathbf{x} \in X. \end{cases} \quad (1.17)$$

Problem (1.17) will be solved through a sequence of explicit sub-problems which are approximations of (1.17). The optimization algorithms used to solve the sub-problems will need some information of object and constraints functions and also their derivatives. In structural optimization, first order methods are common. Zero order methods, which do not use any derivatives, but only need  $\hat{g}_i$ ,  $i = 1, \dots, l$ , are employed at least for small-scale problems. Second or higher order methods are barely used as the calculation of higher order derivatives is expensive.

### Resolution procedure of a nested problem

1. Set counter  $k = 0$  and initialize the design variable  $\mathbf{x}^0$ ;
2. Compute  $\mathbf{u}(\mathbf{x}^k)$ ;
3. Compute  $\hat{g}_0(\mathbf{x}^k)$ ;
4. Produce a convex approximation of the problem (1.17) in  $\mathbf{x}^k$ ;
5. Solve the approximation with an algorithm to have  $\mathbf{x}^{k+1}$ ;
6. Return at the step 2 unless the stopping criterion is satisfied;

Next, for simplicity of notation,  $\hat{g}_i(\mathbf{x})$  will be written as  $g_i(\mathbf{x})$ .

### Sequential Linear Programming (SLP)

In this procedure, objective function and constraints are linearized in  $\mathbf{x}_k$ , so the problem (1.17) can be written at the generic iteration  $k$  as:

$$\begin{cases} \min_{\mathbf{x}} & g_0(\mathbf{x}^k) + \nabla g_0(\mathbf{x}^k)^T(\mathbf{x} - \mathbf{x}^k) \\ \text{s.t.} & g_i(\mathbf{x}^k) + \nabla g_i(\mathbf{x}^k)^T(\mathbf{x} - \mathbf{x}^k) \leq 0, \quad i = 1, \dots, l \\ & \mathbf{x} \in X \\ & -l_j^k \leq x_j - x_j^k \leq -u_j^k, \quad j = 1, \dots, l \end{cases} \quad (1.18)$$

where  $l_j^k$  and  $u_j^k$  are so-called *move limits*. The move limits are chosen by the user; their values deeply influenced the optimization results. The sub-problem is convex since the objective function and constraints can be written as  $\mathbf{a}^T \mathbf{x} + b$  where  $b$  and  $\mathbf{a}$  are constants. To resolve (1.18), for instance, we can use the Simplex Algorithm.

### Sequential Quadratic Programming (SQP)

The problem (1.17) assumes the following form:

$$\begin{cases} \min_{\mathbf{x}} & g_0(\mathbf{x}^k) + \nabla g_0(\mathbf{x}^k)^T(\mathbf{x} - \mathbf{x}^k) + (1/2)(\mathbf{x} - \mathbf{x}^k)\mathbf{H}(\mathbf{x}^k)(\mathbf{x} - \mathbf{x}^k) \\ \text{s.t.} & g_i(\mathbf{x}^k) + \nabla g_i(\mathbf{x}^k)^T(\mathbf{x} - \mathbf{x}^k) \leq 0, \quad i = 1, \dots, l \\ & \mathbf{x} \in X \end{cases} \quad (1.19)$$

where  $\mathbf{H}(\mathbf{x}^k)$  is a positive definite Hessian function of  $g_0$  defined in  $\mathbf{x}^k$ . It follows that (1.19) is a convex problem. For more information about SLP and SQP see [31].

### Convex Linearization (CONLIN)

In the Convex Linearization algorithm, one assumes that all design variables are strictly positive. The set  $X$  in (1.17) become:

$$X = \{\mathbf{x} \in \mathbb{R}^n : 0 < x_j^{min} \leq x_j \leq x_j^{max}, j = 1, \dots, n\}. \quad (1.20)$$

The objective function  $g_0(\mathbf{x})$  and the constraint functions  $g_i(\mathbf{x})$ ,  $i = 1, \dots, l$ , are linearized at the design  $\mathbf{x}^k$  in the *intervening variables*  $y_j = y_j(x_j)$ ,  $j = 1, \dots, n$ , where  $y_j$  will be either  $x_j$  or  $1/x_j$ :

$$g_i(\mathbf{x}) \approx g_i(\mathbf{x}^k) + \sum_{j=1}^n \frac{\partial g_i(\mathbf{x}^k)}{\partial y_j} \left( y_j(x_j) - y_j(x_j^k) \right). \quad (1.21)$$

The partial derivative of  $g_i$  with respect to the intervening variable  $y_j$  is obtained simply using the chain rule, that is

$$\frac{\partial g_i(\mathbf{x}^k)}{\partial y_j} = \frac{\partial g_i(\mathbf{x}^k)}{\partial x_i} \frac{dx_j(x_j^k)}{dy_j} = \frac{\partial g_i(\mathbf{x}^k)}{\partial x_i} \frac{1}{\frac{dy_j(x_j^k)}{dx_j}}. \quad (1.22)$$

Next, we determine the contribution to the sum in (1.21) for the case  $y_j = x_j$  and  $y_j = 1/x_j$ . The contribution of  $y_j = x_j$  is

$$g_{ij}^{L,k}(\mathbf{x}) = \frac{\partial g_i(\mathbf{x}^k)}{\partial x_j} (x_j - x_j^k) \quad (1.23)$$

and  $y_j = 1/x_j$  is

$$g_{ij}^{R,k}(\mathbf{x}) = \frac{\partial g_i(\mathbf{x}^k)}{\partial x_j} \frac{x_j^k (x_j - x_j^k)}{x_j}. \quad (1.24)$$

Now, it is necessary to define the following approximation of  $g_i$  at  $\mathbf{x}^k$ :

$$g_i^{RL,k}(\mathbf{x}) = g_i(\mathbf{x}^k) + \sum_{j \in \Omega_L} g_{ij}^{L,k}(\mathbf{x}) + \sum_{j \in \Omega_R} g_{ij}^{R,k}(\mathbf{x}) \quad (1.25)$$

where  $\Omega_L = \{j : y_j = x_j\}$  and  $\Omega_R = \{j : y_j = 1/x_j\}$ . What variables should be linearized in the direct variables  $x_i$  and what variables should be linearized in the reciprocal variables? In CONLIN we apply

$$\Omega_L = \left\{ j : \frac{\partial g_i(\mathbf{x}^k)}{\partial x_j} > 0 \right\} \quad \Omega_R = \left\{ j : \frac{\partial g_i(\mathbf{x}^k)}{\partial x_j} \leq 0 \right\}. \quad (1.26)$$

The CONLIN approximation turns out to be the most conservative approximation that can be obtained for an approximation on the form (1.25). Some significant properties of the CONLIN approximation are:

- $g_i^{RL,k}$  is a first order approximation of  $g_i$ , indeed the function values and the first order partial derivatives are exact for  $\mathbf{x} = \mathbf{x}^k$ ,
- $g_i^{RL,k}$  is an explicit, convex approximation.

The optimization problem at iteration  $k$  can be rewritten as

$$\begin{cases} \min_{\mathbf{x}} g_0^{RL,k}(\mathbf{x}) \\ \text{s.t.} & g_i^{RL,k}(\mathbf{x}) \leq 0, \quad i = 1, \dots, l \\ & \mathbf{x} \in X \end{cases} \quad (1.27)$$

resolvable using KKT or Lagrangian duality already seen in the previous part. For more information about CONLIN see [23].

### The Method of Moving Asymptotes (MMA)

The Method of Moving Asymptotes (MMA) was developed by Svanberg [22] and employs the intervening variables:

$$y_j(x_j) = \frac{1}{x_j - L_j} \quad y_j(x_j) = \frac{1}{U_j - x_j} \quad j = 1, \dots, n \quad (1.28)$$

where  $L_j$  and  $U_j$  are the *moving asymptotes* which can change during the iterations, but always satisfy:

$$L_j^k < x_j^k < U_j^k. \quad (1.29)$$

The approximation of  $g_i$ ,  $i = 0, \dots, l$  at the design  $\mathbf{x}_k$  is:

$$g_i^{M,k} = r_i^k + \sum_{j=1}^n \left( \frac{p_{ij}^k}{U_j^k - x_j} + \frac{q_{ij}^k}{x_j - L_j^k} \right) \quad (1.30)$$

where

$$p_{ij}^k = \begin{cases} (U_j^k - x_j^k)^2 \frac{\partial g_i(\mathbf{x}^k)}{\partial x_j} & \text{if } \frac{\partial g_i(\mathbf{x}^k)}{\partial x_j} > 0 \\ 0 & \text{otherwise} \end{cases}, \quad (1.31)$$

$$q_{ij}^k = \begin{cases} -(x_j^k - L_j^k)^2 \frac{\partial g_i(\mathbf{x}^k)}{\partial x_j} & \text{otherwise} \\ 0 & \text{if } \frac{\partial g_i(\mathbf{x}^k)}{\partial x_j} > 0 \end{cases} \quad (1.32)$$

and

$$r_i^k = g_i(\mathbf{x}^k) - \sum_{j=1}^n \left( \frac{p_{ij}^k}{U_j^k - x_j^k} + \frac{q_{ij}^k}{x_j^k - L_j^k} \right). \quad (1.33)$$

Differentiation of  $g_i^{M,k}$  twice gives:

$$\frac{\partial g_i^{M,k}(\mathbf{x})}{\partial x_j} = \frac{p_{ij}^k}{(U_j^k - x_j)^2} - \frac{q_{ij}^k}{(x_j - L_j^k)^2}, \quad (1.34)$$

$$\frac{\partial^2 g_i^{M,k}(\mathbf{x})}{\partial x_j^2} = \frac{2p_{ij}^k}{(U_j^k - x_j)^3} + \frac{2q_{ij}^k}{(x_j - L_j^k)^3} \quad (1.35)$$

and

$$\frac{\partial^2 g_i^{M,k}(\mathbf{x})}{\partial x_j \partial x_p} = 0 \quad \text{if} \quad j \neq p. \quad (1.36)$$

MMA shares some nice features:

- the MMA approximation is a first order approximation,
- $g_i^{M,k}$  is an explicit, convex function.

The optimization problem at iteration  $k$  can be rewritten as

$$\begin{cases} \min_{\mathbf{x}} g_0^{M,k}(\mathbf{x}) \\ \text{s.t.} \quad g_i^{M,k}(\mathbf{x}) \leq 0, \quad i = 1, \dots, l \\ \alpha_j^k \leq x_j \leq \beta_j^k, \quad j = 1, \dots, n \end{cases} \quad (1.37)$$

where  $\alpha_j^k$  and  $\beta_j^k$  are called *move limits* to be defined below. As in the case of CONLIN, this problem may be solved using Lagrangian duality or KKT conditions. But how to define the values of the moving asymptotes?

For iteration  $k = 0$  and  $k = 1$

$$\begin{cases} L_j^k = x_j^k - s_{in}(x_j^{max} - x_j^{min}) \\ U_j^k = x_j^k + s_{in}(x_j^{max} - x_j^{min}) \end{cases} \quad (1.38)$$

where  $0 < s_{in} < 1$  and  $x_j^{max}/x_j^{min}$  are the lower and upper bounds of design variable  $x_j$ . For  $k > 1$

$$\begin{cases} L_j^k = x_j^k - s_{slow}(x_j^{k-1} - L_j^{k-1}) \\ U_j^k = x_j^k + s_{slow}(U_j^{k-1} - x_j^{k-1}) \end{cases} \quad (1.39)$$

where  $0 < s_{slow} < 1$  and  $x_j^{max}/x_j^{min}$  are the lower and upper bounds of design variable  $x_j$ . In order to accelerate the convergence we can take  $s_{slow} > 1$ . In each iteration, the design variables are made to satisfy the constraint:

$$\alpha_j^k \leq x_j^k \leq \beta_j^k \quad (1.40)$$

where:

$$\begin{cases} \alpha_j^k = \max(x_j^{min}, (L_j^k + \mu(x_j^k - L_j^k))) \\ \beta_j^k = \min(x_j^{max}, (U_j^k - \mu(U_j^k - x_j^k))) \end{cases} \quad (1.41)$$

with  $0 < \mu < 1$ .

### 1.3 On topology optimization

Through topology optimization we are able to determine the overall configuration of elements in a design problem. Frequently, the results are used as inputs to subsequent size or shape optimization problems. Two main approaches have been developed: *truss-based approach* (part of discrete problems) and *density-based approach* (derived by continuum problems).

In the truss-based approach [Fig. 1.6], a mesh of bars connecting nodes is defined in a predetermined volume, where the mesh can represent a complete graph (*ground truss*) or it is based on unit cells (which is typical for the study of lattice structure). As already mentioned, topology optimization proceeds to identify which bars are most important for the problem, determines their size (especially area or radius) and removes bars so small that they have an insignificant contribution. Often result quality is a strong function of the starting mesh of bars. Results will resemble a lattice structure, with evident variations in bar radius.

The second approach is based on determining the appropriate material density in a set of elements called *voxels* which make up the spatial domain [Fig. 1.7]. This approach is the most common and famous and is employed in many commercial software packages; it became explicit through a process known as the *SIMP (Solid Isotropic Material with Penalization)* method. The starting geometry for the problem is a rectilinear block, which is composed of a set of voxels. Each voxel has a density value which is used as its design variable. A density value of 1 indicates that the material is fully dense, whereas a value of 0 indicates that no material is present. Intermediate values indicate which the material needs not be fully solid to support the local stress state in that voxel. Preferred solutions have voxels that are either fully dense or near 0 density, since typically partially dense materials are difficult to manufacture. Density values are employed to scale voxel stiffness values in the FEM models used during the optimization process.

Here are some examples where topology optimization has been used:

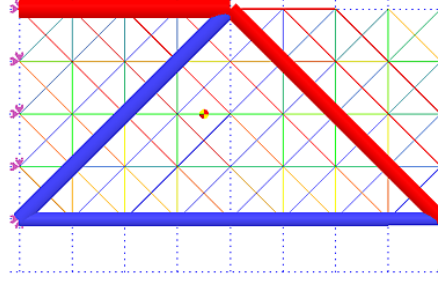


Figure 1.6: Discrete topology optimization for a cantilever. Figure taken from [24].

- in the design of an aircraft to significantly reduce the weight of several different components;
- for the minimization of mass sheet metal chassis components for lightweight, fuel efficient vehicles;
- for the creation of lighter, safer passenger seats for airline passengers;
- to reduce weight in the NASA Altair Lunar Lander Descent Module;
- to decrease the use and cost of materials in the packaging of home appliances;
- for architectural and aesthetic purposes in construction of buildings.

### 1.3.1 Truss-based approach

#### Maximization of the stiffness

The first question we have to answer is:

How can we measure the stiffness of a structure? Most authors suggest to use the compliance  $\mathbf{C}$  of the bars, i.e.  $\mathbf{F}^T \mathbf{u}$ , where  $\mathbf{u}$  are the displacements of the bar nodes and  $\mathbf{F}$  are the given external forces at these nodes. Therefore if the bar is very stiff then its section is very wide.

And, consequently, the second question is:

What are the advantages for this choice? First, in a nested formulation, the compliance



Figure 1.7: Continuum topology optimization for a cantilever. Figure taken from [20].

is a convex function of the design variables, which are the cross-sectional areas of the bars. Second, in a bar where the compliance has been minimized for a given amount of material, all bars have the same stress which means a good use of the available material. Here is the optimization problem in nested formulation that we will tackle:

$$\begin{cases} \min_{\mathbf{x}, \mathbf{u}} \mathbf{F}^T \mathbf{u} \\ \text{s.t.} \quad \mathbf{K}(\mathbf{x}) \mathbf{u} = \mathbf{F} \\ \sum_{j=1}^n l_j x_j \leq V_{max} \\ \mathbf{x} \in X = \{\mathbf{x} \in \mathbb{R}^n : x_j^{min} \leq x_j \leq x_j^{max}, j = 1, \dots, n\} \end{cases} \quad (1.42)$$

where:

- $n$  is the number of bars;
- $\mathbf{K}(\mathbf{x})$  is the global stiffness matrix of the structure;
- $V_{max}$  is the maximum allowed volume of the bars;
- $l_j$  is the length of bar  $j$ ;
- $x_j$  is the cross-sectional area of bar  $j$ .

The external load  $\mathbf{F}$  does not depend on the design variables (we assume that). Since the cross-sectional area cannot be negative or infinite, it is assumed  $x_j^{min} \geq 0$  and

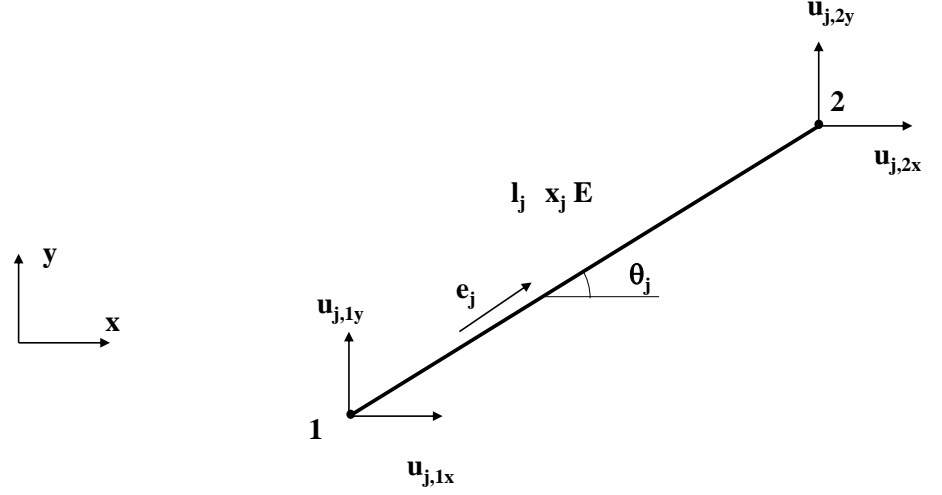


Figure 1.8: Schematization of the bar to be studied.

$x_j^{max} < +\infty$ . Next we will define the process to find the global stiffness. Consider the bar in [Fig. 1.8], the versor  $e_j$  can be written as

$$e_j = \begin{bmatrix} \cos \theta_j \\ \sin \theta_j \end{bmatrix}.$$

The displacements at the ends of the bar in a vectorial way are

$$u_j = \begin{bmatrix} u_{j,1} \\ u_{j,2} \end{bmatrix}$$

where

$$u_{j,1} = \begin{bmatrix} u_{j,1x} \\ u_{j,1y} \end{bmatrix} \quad u_{j,2} = \begin{bmatrix} u_{j,2x} \\ u_{j,2y} \end{bmatrix}.$$

How to define the elongation  $\delta_j$  of the bar and the external forces  $f_j$  applied at the ends?

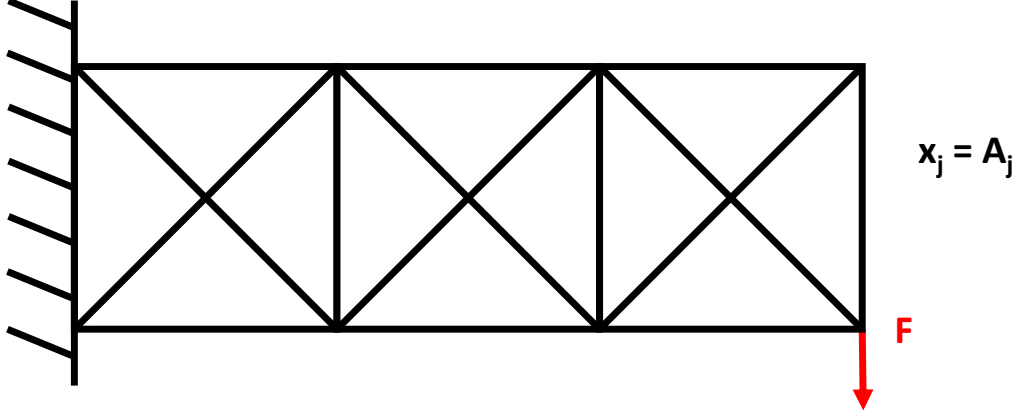


Figure 1.9: Example of optimizing cantilever.

$$\delta_j = \underbrace{[-e_j^T \quad e_j^T]}_{\mathbf{B}_j} \mathbf{u}_j \quad (1.43)$$

$$\mathbf{f}_j = \mathbf{B}_j^T \mathbf{s}_j \quad (1.44)$$

where  $\mathbf{s}_j$  is the force in the bar. If  $s_j > 0$ , bar  $j$  is in tension, otherwise it is in compression. Hook's law states that  $s_j = \sigma_j x_j$  and, since we know that the stress in the bar is

$$\sigma_j = E \epsilon_j \quad (1.45)$$

and the strain

$$\epsilon_j = \frac{\delta_j}{l_j} \quad (1.46)$$

where  $E$  is Young's modulus which is assumed to be the same for all the bars of the structure, it is possible to write  $s_j$  as function of  $\delta_j$

$$s_j = \frac{E \delta_j x_j}{l_j}. \quad (1.47)$$

For simplicity we define  $D_j$  as

$$D_j = \frac{E x_j}{l_j}. \quad (1.48)$$

Inserting the equation (1.43) in (1.47), and then in (1.44) we obtain

$$\mathbf{f}_j = \mathbf{k}_j \mathbf{u}_j \quad (1.49)$$

where

$$\mathbf{k}_j = \mathbf{B}_j^T D_j \mathbf{B}_j \quad (1.50)$$

is the stiffness of bar  $j$ . It is proved that  $\mathbf{k}_j$  is a function of the design variables, hence  $\mathbf{k}_j(\mathbf{x}_j) = \mathbf{k}_j^0 \mathbf{x}_j$ , where  $\mathbf{k}_j^0$  is constant and can be written as

$$\mathbf{k}_j^0 = \frac{E}{l_j} \begin{bmatrix} \cos^2 \theta_j & \cos \theta_j \sin \theta_j & -\cos^2 \theta_j & -\cos \theta_j \sin \theta_j \\ \cos \theta_j \sin \theta_j & \sin^2 \theta_j & -\cos \theta_j \sin \theta_j & -\sin^2 \theta_j \\ -\cos^2 \theta_j & -\cos \theta_j \sin \theta_j & \cos^2 \theta_j & \cos \theta_j \sin \theta_j \\ -\cos \theta_j \sin \theta_j & -\sin^2 \theta_j & \cos \theta_j \sin \theta_j & \sin^2 \theta_j \end{bmatrix}. \quad (1.51)$$

Furthermore the displacements  $\mathbf{u}_j$  of bar  $j$  can be expressed as function of the global displacements  $\mathbf{u}$  as

$$\mathbf{u}_j = \mathbf{C}_j \mathbf{u} \quad (1.52)$$

where  $\mathbf{C}_j$  is a matrix made of 1 and 0. Now inserting the previous equation (1.52) in (1.49) and premultiplying by  $\mathbf{C}_j^T$ , we get the global equilibrium equations for the structure

$$\mathbf{F} = \mathbf{K}(\mathbf{x}) \mathbf{u}. \quad (1.53)$$

It is clear that the global stiffness matrix  $\mathbf{K}(\mathbf{x})$  appears as

$$\mathbf{K}(\mathbf{x}) = \sum_{j=1}^n \mathbf{K}_j(\mathbf{x}) = \sum_{j=1}^n \mathbf{C}_j^T \mathbf{k}_j(\mathbf{x}) \mathbf{C}_j. \quad (1.54)$$

The matrix  $\mathbf{K}_j(\mathbf{x})$  is a global version of the element stiffness matrix  $\mathbf{k}_j(\mathbf{x})$ , whose nonzero elements are the elements of  $\mathbf{k}_j(\mathbf{x})$  that correspond to the degrees of freedom in the global displacement vector  $\mathbf{u}$ . We can express  $\mathbf{K}_j(\mathbf{x})$  as

$$\mathbf{K}_j(\mathbf{x}) = \mathbf{K}_j^0 \mathbf{x}_j = \mathbf{C}_j^T \mathbf{k}_j^0(\mathbf{x}) \mathbf{C}_j \mathbf{x}_j \quad (1.55)$$

and then the global stiffness matrix becomes

$$\mathbf{K}(\mathbf{x}) = \sum_{j=1}^n \mathbf{K}_j^0 \mathbf{x}_j. \quad (1.56)$$

In (1.53)  $\mathbf{F}$  is

$$\mathbf{F}(\mathbf{x}) = \sum_{j=1}^n \mathbf{C}_j^T \mathbf{f}_j. \quad (1.57)$$

Since the contribution from the unknown reaction forces from supports and the unknown forces from neighboring bars will be zero, we may rewrite equation (1.57) as

$$\mathbf{F}(\mathbf{x}) = \sum_{j=1}^n \mathbf{C}_j^T \mathbf{f}_j^a \quad (1.58)$$

where  $\mathbf{f}_j^a$  is the vector of forces on the end points of bar  $j$  and  $\mathbf{F}$  is the vector of the total applied force on the structure. The total element external forces  $\mathbf{f}_j$  may be calculated once has been solved for the displacements. The elongation  $\bar{\delta}$  of all bars in the structure is given by

$$\bar{\delta} = \bar{\mathbf{B}}\mathbf{u} \quad (1.59)$$

where

$$\bar{\mathbf{B}} = \begin{bmatrix} \mathbf{B}_1 \mathbf{C}_1 \\ \mathbf{B}_2 \mathbf{C}_1 \\ \vdots \\ \mathbf{B}_n \mathbf{C}_n \end{bmatrix}. \quad (1.60)$$

If (1.44) is written for the whole structure, it becomes:

$$\mathbf{F} = \bar{\mathbf{B}}^T \mathbf{s} \quad (1.61)$$

where  $\mathbf{s}$  are the forces in all bars. If  $\bar{\mathbf{B}}$  is invertible then:

$$\mathbf{u} = \bar{\mathbf{B}}^{-1} \bar{\delta} = \bar{\mathbf{B}}^{-1} \text{diag}\left(\frac{l_1}{Ex_1}, \dots, \frac{l_n}{Ex_n}\right) \bar{\mathbf{B}}^{-T} \mathbf{F} \quad (1.62)$$

and we can define the stress in all the bars:

$$\sigma = \text{diag}\left(\frac{1}{x_1}, \dots, \frac{1}{x_n}\right) \bar{\mathbf{B}}^{-T} \mathbf{F}. \quad (1.63)$$

### Nested formulation

If the global stiffness matrix of the structure is non-singular, it is possible to use the nested formulation. Generally in topology optimization global stiffness is singular. We might prevent the simultaneous formulation by putting the lower bounds (that is null) to a very small and positive value:  $x_{min}^j = \epsilon > 0$ . It may be proven that as  $\epsilon \rightarrow 0$ , the solution of for  $x_{min}^j = \epsilon$  approaches that of for  $x_{min}^j = 0$ .

The main difficulty is to find a suitable value for the lower bound  $\epsilon$ . If  $\epsilon$  is too small  $\mathbf{K}(\mathbf{x})$  can be ill conditioning, if  $\epsilon$  is too large, the deleted bars may posses structural

importance. We write the nested formulation:

$$\begin{cases} \min_{\mathbf{x}} \mathbf{F}^T \mathbf{u}(\mathbf{x}) \\ \sum_{j=1}^n l_j x_j \leq V_{max} \\ \mathbf{x} \in X = \{\mathbf{x} \in \mathbb{R}^n : x_j^{min} \leq x_j \leq x_j^{max}, j = 1, \dots, n\} \end{cases} \quad (1.64)$$

Why should we prefer nested formulation to simultaneous formulation? The main reason is that the nested formulation is convex and simultaneous formulation is not [24]. The problem (1.64) can be resolved through the application of techniques seen in 1.2.3.

### Minimization of volume

Before starting to discuss the issue in general terms, we focus our attention on the following problem taken from [24].

**Exercise** Consider a cantilever beam, fixed at the left end and subject to a vertical force  $F$  at the right end. The beam consists of 2 segments, each of length  $L$ . The density is called  $\rho$ . Each segment cross section has a hollow square form, see [Fig. 1.10]. The thickness is called  $t$  for all segments and the side length  $x_S$  for segment  $S = 1, 2$ . The moment of inertia,  $I_S$  can be calculated from classical formulation. If it is assumed  $t \ll x_S$ , for all  $S$ , then

$$I_S = \frac{x_S^4}{12} - \frac{(x_S - 2t)^4}{12} = \frac{2tx_S^3}{3}. \quad (1.65)$$

We want to minimize the weight of the beam under the constraint that the displacement at the tip  $\delta$  is lower than  $\delta_0$ . The design variables are the cross-sectional sizes. The weight can be written ( $t \ll x_S$ ) as:

$$f(x_S) = 4\rho t \sum_{S=1}^N x_S. \quad (1.66)$$

The displacement at the tip of the beam can be seen as the sum of contributions from each segment when other segments are considered as rigid, that is

$$\delta = \sum_{S=1}^N \delta^S \quad (1.67)$$

where  $\delta^S$  is the displacement at the tip of the cantilever for a system where only segment  $S$  is elastic. Since we consider small displacements such that  $\sin \theta_S \approx \theta_S$  hence:

$$\delta^S = \delta_S + (S - 1)\theta_S \quad (1.68)$$

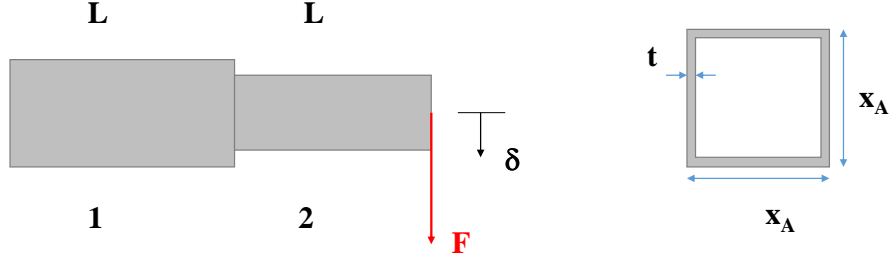


Figure 1.10: Cantilever and the cross section.

where  $\delta_S$  and  $\theta_S$  are the displacement and the rotation at the right-hand side of segment  $S$  when only this segment is elastic [Fig. 1.11].  $\delta_S$  and  $\theta_S$  can be found with through the following equations:

$$\delta_S = \frac{M_S L^2}{2EI_S} + \frac{F_S L^3}{3EI_S}, \quad \theta_S = \frac{M_S L}{EI_S} + \frac{F_S L^2}{2EI_S} \quad (1.69)$$

where  $E$  is Young modulus,  $M_S = (S - 1)LF$  and  $F_S = F$ . Inserting (1.69) in (1.68) and then the results in (1.67) we obtain:

$$\delta = \frac{FL^3}{2Et} \sum_{s=1}^N (S_2 - S + \frac{1}{x_s^3}) \quad (1.70)$$

The minimization problem we have to resolve is:

$$\begin{cases} \min_{x_1, x_2} f(x_1, x_2) = 4\rho Lt(x_1 + x_2) \\ \text{s.t.} \quad \frac{1}{x_1^3} + \frac{7}{x_2^3} \leq \frac{2\delta_0 Et}{FL^3} \\ x_1 > 0, \quad x_2 > 0 \end{cases} \quad (1.71)$$

Assuming equality in the non strict inequality constraint we solve:

$$x_1^* = \left( \frac{1 + 7^{1/4}}{\frac{2\delta_0 Et}{FL^3}} \right)^{1/3} \quad x_2^* = 7^{1/4} \left( \frac{1 + 7^{1/4}}{\frac{2\delta_0 Et}{FL^3}} \right)^{1/3} \quad (1.72)$$

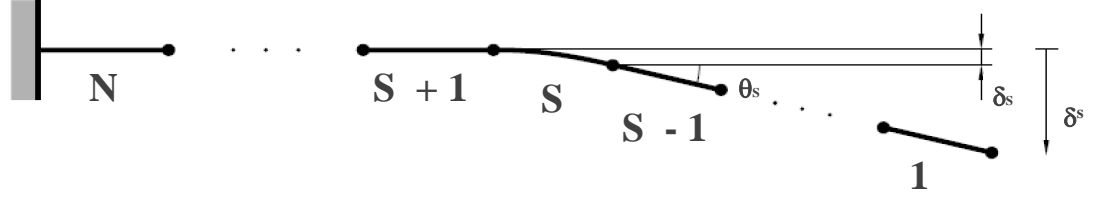


Figure 1.11: Cantilever when only A is elastic.

what happens if we minimize the tip displacement having the weight as constraint?

$$\begin{cases} \min_{x_1, x_2} \frac{1}{x_1^3} + \frac{7}{x_2^3} \\ \text{s.t.} \quad 4\rho L t(x_1 + x_2) < W_{lim} \\ x_1 > 0, \quad x_2 > 0 \end{cases} \quad (1.73)$$

where  $W_{lim}$  is the upper bound of the weight. We resolve the problem as before and we find:

$$x_1^{**} = \left( \frac{W_{lim}}{\frac{2\delta_0 E t}{F L^3} (1 + 7^{1/4})} \right)^{1/3} \quad x_2^{**} = 7^{1/4} \left( \frac{W_{lim}}{\frac{2\delta_0 E t}{F L^3} (1 + 7^{1/4})} \right)^{1/3}. \quad (1.74)$$

Thus, the solution of (1.73) can be obtained by scaling the solution of the reversed problem and viceversa.

We will now generalize this result for the truss-based approach. We write the problem of minimizing the compliance under a volume constraint and the problem of minimizing the volume under a compliance constraint as:

$$\begin{cases} \min_{\mathbf{x}} \mathbf{F}^T \mathbf{u}(\mathbf{x}) \\ \text{s.t.} \quad \mathbf{l}^T \mathbf{x} - V_{max} \leq 0 \\ \mathbf{x} \in X \end{cases} \quad (1.75)$$

$$\begin{cases} \min_{\mathbf{x}} \mathbf{l}^T \mathbf{x} \\ \text{s.t.} \quad \mathbf{F}^T \mathbf{u}(\mathbf{x}) - C_{max} \leq 0 \\ \mathbf{x} \in X \end{cases} \quad (1.76)$$

(we will call (1.75) as (A) and (1.76) as (B)); where  $\mathbf{l}$  is a vector with the lengths of the bars,  $C_{max} > 0$  is the maximum allowed compliance in problem (B) and  $V_{max} > 0$  is the maximum allowed volume in problem (A). Under the assumption that the lower and upper bounds are not active in (A) and (B), we have to prove:

$$\mathbf{x}_B^* = \frac{C_A^*}{C_{max}} \mathbf{x}_A^*, \quad C_A^* = \mathbf{F}^T \mathbf{u}(\mathbf{x}_A^*) \quad (1.77)$$

$$\mathbf{x}_A^* = \frac{V_{max}}{V_B^*} \mathbf{x}_B^*, \quad V_B^* = \mathbf{l}^T \mathbf{x}_B^* \quad (1.78)$$

where  $\mathbf{x}_A^*$  is the solution of problem (A) and  $\mathbf{x}_B^*$  is the solution of problem (B). We write KKT condition for (A):

$$-\mathbf{u}(\mathbf{x}_A)^T \mathbf{K}_j^0 \mathbf{u}(\mathbf{x}_A) + \lambda_A l_j = 0 \quad (1.79)$$

$$\lambda_A (\mathbf{l}^T \mathbf{x}_A - V_{max}) = 0 \quad (1.80)$$

$$\mathbf{l}^T \mathbf{x}_A - V_{max} \leq 0 \quad (1.81)$$

$$\lambda_A \geq 0 \quad (1.82)$$

and for (B):

$$l_j - \lambda_B \mathbf{u}(\mathbf{x}_B)^T \mathbf{K}_j^0 \mathbf{u}(\mathbf{x}_B) = 0 \quad (1.83)$$

$$\lambda_B (\mathbf{F}^T \mathbf{u}(\mathbf{x}_B) - C_{max}) = 0 \quad (1.84)$$

$$\mathbf{F}^T \mathbf{u}(\mathbf{x}_B) - C_{max} \leq 0 \quad (1.85)$$

$$\lambda_B \geq 0. \quad (1.86)$$

Let  $\mathbf{x}_A$  the solution to (A) and  $\mathbf{x}_B^* = \frac{C_A^*}{C_{max}} \mathbf{x}_A^*$ . We will show that exists a  $\lambda_B^* \geq 0$  such as  $(\lambda_B^*, \mathbf{x}_B^*)$  is a KKT point for (B). Since the problem is convex,  $\mathbf{x}_B^*$  is a solution to (B).

**Definition 5** Admit that the positive definite global stiffness matrix be written as in (1.56) for any  $\mathbf{x}$  and  $\mathbf{x}^* = \alpha \mathbf{x}$ ,  $\alpha \neq 0$ . Hence  $\mathbf{u}(\mathbf{x}^*) = \mathbf{u}(\mathbf{x})/\alpha$  solves  $\mathbf{K}(\mathbf{x}^*)\mathbf{u}(\mathbf{x}^*) = \mathbf{F}$  if, and only if,  $\mathbf{u}(\mathbf{x})$  solves  $\mathbf{K}(\mathbf{x})\mathbf{u}(\mathbf{x}) = \mathbf{F}$ .

Demonstration of what it is said in the previous definition:

$$\sum_{j=1}^n x_j \mathbf{K}_j^0 \mathbf{u}(\mathbf{x}) = \mathbf{F} \iff \sum_{j=1}^n \alpha x_j \mathbf{K}_j^0 \frac{\mathbf{u}(\mathbf{x})}{\alpha} = \mathbf{F} \iff \mathbf{K}(\mathbf{x}^*) \frac{\mathbf{u}(\mathbf{x})}{\alpha} = \mathbf{F}. \quad (1.87)$$

Thus,  $\mathbf{u}(\mathbf{x}^*) = \mathbf{u}(\mathbf{x})/\alpha$  is the unique solution to equilibrium equations for the design  $\mathbf{x}^*$ . This definition is useful, in fact:

$$\mathbf{u}(\mathbf{x}_B^*) = \mathbf{u}(\mathbf{x}_A^*) \frac{C_{max}}{\mathbf{F}^T \mathbf{u}(\mathbf{x}_A^*)}. \quad (1.88)$$

In this equation the denominator cannot be zero since the compliance  $\mathbf{C}$  is always *definite positive*, in fact  $\mathbf{C} = \mathbf{F}_T^T \mathbf{u}(\mathbf{x}) = \mathbf{u}(\mathbf{x})^T \mathbf{K} \mathbf{u}(\mathbf{x})$ , where  $\mathbf{K}$  is definite positive and  $\mathbf{u} \neq 0$  since  $\mathbf{F} \neq 0$ . From (1.79) we have

$$\lambda_A^* = \frac{\mathbf{u}(\mathbf{x}_A^*)^T \mathbf{K}_j^0 \mathbf{u}(\mathbf{x}_A^*)}{l_j} \quad (1.89)$$

where  $\lambda_A^*$  is positive, because, if it were zero, the strain energy should be zero for all elements. From (1.83) and (1.88) we get

$$l_j - \lambda_B^* \left( \frac{C_{max}}{\mathbf{F}^T \mathbf{u}(\mathbf{x}_A^*)} \right)^2 \mathbf{u}(\mathbf{x}_A^*)^T \mathbf{K}_j^0 \mathbf{u}(\mathbf{x}_A^*) = 0. \quad (1.90)$$

Inserted in (1.89):

$$\lambda_B^* = \frac{1}{\left( \frac{C_{max}}{\mathbf{F}^T \mathbf{u}(\mathbf{x}_A^*)} \right)^2 \lambda_A^*} > 0. \quad (1.91)$$

So (1.86) is proved. From (1.88) we have

$$\mathbf{F}^T \mathbf{u}(\mathbf{x}_B^*) - C_{max} = \mathbf{F}^T \left( \frac{C_{max}}{\mathbf{F}^T \mathbf{u}(\mathbf{x}_A^*)} \right) \mathbf{u}(\mathbf{x}_A^*) - C_{max} = 0. \quad (1.92)$$

Thus, (1.80) and (1.81) are satisfied. Since all KKT conditions of (B) are satisfied, we know that  $\mathbf{u}(\mathbf{x}_B^*)$  as defined above is a solution to (B). Now let  $\mathbf{x}_B^*$  be a solution to (B), and let  $\mathbf{x}_A^* = \mathbf{x}_B^* (\mathbf{V}_{max} / \mathbf{l}^T \mathbf{x}_B^*)$  then

$$\mathbf{u}(\mathbf{x}_A^*) = \frac{\mathbf{l}^T \mathbf{x}_B^*}{V_{max}} \mathbf{u}(\mathbf{x}_B^*) \quad (1.93)$$

using (1.79) and (1.83)

$$\lambda_A^* = \frac{\left( \frac{\mathbf{l}^T \mathbf{x}_B^*}{V_{max}} \right)^2}{\lambda_B^*} > 0 \quad (1.94)$$

so (1.86) is valid and (1.78) yields

$$\mathbf{l}^T \mathbf{x}_A^* - V_{max} = \mathbf{l}^T \left( \frac{V_{max}}{\mathbf{l}^T \mathbf{x}_B^*} \right) \mathbf{x}_B^* - V_{max} = 0. \quad (1.95)$$

Hence (1.80) and (1.81) is valid, proving that  $\mathbf{x}_A^*$  is a solution to (A).

### Sensitivity Analysis

To solve optimization problems, it is often necessary to differentiate the objective functions and the constraint functions with respect to the design variables. The procedure

which is carried out to obtain the derivatives is called *sensitivity analysis* where *sensitivity* means nothing but derivative. The theme, though relatively simple from a mathematical point of view, is fundamental for the use of optimization theory, especially in the case of the approximated problems. The main methods employed to obtain the derivatives are:

- analytical methods
- numerical methods

Beside these main procedures, however, there are other methods which combine the two listed above. Subsequently, we will describe briefly the principles of the operation.

**Analytical methods** Consider  $g_i(\mathbf{x}) : \mathbb{R}^n \rightarrow \mathbb{R}^l$ , in order to obtain the analytical expression for  $\partial g_i(\mathbf{x}^k) \backslash \partial x_j$  at  $k$  iteration, we apply the chain rule:

$$\frac{\partial g_i(\mathbf{x}^k)}{\partial x_j} = \frac{\partial g_i(\mathbf{x}^k, \mathbf{u}(\mathbf{x}^k))}{\partial x_j} + \frac{\partial g_i(\mathbf{x}^k, \mathbf{u}(\mathbf{x}^k))}{\partial \mathbf{u}} \frac{\partial \mathbf{u}(\mathbf{x}^k)}{\partial x_j} \quad (1.96)$$

where  $\partial g_i \backslash \partial \mathbf{u}$  is a row matrix, and  $\partial \mathbf{u} \backslash \partial x_j$  is a column matrix.

In the analytical method,  $\partial \mathbf{u} \backslash \partial x_j$  is obtained by differentiation of the equilibrium equations  $\mathbf{K}(\mathbf{x})\mathbf{u}(\mathbf{x}) = \mathbf{F}(\mathbf{x})$ . The result is then inserted into (1.96). In order to avoid writing all the passages, we get

$$\frac{\partial \mathbf{u}(\mathbf{x}^k)}{\partial x_j} = \mathbf{K}(\mathbf{x}^k)^{-1} \left( \frac{\partial \mathbf{F}(\mathbf{x}^k)}{\partial x_j} - \frac{\partial \mathbf{K}(\mathbf{x}^k)}{\partial x_j} \mathbf{u}(\mathbf{x}^k) \right). \quad (1.97)$$

Since our purpose is not to describe verbosely, we will use a good example. We want to calculate the sensitivity of compliance  $g_0(\mathbf{x}, \mathbf{u}(\mathbf{x})) = \mathbf{F}(\mathbf{x})^T \mathbf{u}(\mathbf{x})$ . First we differentiate the sensitivity

$$\frac{\partial g_0(\mathbf{x}^k, \mathbf{u}(\mathbf{x}^k))}{\partial x_j} = \frac{\partial \mathbf{F}(\mathbf{x}^k)^T}{\partial x_j} \mathbf{u}(\mathbf{x}^k) + \frac{\partial g_0(\mathbf{x}^k, \mathbf{u}(\mathbf{x}^k))}{\partial \mathbf{u}} = \mathbf{F}(\mathbf{x}^k)^T \quad (1.98)$$

Inserting (1.97) and the equation just written in (1.96) we obtain, after few passages,

$$\frac{\partial g_0(\mathbf{x}^k)}{\partial x_j} = 2\mathbf{u}(\mathbf{x}^k)^T \frac{\partial \mathbf{F}(\mathbf{x}^k)^T}{\partial x_j} - \mathbf{u}(\mathbf{x}^k)^T \frac{\partial \mathbf{K}(\mathbf{x}^k)^T}{\partial x_j} \mathbf{u}(\mathbf{x}^k). \quad (1.99)$$

It is remarkable that the method just presented is *exact method*.

**Numerical methods** Frequently, analytical methods are difficult to implement from the mathematical point of view and from a computational point of view, so we resort to numerical methods which are an approximation of the former. The numerical methods employed to approximate the value of the derivatives are essentially two: the *forward difference approximation* and *central difference approximation*. Here is the formulation for the two method:

- For forward difference approximation

$$\frac{\partial \mathbf{g}_i(\mathbf{x}^k)}{\partial x_j} \approx \frac{g_i(\mathbf{x}^k + h\mathbf{e}_j) - g_i(\mathbf{x}^k)}{h} \quad (1.100)$$

where  $\mathbf{e}_j = [0, \dots, 0, 1, 0, \dots, 0]^T$  and  $h$  is a small number greater than one;

- For central difference approximation

$$\frac{\partial \mathbf{g}_i(\mathbf{x}^k)}{\partial x_j} \approx \frac{g_i(\mathbf{x}^k + h\mathbf{e}_j) - g_i(\mathbf{x}^k - h\mathbf{e}_j)}{2h} \quad (1.101)$$

where  $\mathbf{e}_j = [0, \dots, 0, 1, 0, \dots, 0]^T$  and  $h$  is a small number greater than one.

### 1.3.2 Density-based approach

The *density-based approach* is a type of approach much more general than the truss-based approach, and reflects the purest conception of topology optimization. There is much interest for this technique mainly due to the fact that the obtained outcomes are often surprising [Fig. 1.12]. The goal is to find the optimal distribution of material in a determined domain in order to maximize an objective function satisfying a set of constraints. Loads, boundary conditions and maximum volume allowed for the structure are known; shape and connectivity, instead, are not and are found as a result of the optimization. The final result shows the locations in space where there should be material and the locations which should be void.

Consider the design domain  $\Omega$  discretized by  $n$  finite elements, to each element can be assigned a design variable  $\rho_e \in (0, 1]$  to represent its relative density, where  $e = 1 \dots n$ . These design variables can be collected into a vector  $\boldsymbol{\rho} \in \mathbb{R}^n$ . The assembled global stiffness matrix  $\mathbf{K}(\boldsymbol{\rho})$  is dependent on the design variables and it has dimension of  $d \times d$ , where  $d$  is the number of degrees of freedom. The displacements vector  $\mathbf{u} \in \mathbb{R}^d$  can be determined by the equilibrium equations

$$\mathbf{K}(\boldsymbol{\rho})\mathbf{u} = \mathbf{F} \quad (1.102)$$

where  $\mathbf{F} \in \mathbb{R}^d$  the external load.

Assuming linear elasticity, the strain and stress tensors can be related to the displacement vector through the kinematic and constitutive equations, that is

$$\epsilon_{ij} = \frac{1}{2}(\mathbf{u}_{i,j} + \mathbf{u}_{j,i}) \quad (1.103)$$

$$\sigma_{ij} = D_{ijkl}\epsilon_{kl} \quad (1.104)$$

where  $\mathbf{D}$  is the constitutive matrix dependent on Poisson's ratio  $\nu$  and Young's modulus  $E_0$ . The density design variable, at the end of the optimization, should be maximum or minimum (1 or 0), such that the discretized domain appears black and white. A common

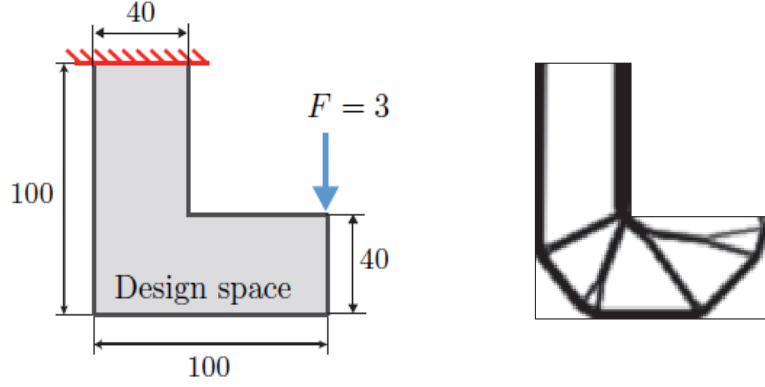


Figure 1.12: Example of density-based approach. Figure taken from [4].

approach to enforce this bi-color solution is to use the *Solid Isotropic Material with Penalization (SIMP)* approach to penalize the intermediate densities. According to this approach, the Young's modulus  $E_e$  of each element can be written as

$$E_e = \rho_e^p E_0 \quad (1.105)$$

where  $E_0$  is the Young's modulus of the solid material, and  $p$  is the penalization power. By using a penalized Young modulus, the assembled stiffness matrix has an explicit dependence on each density design variables, with

$$\mathbf{K}(\rho) = \sum_{e=1}^n \rho_e^p \mathbf{k}_0 \quad (1.106)$$

where  $\mathbf{k}_0$  is the element stiffness matrix which employs the solid material's Young's modulus  $E_0$ .

For the discretized domain  $\Omega$ , the mass can be calculated as:

$$M(\rho) = \sum_{e=1}^n V_e \rho_{eff,e} \quad (1.107)$$

where  $V_e$  is the volume of a mesh element and  $\rho_{eff,e}$  represents the effective density of the material for a single element. If the elements of the mesh have unitary volume, as

often happens, (1.110) becomes:

$$M(\rho) = \sum_{e=1}^n \rho_{eff,e} \quad (1.108)$$

Since the effective density can be written as:

$$\rho_{eff,e} = \rho_{mat}\rho_e \quad (1.109)$$

where  $\rho_{mat}$  is the density of the solid material. Then we define the *mass function*, the one which should be minimized, such as

$$m(\rho) = \sum_{e=1}^n \rho_e \quad (1.110)$$

$\rho_{mat}$  is neglected as a constant.

Frequently, in order to ensure a black and white resulting scheme, it is useful to penalize the mass. Initially mass function is

$$m(\rho) = \sum_{e=1}^n \rho_e, \quad (1.111)$$

but with penalization becomes

$$m(\rho) = \sum_{e=1}^n \rho_e + \alpha \rho_e (1 - \rho_e) \quad (1.112)$$

where  $\alpha$  is a penalty coefficient. The second term is different from zero when the density assumes intermediate value.

### Minimization of compliance with mass constraint

One common objective for topology optimization problems is the minimization of the compliance subject to a mass constraint. In this formulation, the purpose is to distribute a given amount of material to achieve a structure with maximum stiffness, i.e. minimizing compliance. The problem can be mathematically described as

$$\begin{cases} \min_{\rho} C(u) = \mathbf{u}^T \mathbf{K} \mathbf{u} \\ \text{s.t.} & \sum_{e=1}^n \rho_e \leq m_0 \quad e = 1, \dots, n. \\ & \mathbf{K} \mathbf{u} = \mathbf{F} \\ & 0 < \rho_{min} \leq \rho_e \leq \rho_{max} \end{cases} \quad (1.113)$$

where:

- $\mathbf{u}$  are the global displacements,

- $\mathbf{K}$  is the global stiffness matrix,
- $m_0$  is the maximum allowed for mass function,
- $\rho_{min}$  is the minimum relative density (typically set to  $10^{-3}$ ).

$\rho$  is non zero to avoid singularities in the stiffness matrix. [42] is a synthetic paper on minimization of compliance.

### Minimization of mass with stress constraints

Despite the well-known mathematical background of compliance minimization in topology optimization, this problem is not representative of practical structural issues. To determine the lightest structure that does not fail would be a more useful goal. Once we know the value of the stress tensor, it is possible to replace the stress values obtained in the chosen material failure function  $F(\sigma)$ . Thus, the stress-constrained mass minimization optimization problem can be written as

$$\begin{cases} \min_{\rho} m(\rho) = \sum_{e=1}^n \rho_e \\ \text{s.t.} & F(\sigma_e)/\sigma_y \leq 1 \quad e = 1, \dots, n. \\ & \mathbf{K}\mathbf{u} = \mathbf{F} \\ & 0 < \rho_{min} \leq \rho_e \leq \rho_{max} \end{cases} \quad (1.114)$$

where  $\sigma_y$  is the material yield strength. Clearly failure occurs when  $F(\sigma_e) > \sigma_y$ . One of the most basic failure criteria is the Von Mises stress criterion. For isotropic materials with mainly ductile behavior, the Von Mises failure criterion is the most widely used failure function, and is given by

$$\sigma_{vm} = \sqrt{\frac{1}{2}[(\sigma_{22} - \sigma_{11})^2 + (\sigma_{33} - \sigma_{22})^2 + (\sigma_{33} - \sigma_{11})^2] + 3(\sigma_{12}^2 + \sigma_{23}^2 + \sigma_{31}^2)}. \quad (1.115)$$

However, it has been recognized that topology optimization with stress constraints may encounter singularities as noted in [43] and [45]. In both cases, a three-bar truss problem was analyzed, and it was discovered that the the global optimum can only be obtained if one of the trusses is removed, which would in effect violate that member's stress constraint.

This phenomenon is caused by the discontinuous nature of the stress function: as  $\rho \rightarrow 0$ , the stress approaches infinity; while when  $\rho = 0$ , the stress is undefined. As the truss area approaches zero, the stress approaches a large value and the constraint becomes violated. Physically, however, this stress constraint should be eliminated when the area is exactly zero. A stress-constrained structural topology optimization approach which does not treat this singularity appropriately prevents material from being removed completely. There are several papers covering the topic, the more interesting being [40] and [41].

### Problem of singularities: relaxation techniques

Cheng and Guo [36] proposed  $\epsilon$ -relaxation as a solution to the inaccessibility of singular optima. This strategy was first introduced to truss optimization and has also proved to be effective for continuum topology optimization. To make sure that the constraint on the stress is always satisfied when the density vanishes, the stress constraint can be written as

$$\rho_e \left( \frac{\sigma_{vm}}{\sigma_y} \right) \leq 0. \quad (1.116)$$

However, one can see that as the density approaches zero, the stress remains finite and the constraint is violated. The relaxation approach implies that the stress constraint and the variable lower bounds are perturbed by a small parameter,  $\epsilon > 0$ , such that the degenerate part in the feasible region is smoothed. This relaxation modifies (1.116) to

$$\rho_e \left( \frac{\sigma_{vm}}{\sigma_y} \right) \leq \epsilon \quad (1.117)$$

where  $\epsilon$  is called relaxation parameter.

The alternative formulation of  $\epsilon$ -relaxation proposed by Duysinx in [38] is often used:

$$\left( \frac{\sigma_{vm}}{\sigma_y} \right) - 1 - \frac{\epsilon}{\rho_e} + \epsilon \leq 0 \quad (1.118)$$

Here, an additional term has been introduced to eliminate any perturbation of the constraints for solid densities  $\rho = 1$ . [Fig. 1.13], [Fig. 1.14], [Fig. 1.15], [Fig. 1.16] show the effect of relaxation on the feasible domain for different values of the relaxation parameter. In these figures, point B is the global minimum in the degenerate region of line segment BC. The contour of the objective function is shown, with the feasible region in gray, and point A being a local minimum. As  $\epsilon$  decreases, point B approaches the true optimum, but remains difficult to achieve. Conversely, as  $\epsilon$  increase, point B moves away from the true optimum, but becomes simpler to achieve.

Bruggi, in [39], introduced an alternative  $\epsilon$ -relaxation scheme known as the *qp*-approach. Here is the stress constraints written with this approach:

$$\rho_e^{\epsilon_{pq}} \left( \frac{\sigma_{vm}}{\sigma_y} \right) \leq 1 \quad (1.119)$$

where

$$\epsilon_{pq} = p - q \quad (1.120)$$

In the equation above  $p$  is the penalization factor and  $q$  is a real number with values  $0 \leq q \leq p$ . In density-based topology optimization the *qp*-approach is generally applied using a relatively large constant relaxation parameter, typically  $0.5 \leq \epsilon \leq 1$ . The formulation proposed by Lee et al. [40] is simpler, showing good results:

$$\rho_e^{\frac{1}{2}} \left( \frac{\sigma_{vm}}{\sigma_y} \right) \leq 1 \quad (1.121)$$

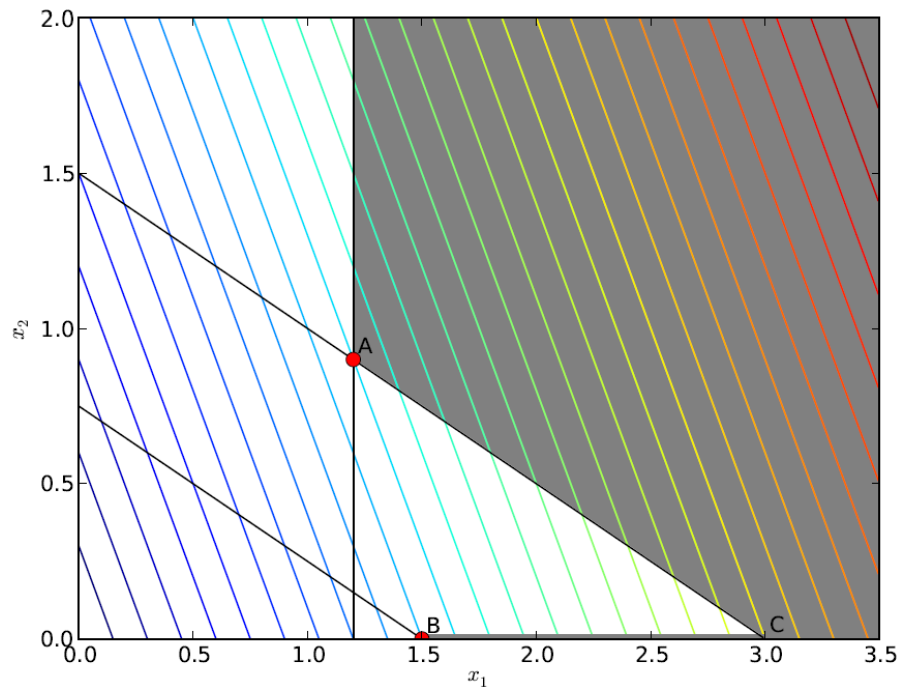


Figure 1.13: No relaxation,  $\epsilon = 0$ . Figure taken from [5].

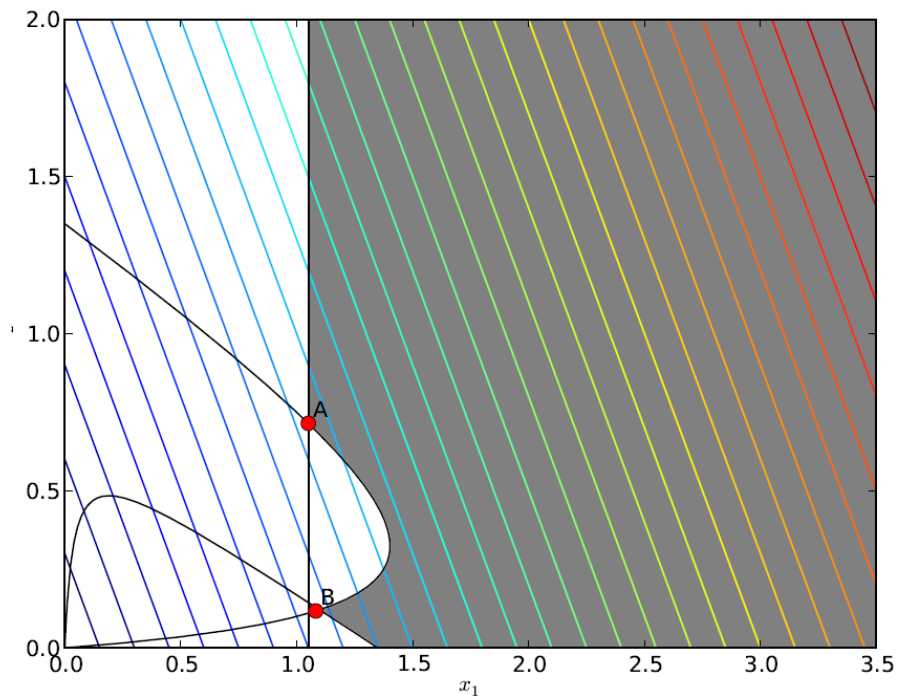


Figure 1.14:  $\epsilon = 0.15$ . Figure taken from [5].

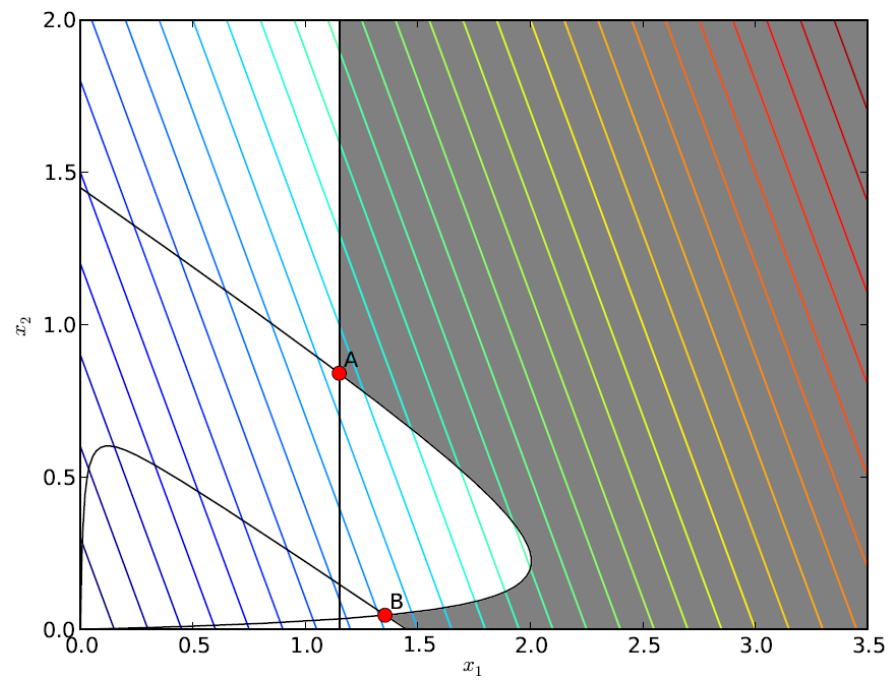


Figure 1.15:  $\epsilon = 0.05$ . Figure taken from [5].

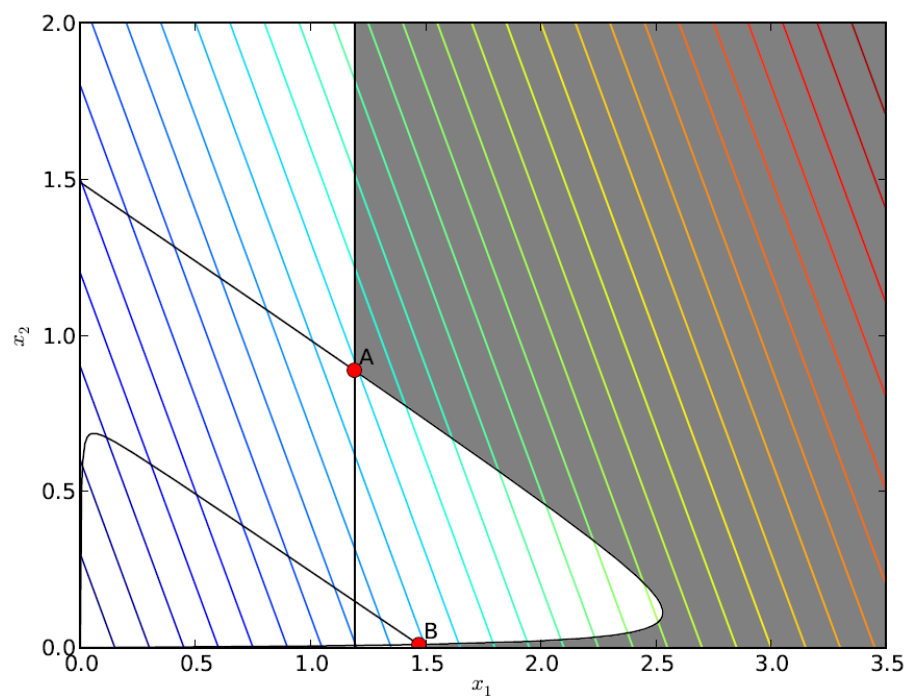


Figure 1.16:  $\epsilon = 0.01$ . Figure taken from [5].

Different formulations of relaxation techniques have been employed in literature; they are often closely related but differ in their exact implementation.

### Continuation Method

The presence of penalization parameter  $p$  creates a complication that plagues the continuum problem of topology optimization. The penalization parameter is essential for obtaining the scheme void-solid, however it causes the onset of a large number of local minima. One approach to avoid local minima is to use a continuation method, a concept first introduced by Allaire and Francfort in [44]. The idea is to begin the optimization with no penalization of intermediate densities, setting  $p = 1$ , and then gradually increasing the SIMP penalization parameter until an acceptable void-solid solution is obtained. Therefore, by delaying the penalization, one prevents the optimizer from prematurely converging to a sub optimal solution. Though this method, as shown by many authors, gives satisfactory results, it cannot be guaranteed with the utmost confidence that the point of minimum found is actually global. Nevertheless, it is the best possible solution currently available.



## Chapter 2

# Cellular materials

### 2.1 Introduction

Mankind has always been looking for materials which might offer great performance. A timeline is the conventional way in which we can observe the evolution of human knowledge about materials over the course of the centuries [Fig. 2.1]; a timeline, however, lacks completely information about the properties of every material. There is a way to overcome the issue and manage to see the progress in the use of different materials in relation to certain properties, and that is using the property charts. Material property charts, like those proposed by Ashby, possess certain properties on the abscissa axis and on the ordinate axis. Many combinations are possible [Tab. 2.1], but there are obvious incentives for seeking materials with greater strength and, frequently, with greater stiffness. Recently, a combination of high strength and stiffness at a low weight is very sought after, especially in the transportation and aerospace industry as direct drivers. In order to show the qualitative development in the use of materials, we include some Ashby charts “strength–density” for three successive points in historical time [Fig. 2.2]. These charts are very useful for visually identifying peculiar features of materials and often highlight issues hardly anticipated by more canonical methods of investigation.

In prehistory, the materials we know cover only a small fraction of strength–density space. But with the Roman empire, around the time of Augustus, there was a great expansion of the knowledge of metals, with a significant filling of the chart. Until the Renaissance, the materials used did not vary much from those used by the Romans. In the following centuries we have the discoveries of cast iron and later aluminum. Around the middle of the 20th century, the metals envelope has expanded considerably and we note a new envelope of synthetic polymers which occupy an important position. Between then and the present day, the expansion has been dramatic [Fig. 2.3].

There are a large amount of materials known today, but it is equally clear that the materials we know do not possess some features. Indeed, observing some of today’s charts, we realize that large parts of the space are populated with materials, but other parts are

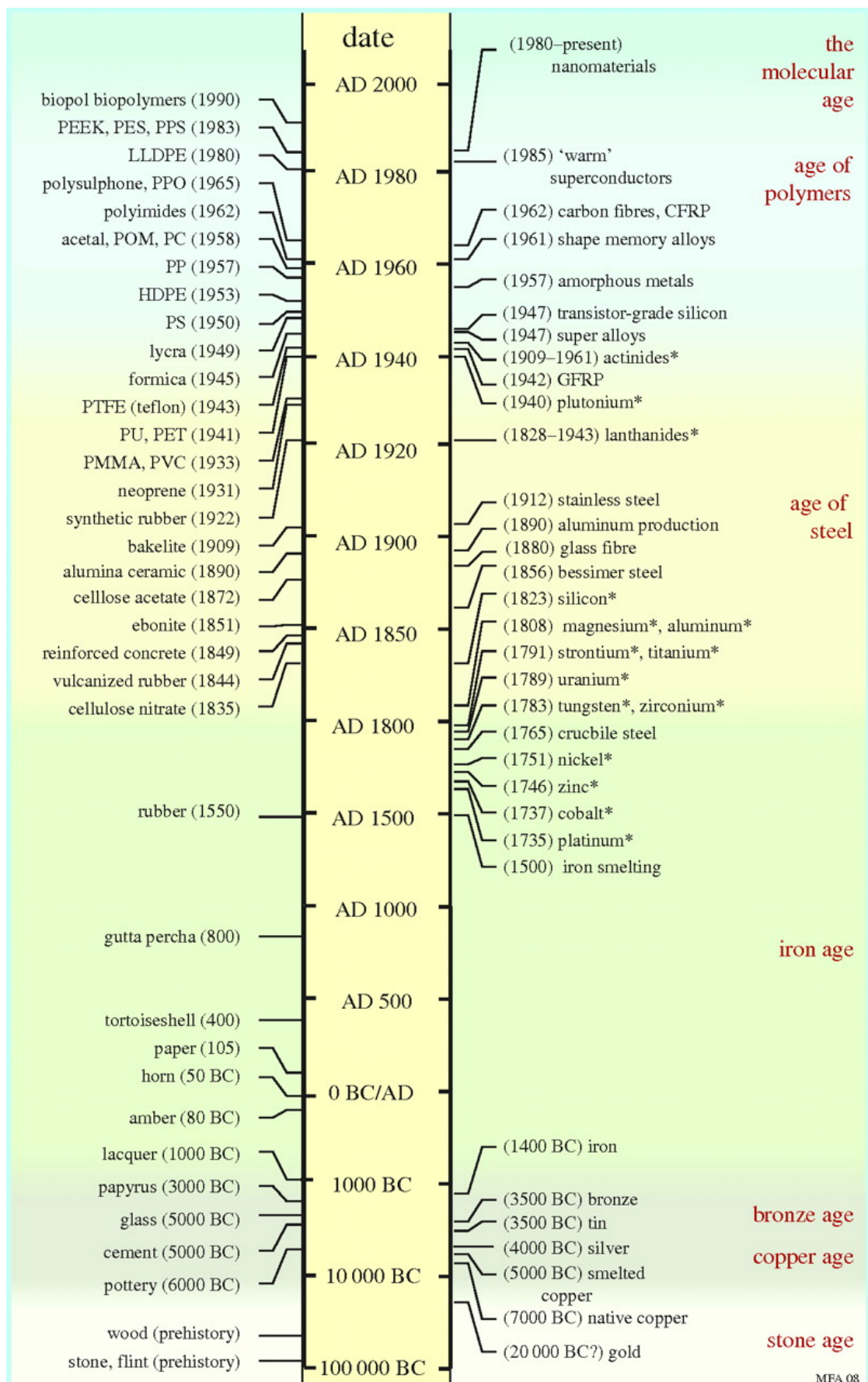
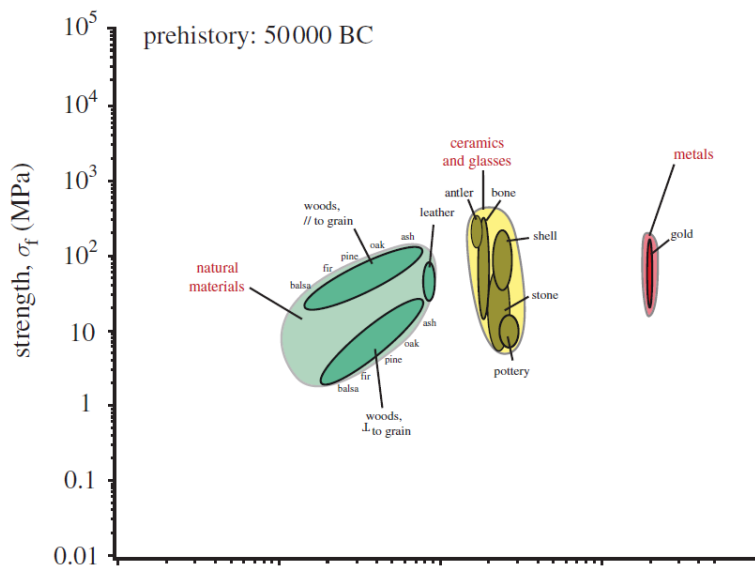
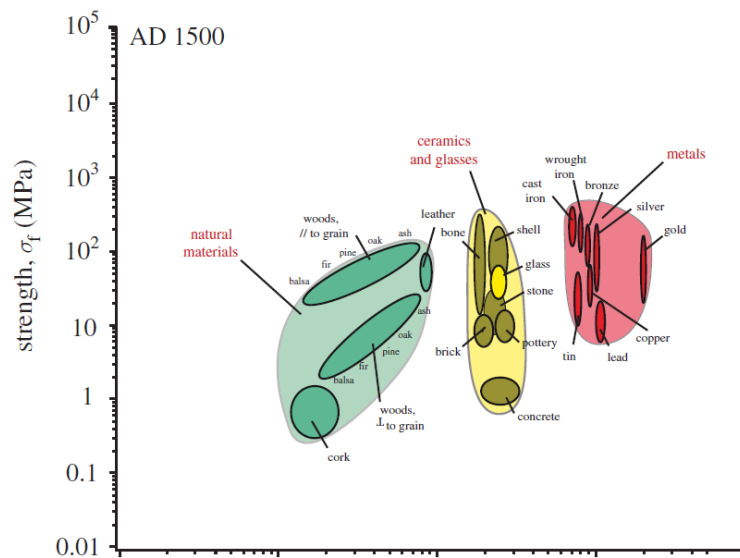


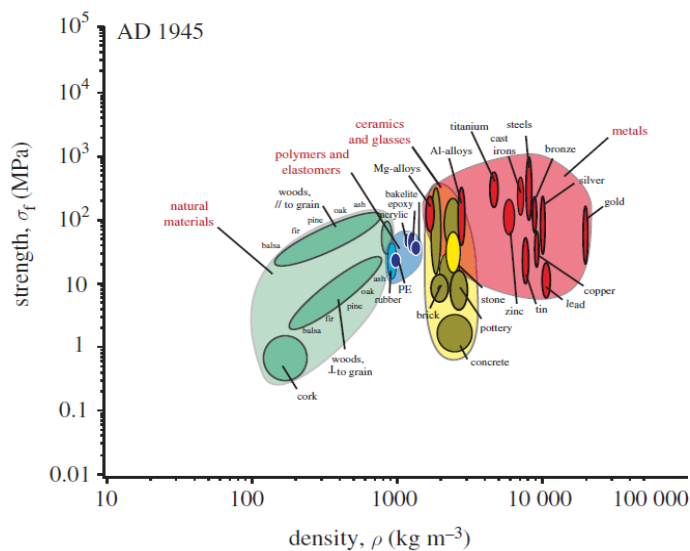
Figure 2.1: Materials time-line. The scale is nonlinear with big steps at the bottom, small ones at the top. Figures taken from [6].



(a)



(b)



(c)

Figure 2.2: Progressive filling of the charts in time. Figures taken from [6].

Table 2.1: Some properties for Ashby charts.

General	Mechanical	Thermal	Electrical
Price	Moduli	Melting Point	Conductivity
Density	Yield strength	Specific heat	Dielectric constant
Embodied energy	Tensile strength	Thermal conductivity	Dielectric strength
Carbon footprint	Hardness	Expansion coefficient	Loss coefficient
	Elongation		
	Fatigue strength		
	Fracture strength		
	Damping coefficient		

not: there are holes.

Some holes, or a part of them, are inaccessible for fundamental reasons, but others are simply empty and in principle they could be filled [50]. We notice that an ideal material with high stiffness and low density would naturally be in the top-left corner and a poor material would be in the bottom-right corner. What kind of materials can fulfill the need of low weight and high strength or stiffness?

- One approach to filling empty spaces in material property charts consist in creating new materials, developing new metal alloys, new polymer formulations and new compositions of glass and ceramic, which will extend the populated areas of the special maps.
- Another approach is that of manipulating microstructure, using thermo-mechanical processing to control the distribution of phases and defects of materials.
- A third approach is to combine two or more existing materials to create hybrids. The great success of composites (e.g. carbon and glass fiber reinforced), at one extreme, and of synthetic cellular materials, at another (hybrids of material and void space), in filling the previously empty areas of the property chart is an encouragement to explore ways in which such hybrids can be designed.

The first two approaches have been explored systematically leaving little room for further gains, while the third has led to the development of very promising materials: the so-called *architected materials*. [Fig. 2.4] illustrates some examples. The basic idea is to optimize of binomial material-geometry in order to obtain materials with better combinations of properties.

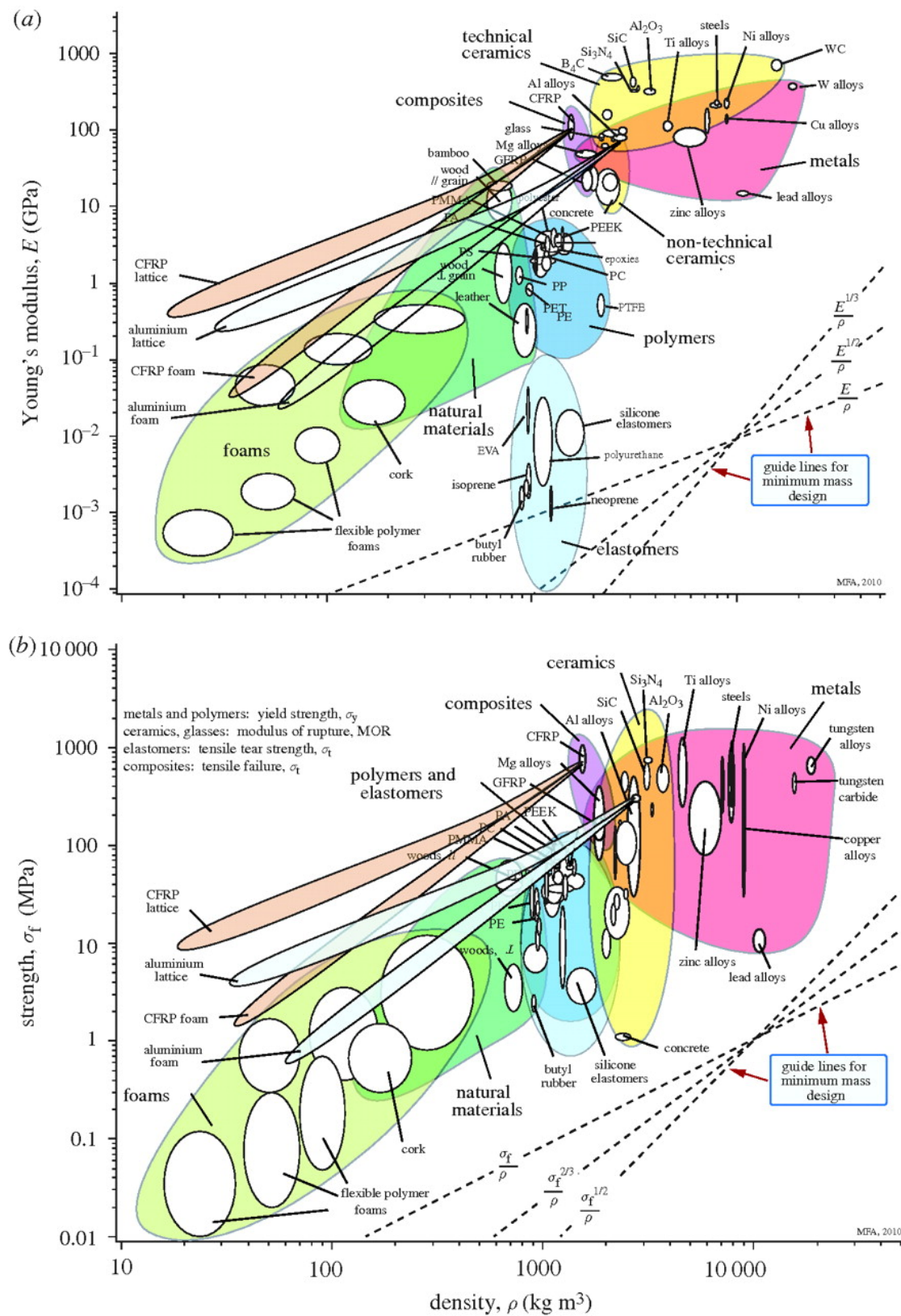


Figure 2.3: Stiffness-density chart and strength-density chart.

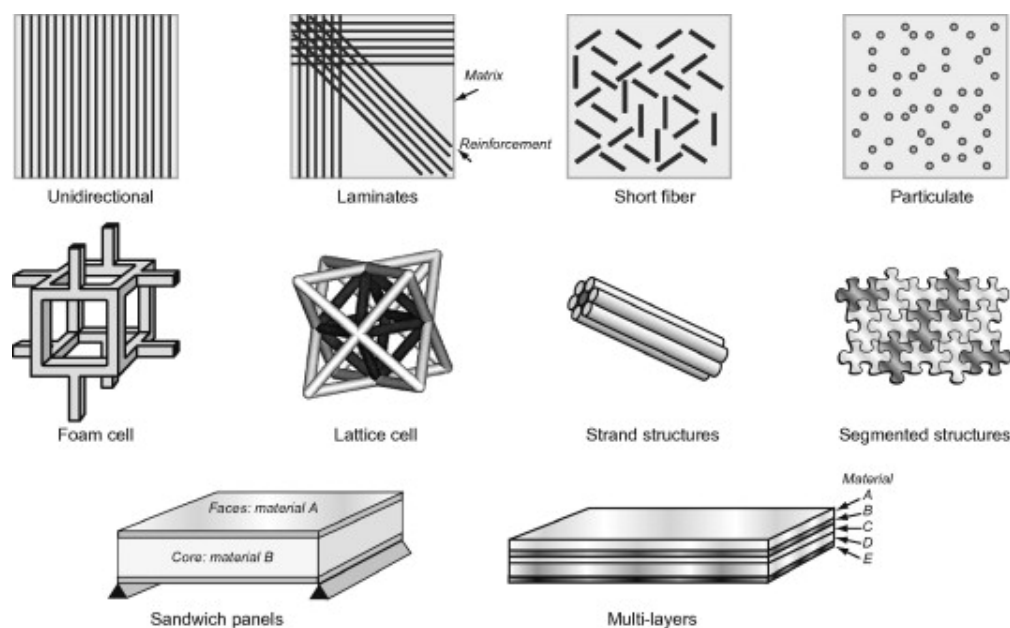


Figure 2.4: Some of the best known architected materials. Figure taken from [8].

## 2.2 Initial considerations

By the terms *cellular material* we mean an assemblage of cells made of solid edges or faces, joined together in order to fill the space [13]. They are commonly found in nature; some examples would be bones [Fig. 2.6], wood [Fig. 2.5], sponge [Fig. 2.7] or coral. They are an important class of engineering materials, but generally neglected. They are produced in enormous scale and, including wood, their business is comparable with that of glass industry. However they are less studied and less understood than any other class of material. In this chapter we will examine them closely.

### Short classification

Generally cellular materials can be divided into two families:

- *foams*
- *lattice materials* or most commonly *lattices*

Foams are characterized by a stochastic disposition of unit cells as it is shown in [Fig. 2.10], while lattice materials are constituted by periodic repetition of a single cell or a group of cells [Fig. 2.11]. Furthermore, cellular materials can be 2D or 3D. For a 2D, the unit cell is repeated in a 2D plane and is infinitely extruded in the perpendicular plane [Fig. 2.8]; for a 3D cellular material, the unit cell is tessellated in three perpendicular

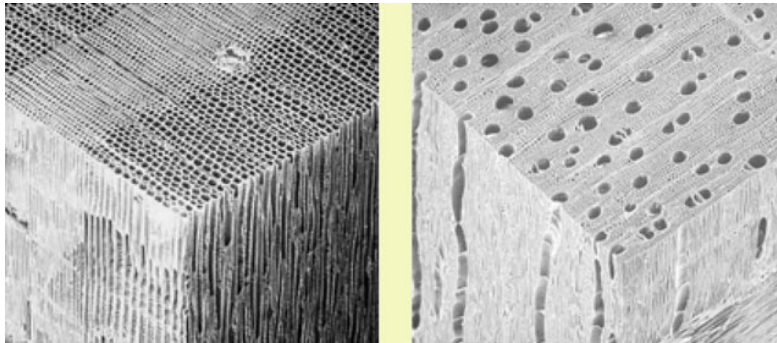


Figure 2.5: Microscopic vision of wood. Figure taken from [87].

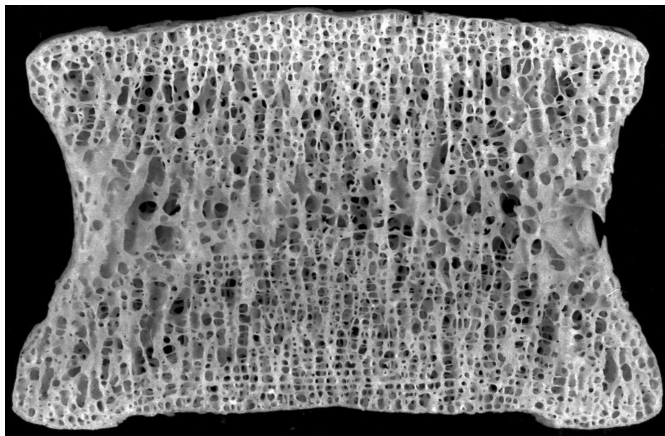


Figure 2.6: Microscopic vision of bone. Figure taken from [88].

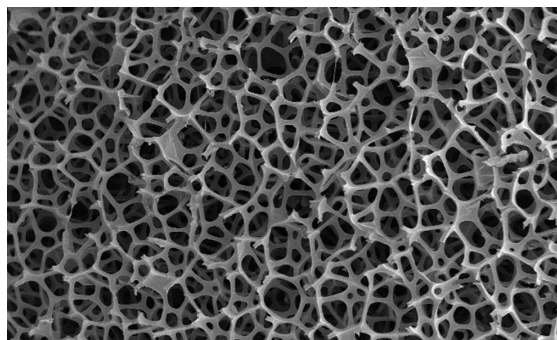


Figure 2.7: Microscopic vision of sponge. Figure taken from [89].

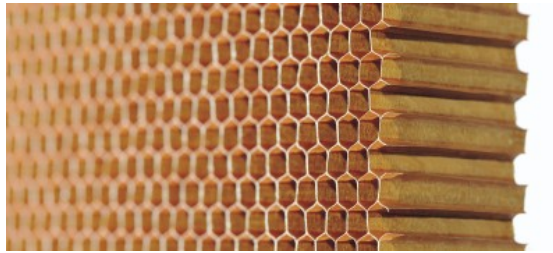


Figure 2.8: 2D extruded honeycomb. Figure taken from [90].

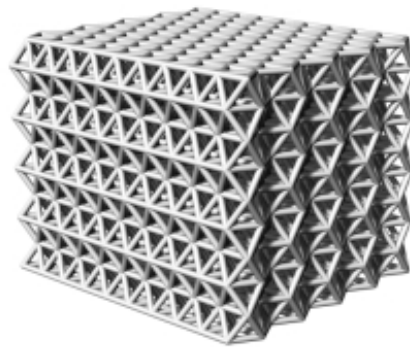


Figure 2.9: 3D lattice. Figure taken from [97].

directions [Fig. 2.9].

In the case of 3D cellular materials, cell-covering provides another distinction: so we define cellular material with *open-cell* if each unit cell is composed of struts and cellular material with *closed-cell* if it is composed of a pockets.

### The current use of cellular materials

Lattice materials have led to a change in material perspective from a structural to a multifunctional point of view. For instance, besides providing superior structural properties about weight, these micro-architected materials can offer multifunctional properties besides high specific stiffness and strength. We report some examples:

**Packaging** The essence of protective packaging is the ability to convert kinetic energy into some other sort of energy via plasticity, visco-elasticity or friction, keeping the peak force under the threshold therefore avoiding damages. The package should be able to convert the energy of the impact in a different direction. See [Fig. 2.12] for the comparison between an elastic solid material and a cellular material made of the same material of the solid. The figure shows clearly the better performance of a cellular material. Nowadays, foams are widely used for that kind of application.

foams@aber.ac.uk

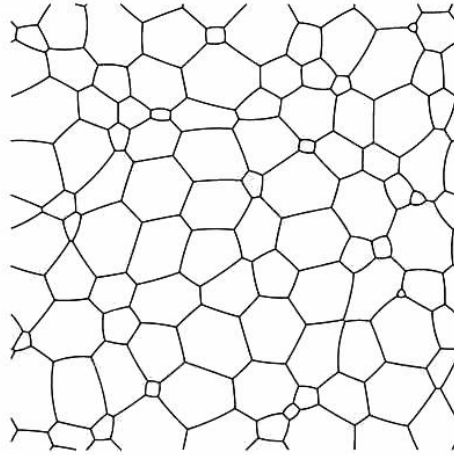


Figure 2.10: Example of cell distribution in a foam. Figure taken from [91].

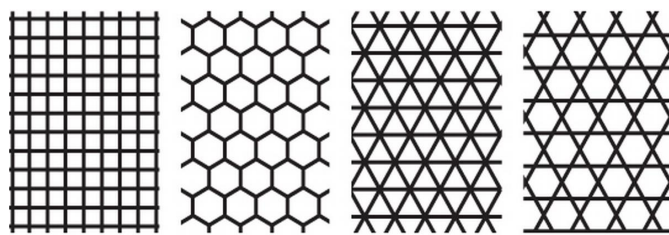


Figure 2.11: Example of cell distribution in a lattice. Figure taken from [10].

**Thermal insulation** Today thermal insulation is the most common use of cellular materials. In particular closed-cell foams have the lowest thermal conductivity than conventional non-vacuum insulation. Many factors contribute to decrease thermal conductivity:

- the low fraction of solid phase,
- the smallness of the cell which avoids convection and also radiation through absorption and reflection at the cell wall,
- poor conductivity of internal gas.

This feature is very useful for several purposes, for example in the insulation for liquid oxygen rocket tanks, in frozen food industry for refrigerated trucks or railway car, in the transport of liquefied gas around the world in tankers lined with foam etc. Furthermore, the thermal expansion coefficient is the same of the solid material which they are made of, but with smaller moduli and, for this reason, they have a good thermal-shock resistance. Their use as heat shields or ablative coatings is thus explained.

**Buoyancy** Already Pliny the Elder (Roman author, naturalist and admiral of Vespasian navy) in his work *Naturalis Historia* describes the use of cork as fishing float. Today plastic lattices are used in this field because they do not corrode and also they retain buoyancy when extensively damaged.

**Acoustic cloaking** It is proved that, enveloping an object with a particular type of foam, this is cloaked from acoustic field. When insulated with this cloaking material, the object no more alters the acoustic pressure field and hence seems invisible.

**Negative Poisson's ratio** The effective material properties not only depend on the relative density, but also on the geometry of the unit cell. For example, the hex-chiral lattice shown in [Fig. 2.14] possesses negative Poisson's ratio and therefore expands in transverse direction when put in traction in a longitudinal direction.

**Effective zero coefficient of thermal expansion** As this material is heated homogeneously, the relative distance between the nodes remains same. This is achieved by suitably contrasting the coefficient of thermal expansion of inner member materials with outer member materials.

**Seismic isolation systems** In [11] the author proposes the use of a particular lattice called *Pentamode* [Fig. 2.13] in order to reduce the effects of seismic waves on the structure. Pentamode lattices are artificial structural crystals showing shear moduli markedly smaller than the bulk modulus. Such systems have, from a mechanical standpoint, zero

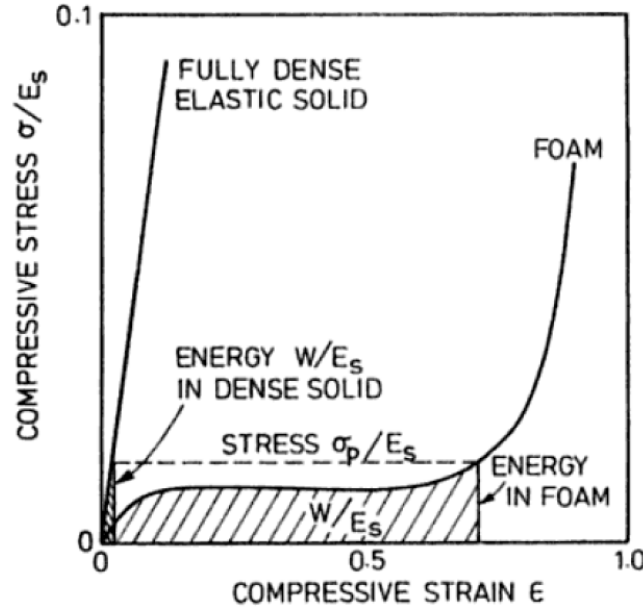


Figure 2.12: Comparison between energy absorption in an elastic solid material and in a foam made of the same material. Figure taken from [13].

or nearly zero shear moduli (five soft modes and only one stiff mode, that is volumetric deformation). This feature is very useful when you need to dampen the horizontal waves of an earthquakes in order to avoid a collapse of the building. The development of this technology could lead to a replacement of the existing dampers.

## 2.3 Mechanical overview

### 2.3.1 Relative density

The most important feature of a cellular solid is its *relative density*  $\bar{\rho}$  [14]:

$$\bar{\rho} = \frac{\tilde{\rho}}{\rho_s} \quad (2.1)$$

where  $\tilde{\rho}$  is the density of cellular solid and  $\rho_s$  is the density of solid of which it is made. Cellular materials resemble frameworks when relative density is less than 0.2. The relative density is directly related to the thickness  $t$  and length  $l$  of the a strut, in according to:

$$\bar{\rho} = A \left( \frac{t}{l} \right) \quad (2.2)$$

for 2D cellular solid.  $A$  is a constant that depends on geometry. As just mentioned, a three dimensional lattice or foam can be either open-cell or closed-cell. Open-cell microstructures comprise a three dimensional disposition of interconnected struts and have

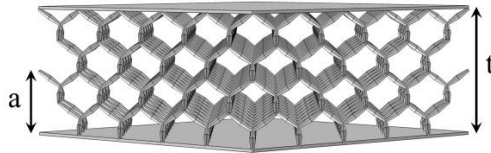


Figure 2.13: Pentamode lattice. Figure taken from [11].

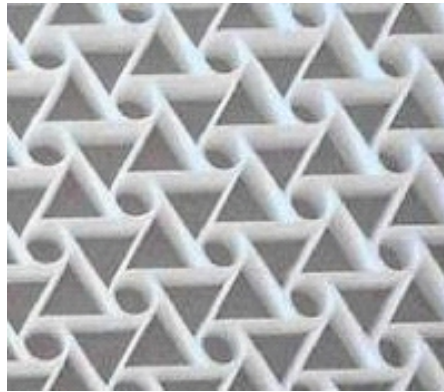


Figure 2.14: Lattice with negative Poisson's ratio. Figure taken from [95].

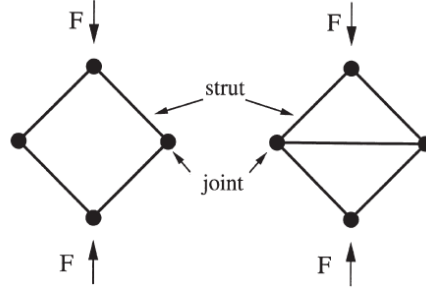


Figure 2.15: Cell to the left collapses due to mechanism. Cell to the right does not collapse. Figure taken from [14].

the property that  $\bar{\rho}$  scales with  $(t/l)^2$ , instead, closed-cell microstructures with plate-like cell faces of thickness  $t$  and side length  $l$ , are characterized by a relative density which scales with  $t/l$ . In general artificial closed-cell microstructures have thicker edges than faces so the relative density is similar to the same feature of an open-cell microstructure.

### 2.3.2 Stretching-dominated and bending-dominated

Consider the pin-jointed frames shown in [Fig. 2.15] to the left. The considered frame is a *mechanism*. It is simple to observe that, when loaded, the struts rotate about the joints causing the frame to collapse because there are neither stiffness nor strength. Conversely, the triangulated frame shown in [Fig. 2.15] to the right is a structure where, when loaded, the struts indeed support axial loads going in compression or in traction. The deformation is *stretching-dominated* and the frame collapses by the stretching of the struts. What if we block the rotations at nodes? For the first frame, the applied load induces bending moments at the blocked joints, and this leads the struts to bend, this is why, this kind of structure is called *bending-dominated*. However, for the triangulated structure the condition of block has no effect on the macroscopic stiffness or strength; although the struts bend, the frame is still stretching-dominated and the collapse load is dictated mainly by the axial strength of the struts. At constant relative density, stretching-dominated frames are 10 times stiffer and 3 times more resistant than structures bending-dominated ones.

### Bending-dominated

Consider the cellular solid as sketched in [Fig. 2.16]. The material behaves as linear elastic at the first stage, hence may collapse in three different ways:

- plastic yielding,
- elastic buckling,
- brittle crushing.

After the collapse, the structure continues to deform with constant stress till the so-called *densification*. This phenomenon involves a great growth of stress with little strain. Roughly, we could say that the cellular material is crushed and internal voids tend to cancel, creating a sort of solid material.

In this part we are going to show that relative density can be easily related to the mechanical properties of cellular materials. Imagine a cell loaded at the edges by forces  $F$  [Fig. 2.17]. We know the deflection of the struts at the center line  $\delta$  has the following relation:

$$\delta \propto \frac{FL^3}{E_s I} \quad (2.3)$$

where  $L$  is the length of the cell edge,  $E_s$  is the Young's modulus of solid material of which the cell is made and  $I$  is the moment of inertia equal to  $t^4/12$ . The compressive strain to which is subject the cell meets:

$$\epsilon \propto \frac{2\delta}{L}. \quad (2.4)$$

Since  $F \propto \sigma L^2$  and  $\sigma = \tilde{E}\epsilon$ , where  $\tilde{E}$  is Young's modulus of cellular material, assembling the previous results:

$$\boxed{\frac{\tilde{E}}{E_s} \propto \left(\frac{\tilde{\rho}}{\rho_s}\right)^2.}$$

The same approach is used in order to define the failure strength  $\tilde{\sigma}_p$ . The cell walls yield when the force exerted on them exceeds their fully plastic moment, i.e.

$$M_p = \left(\frac{\sigma_y t^3}{4}\right) \quad (2.5)$$

where  $\sigma_y$  is the yield strength of solid material. Knowing that  $M \propto \sigma L^3$  we can write:

$$\boxed{\frac{\tilde{\sigma}_p}{\sigma_y} \propto \left(\frac{\tilde{\rho}}{\rho_s}\right)^{3/2}.}$$

Frequently, elastomeric materials fail because of elastic buckling. Since the Eulerian buckling load is:

$$F_b \propto \frac{E_s I}{L^2} \quad (2.6)$$

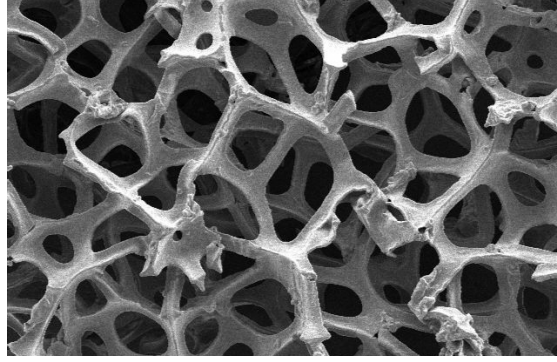


Figure 2.16: Bending-dominated foam. Figure taken from [50].

the stress  $\tilde{\sigma}_b$  responsible of elastic buckling is:

$$\tilde{\sigma}_b \propto E_s \left( \frac{\tilde{\rho}}{\rho_s} \right)^2.$$

Another type of failure is brittle collapse for which it is:

$$\frac{\tilde{\sigma}_{cr}}{\sigma_R} \propto \left( \frac{\tilde{\rho}}{\rho_s} \right)^{3/2}$$

where  $\tilde{\sigma}_{cr}$  is the stress of crushing, whereas  $\sigma_R$  is the stress of rupture of a struts.

### Stretching-dominated

The line of thought used to give an insight on stretching-dominated structure is similar to the one used in the previous paragraph 2.3.2. Consider the tensile loading of the material. The relation between elastic moduli and densities is given by:

$$\frac{\tilde{E}}{E_s} \propto \left( \frac{\tilde{\rho}}{\rho_s} \right).$$

Comparing this results with the ratio of Young's moduli for bending-dominated, it is evident the greater stiffness of stretching-dominated material. When the elastic limit is reached, the structure meets plastic yielding, buckling or fracture. Elastic limit, in terms of stress, follows this relation:

$$\frac{\tilde{\sigma}_p}{\sigma_y} \propto \left( \frac{\tilde{\rho}}{\rho_s} \right).$$

In the same way, we can identify the buckling strength:

$$\frac{\tilde{\sigma}_b}{E_s} \propto \left( \frac{\tilde{\rho}}{\rho_s} \right)^2.$$

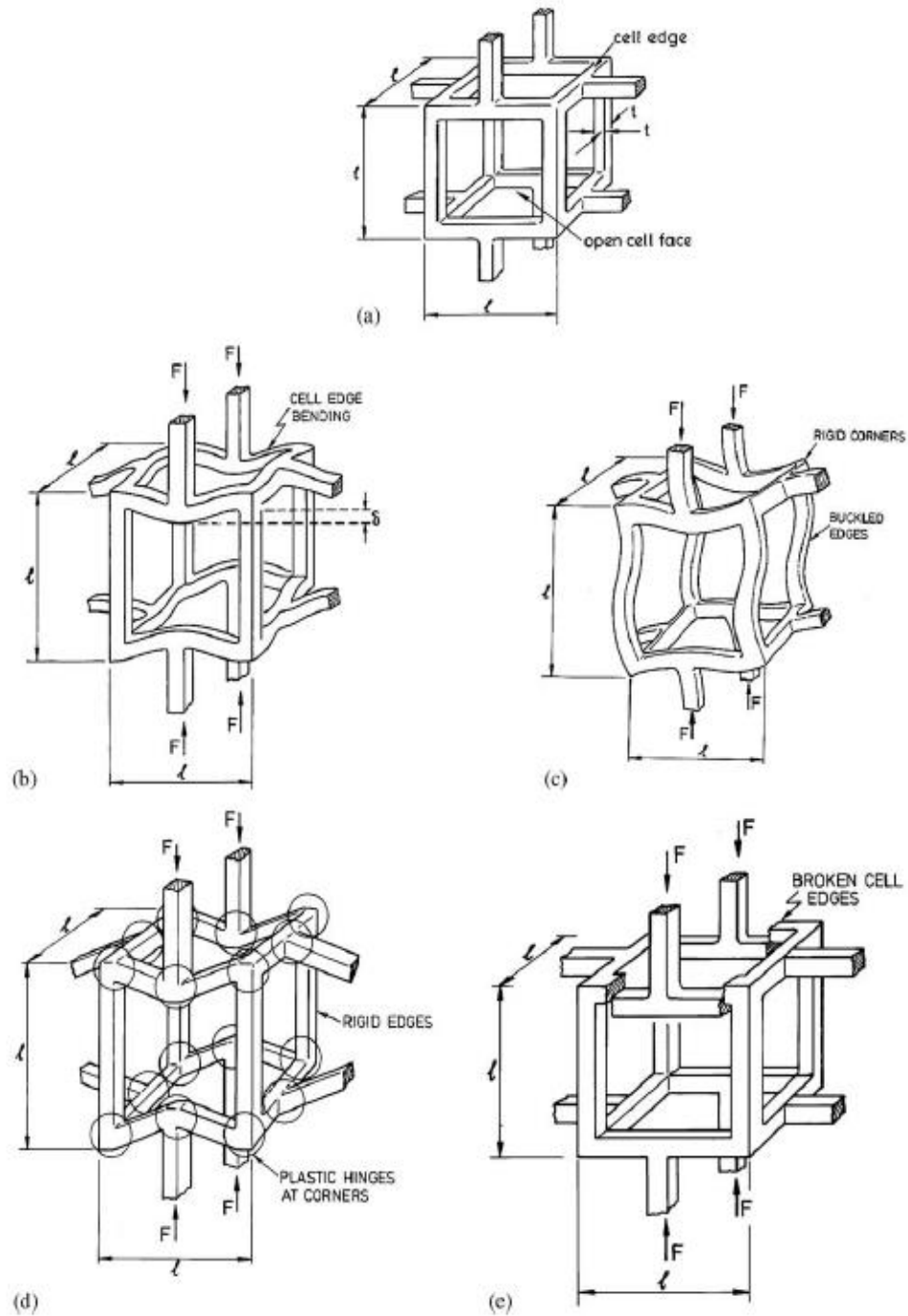


Figure 2.17: Where: (a) is undeformed cell (b) is linear elastic strut bending. Cell collapse by (c) elastic buckling (d) plastic yielding (e) brittle crushing. Figures taken from [13].

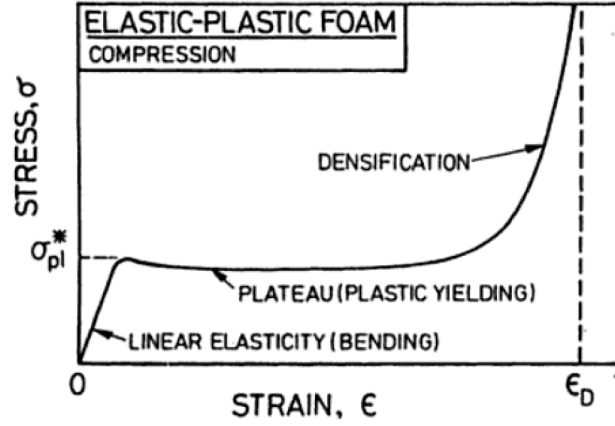


Figure 2.18: Stress–strain curve for a bending-dominated structure. Figure taken from [13].

In this case, the ratio between densities is squared; indeed, buckling depends on the slenderness of struts, i.e.  $t/l$ , which is linked to densities (2.2). The fracture strength, typical for ceramic materials, scale as:

$$\frac{\tilde{\sigma}_{cr}}{\sigma_R} \propto \left( \frac{\tilde{\rho}}{\rho_s} \right)^2.$$

There are many tables in the literature that estimate (from empirical data) the coefficients of proportionality for the formulations above. These results are clear because they show that both the modulus and initial collapse strength of a stretching-dominated material are much greater than those of a bending-dominated one with the same relative density. Observing the figures [Fig. 2.18] and [Fig. 2.19], we note that stretching-dominated structures are more profitable in order to reach the aim of low weight and high stiffness and strength, conversely they have lower performance in energy absorption due primarily to shortness of plateau stress.

The theory linked to 2.3.2 is borrowed from [50].

### 2.3.3 Stretching- or bending-dominated?

#### Maxwell's rule

An arrangement of pin-jointed struts becomes a rigid structure when it is statically and kinematically determinate. Note that a structure is statically determinate if the equilibrium equations can determine the internal member deflections. Kinematic determinacy of a pin jointed frame implies that the position of any joint relative to another joint could be determined purely in terms of individual strut lengths. For a finite pin-jointed lattice in space, the necessary conditions for kinematic and static determinacy, were first given by J. C. Maxwell [34] in the mid-nineteenth century. Maxwell analyzed a pin-jointed

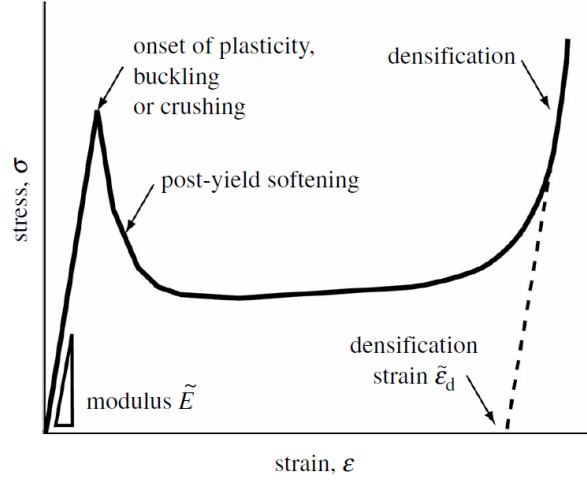


Figure 2.19: Stress-strain curve for a stretching-dominated structure. Figure taken from [13].

frame (hinged at its corners) made up of  $b$  struts and  $j$  frictionless joints. He showed that a two-dimensional statically and kinematically determinate frame has the property that:

$$M = b + 2j + 3 = 0 \quad (2.7)$$

and in 3D:

$$M = b + 3j + 6 = 0. \quad (2.8)$$

Two hundred years after that, 3D relation is generalized by C.R. Calladine as:

$$M = b + 3j + 6 = s - m \quad (2.9)$$

where  $s$  and  $m$  are the states of self-stress and mechanisms, respectively. Each can be determined by finding the rank of the equilibrium matrix describing the frame in a full structural analysis as follow from studies made by C. R. Calladine and S. Pellegrino.

If  $M < 0$  the frame is a mechanism; it has one or more degrees of freedom and in these directions allows displacements so it has no stiffness or strength. Therefore, the blocking of the nodes generates a bending-dominated structure. If  $M = 0$  the frame ceases to be a mechanism and, if it is loaded, its members are subject to tension or compression, so can be classified as stretching-dominated structure. If  $M > 0$  the frame is characterized by self-stress state.

That is valid for finite frameworks, but cellular material is made of several cells, so now we proceed to analyze the rigidity criteria of infinite frameworks. Consider a large pin-jointed framework with an average connectivity (number of struts at a node)  $Z$ . The total number of struts  $b$  in the framework is  $< jZ/2$ . From the Maxwell's criterion we get that the necessary condition for rigidity is  $Z = 4$  in the 2D case and  $Z = 6$  in the 3D case.

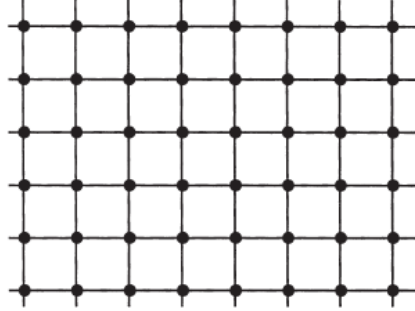


Figure 2.20:  $Z=4$ , presence of mechanisms. Figure taken from [50].

We can observe that, as in the case of finite frameworks, the condition above is not sufficient. In fact, the framework drawn in [Fig. 2.20] has  $Z = 4$  (Maxwell's rule is satisfied) but admits one mechanism and one state of self stress. Conversely, the framework drawn in [Fig. 2.21] has still an average connectivity of four but does not possess mechanism or self-stress state. Detailed information can be found in [14].

The nature of Maxwell's criterion as a necessary rather than sufficient condition gives insight into the design of lattice materials, and reveals why foams are almost always bending-dominated. Since our objective is the study of materials with high strength and stiffness, this thesis will continue considering preponderantly lattice materials.

## 2.4 Effective material properties of lattice material

The characterization seen previously for bending- and stretching-dominated structure represents a good way to approach the mechanical behavior of cellular material and gives us an easy physical insight, but its implementation is difficult for a lattice having a complex unit cell and cannot serve as an efficient way of comparing various new topologies based on their structural capabilities. Effective material properties can be tools of comparison for an engineer, allowing him to confront structural properties of different topologies in order to choose the optimum lattice topology for a specific loading condition. Three main methods are used to derive effective material properties:

- *Finite element approach (FEA)*. Direct computation using the Finite Element approach requires building a finite element model of lattice and applying convenient

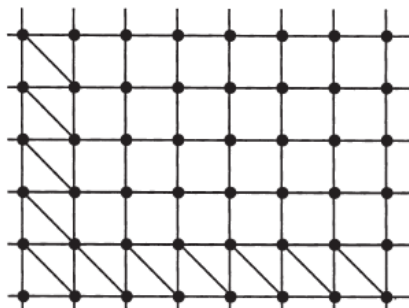


Figure 2.21:  $Z=4$ , absence of mechanisms. Figure taken from [50].

boundary conditions in order to simulate uni-axial tension and pure shear conditions. Through stress and strain measures from these tests, it is possible to estimate the effective material properties of lattice materials.

In their famous paper [32], Wallach and Gibson managed to predict the effective material properties and shear modulus of a 3D octet lattice (a particular type of lattice). Though it is relatively simple to build a finite element model, the method has disadvantages linked to an accurate judgment of boundary conditions to capture the global effects (which are not so immediate) and high computational cost for large lattice. Furthermore, anisotropy is a problem when cumbersome finite element computations have to be repeated multiple times in order to deduce strain tensor and stress tensor.

- *Homogenization method.* In order to deduce the effective material properties, the lattice is seen as an effective continuum; therefore, the size of the unit cell should be much more smaller than the macroscopic size of the material as a whole. This is a necessary condition to avoid size effects. Literature about homogenization is very rich. The homogenization method was applied by Chen et al. [33] by equating the strain energy of a discrete structure to the strain energy of an equivalent micropolar continuum. However, their model gives moduli that are too large (i. e. the structure is too stiff), as reported by Fleck and Qui [35]. Kumar et al. [46] have recently used homogenization method by taking terms until second order derivatives in the Taylor series expansion for displacements and rotations. However, their model cannot be employed for lattices such as in Kagome and Hexagonal honey-

comb. Gonella et al. [47] have incorporated higher order terms in the Taylor series expansion and have used their model to predict the wave-bearing characteristics of lattice materials pertaining to the lower branches of the dispersion curves. However, their model shows the same restriction on the choice of unit cell as [46], which limits its functionality.

- *Wave-based dynamic method (WDM)*. This approach has been shown in [48] using the theory of Timoshenko to find the effective moduli of infinite Triangular, Hexagonal, Square and Kagome lattices. Numerical results agree with the analytical predictions. Phani et al. have employed this approach to predict the wave bearing characteristics of the lattice materials through the so-called *dispersion curves*. Their approach essentially uses *Floquet-Bloch* formalism to take advantage from the repeatability of the unit cell and finite element analysis. It is true that the Wave-based dynamic method requires only the finite element modeling of a unit cell becoming computationally efficient and, because of this, it could be employed also for complex isotropic lattice topology. However, their model is limited to effective property estimation of isotropic topologies.

### 2.4.1 Homogenization method

#### Preliminary concepts

As the amount of articles and books shows, the homogenization method is the most used and studied. The principle of homogenization, which makes it easier to calculate the properties of a composite material, is particularly interesting.

The characteristics of microstructure of a lattice structure control the macroscopic characteristics. The main goal of the homogenization approach is to derive effective mechanical properties (elastic modulus, yield strength, strength) from the microstructure. This concept can be applied to periodic lattice structures; indeed, lattice structure can be thought as a heterogeneous material made of solid material and voids. In order to explain the relationship between macroscopic mechanical properties and microscopic characteristics, several methods have been proposed. We propose the discrete homogenization approach by [49] since it can be applied to lattice structures made of any structural elements, which can be modeled using finite element analysis. Moreover the analysis in [49] is very clear and intuitive. The approach is based on multi-scale analysis. There are two different length scales:

- (a) the length scale of a unit cell as microscopic scale,
- (b) the length scale of a lattice part as macroscopic scale.

As already mentioned, the dimension of a unit cell is much smaller than the dimension of the whole lattice structure. We introduce periodic direction vectors defined as quantity at the microscopic scale, which represents periodic directions and periodic lengths of unit cells. For the characteristic quantity at macro scale, the macroscopic strain tensor is se-

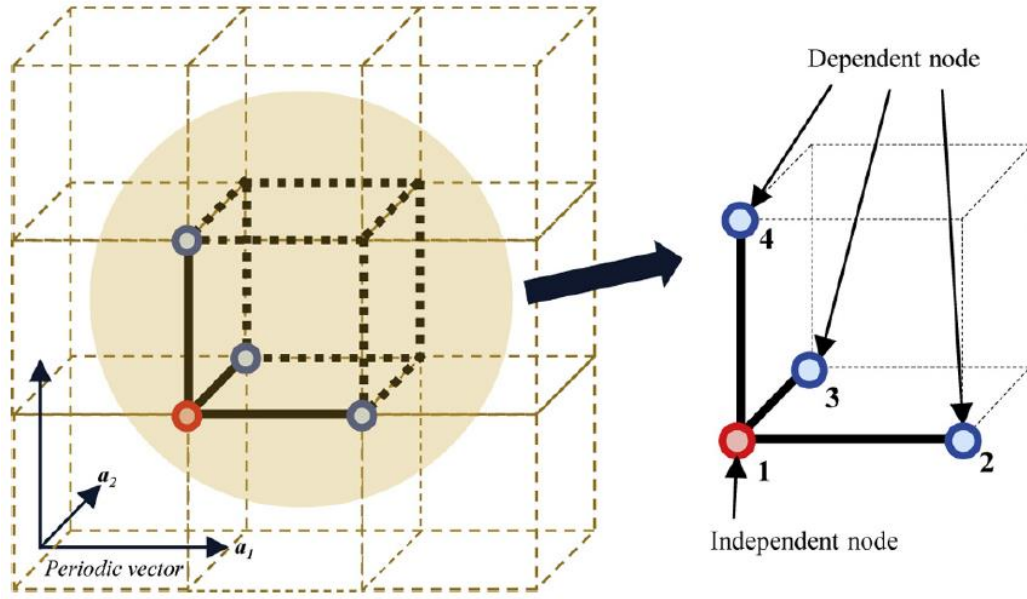


Figure 2.22: Example of representative unit cell. In this case a cubic unit cell.

lected, which describes the deformation of the lattice structure. The cardinal principle of the method we are going to illustrate is the equation between macroscopic strain energy after deformation (due to a given macroscopic strain field) and the microscopic strain energy of a *representative unit cell* (due to changes in periodic direction vectors after deformation). This way, the homogenized mechanical properties are often determined in terms of strut diameter and strut length by comparing the macroscopic and microscopic strain energy.

### Approach

Since a lattice structure is made of several unit cells located periodically, the position and displacement can be expressed through a representative unit cell [Fig. 2.22]. The representative unit cell is a unit cell which does not have duplicated edges along the periodic direction. Two classes of nodes in a unit cell are defined: the *internal nodes* connecting elements of a given unit cell and the *boundary nodes* that link elements of confining cells. Due to periodicity, we observe that the boundary nodes must correspond along the periodic vectors; it can be concluded then that a subset of the unit cell nodes is sufficient to generate all the nodes of the lattice. These *independent nodes* comprise the internal nodes (which do not have a corresponding node in the unit cell) and a selection of boundary nodes. When the representative unit cell is repeated in the  $X$ ,  $Y$ , and  $Z$  directions, a lattice structure is created. For simplicity, consider the cell in [Fig. 2.22].

The position of arbitrary nodes in the lattice structure is represented as follows:

$$\mathbf{r}_k = \mathbf{r}_0 + n_i \mathbf{a}_i \quad i = 1, 2, 3 \quad n_i \in \mathbb{N} \quad (2.10)$$

where

- $\mathbf{r}_0$  is a position vector of the independent node,
- $n_i$  is an integer multiplier,
- $\mathbf{a}_i$  is a periodic direction vector which defines the size of unit cell.

The subscript  $k$  indexes the nodes in the unit cell and subscript  $i$  generates repeated unit cells. Under a uniform macroscopic stress, an infinite lattice gets deformed while keeping its periodicity. If  $\mathbf{r}_k$  represents the undeformed situation and

$$\mathbf{r}'_k = \mathbf{r}'_0 + n_i \mathbf{a}'_i \quad i = 1, 2, 3 \quad n_i \in \mathbb{N} \quad (2.11)$$

the deformed situation, it is possible, by subtracting  $\mathbf{r}'_k$  to  $\mathbf{r}_k$ , to write the nodal displacement as

$$\mathbf{u}_k = \mathbf{u}_0 + n_i \Delta \mathbf{a}_i \quad i = 1, 2, 3 \quad n_i \in \mathbb{N} \quad (2.12)$$

where  $\mathbf{u}_0$  is the displacement vector of the independent node and  $\Delta \mathbf{a}_i$  the change in periodic vectors from their undeformed configuration to deformed configuration. We collect all nodal degrees of freedom (DOFs) of a unit cell in an array defined as:

$$\mathbf{d} = \begin{bmatrix} \mathbf{d}_1 \\ \mathbf{d}_2 \\ \vdots \\ \mathbf{d}_k \end{bmatrix} \quad (2.13)$$

where  $\mathbf{d}_k$  is the  $kth$  nodal DOFs including translation and rotation

$$\mathbf{d}_k = \begin{bmatrix} u_k & v_k & w_k & \theta_{xk} & \theta_{yk} & \theta_{zk} \end{bmatrix} \quad (2.14)$$

so that  $\mathbf{d}$  is a  $k \times 6$  matrix. In the same way, the collection of independent nodal DOFs  $\mathbf{d}_0$  is defined. The nodal DOFs  $\mathbf{d}$  are represented in terms of independent nodal DOFs and periodic vectors as

$$\mathbf{d} = \mathbf{B}_0 \mathbf{d}_0 + \mathbf{B}_a \Delta \mathbf{a} \quad (2.15)$$

$\mathbf{B}_0$  expresses the dependencies between the nodes of the unit cell in relation to the periodic vectors; it has as many row blocks as the number of nodes of the unit cell and as many column blocks as the numbers of independent nodes; for each row only one column block is non zero; the blocks are identity matrices of the size of the number of DOFs for

each node.

$\mathbf{B}_a$  expresses the relative displacements between corresponding boundary nodes of the unit cells, as a function of the change in the periodic vectors; it has as many row blocks as the number of nodes of the unit cell and many column blocks as the number of independent periodic vectors; the blocks are signed in order to consider negative translations. The next step is to formulate the static equilibrium expression for the periodic lattice structure using the finite element analysis technique. In the deformed configuration, the internal forces of any cell of the lattice must balance the forces applied by the surrounding cells. In the linear case, the nodal forces of the unit cell can be written as

$$\mathbf{F}_{uc} = \mathbf{K}_{uc}\mathbf{d} \quad (2.16)$$

where  $\mathbf{K}_{uc}$  is the unconstrained stiffness matrix for the unit cell and  $\mathbf{F}_{uc}$  is the nodal force vector. In the deformed configuration, the resultant force applied by surrounding edges at each node must be null. Due to the periodicity of lattice structure, the equilibrium equation can be represented by nodal forces in the unit cell using  $\mathbf{B}_0$  which describes the periodicity in the unit cell

$$\mathbf{B}_0^T \mathbf{F}_{uc} = \mathbf{B}_0^T \mathbf{K}_{uc} \mathbf{d} = 0. \quad (2.17)$$

Inserting (2.15) in (2.17) we obtain

$$\mathbf{B}_0^T \mathbf{K}_{uc} \mathbf{B}_0 \mathbf{d}_0 = -\mathbf{B}_0^T \mathbf{K}_{uc} \mathbf{B}_a \Delta \mathbf{a} = 0 \quad (2.18)$$

Since the unconstrained stiffness matrix is singular, the equation cannot be solved directly. Then we use the *pseudo-inverse technique* indicated with  $(-)^+$ :

$$\mathbf{d}_0 = -(\mathbf{B}_0^T \mathbf{K}_{uc} \mathbf{B}_0)^+ \mathbf{B}_0^T \mathbf{K}_{uc} \mathbf{B}_a \Delta \mathbf{a} = \mathbf{D}_0 \Delta \mathbf{a}. \quad (2.19)$$

After substituting (2.19) into (2.15), the nodal DOFs are calculated as

$$\mathbf{d} = (\mathbf{B}_0 \mathbf{D}_0 + \mathbf{B}_a) \Delta \mathbf{a} = \mathbf{D}_a \Delta \mathbf{a}. \quad (2.20)$$

The strain energy stored in a unit cell after deformation is

$$W = \frac{1}{2} \mathbf{d}^T \mathbf{K}_{uc} \mathbf{d} = \frac{1}{2} \Delta \mathbf{a}^T \mathbf{D}_a^T \mathbf{K}_{uc} \mathbf{D}_a \Delta \mathbf{a} = \frac{1}{2} \Delta \mathbf{a}^T \mathbf{K}_{\Delta a} \Delta \mathbf{a} \quad (2.21)$$

It is necessary to write the deformation work as a function of the components of a uniform macroscopic strain field acting on the lattice. The changes in periodic vectors can be evaluated using the macroscopic strain field as below:

$$\Delta \mathbf{a} = \epsilon_M \mathbf{a} \quad (2.22)$$

where  $\epsilon_M$  is the Cauchy strain tensor. It is possible to group the equations for all periodic vectors as

$$\Delta \mathbf{a} = \mathbf{B}_\epsilon \epsilon_M = \begin{bmatrix} a_{1x} & 0 & 0 & \frac{a_{1y}}{2} & 0 & \frac{a_{1z}}{2} \\ 0 & a_{1y} & 0 & \frac{a_{1x}}{2} & \frac{a_{1z}}{2} & 0 \\ 0 & 0 & a_{1z} & 0 & \frac{a_{1y}}{2} & \frac{a_{1x}}{2} \\ a_{2x} & 0 & 0 & \frac{a_{2y}}{2} & 0 & \frac{a_{2z}}{2} \\ 0 & a_{2y} & 0 & \frac{a_{2x}}{2} & \frac{a_{2z}}{2} & 0 \\ 0 & 0 & a_{2z} & 0 & \frac{a_{2y}}{2} & \frac{a_{2x}}{2} \\ a_{3x} & 0 & 0 & \frac{a_{3y}}{2} & 0 & \frac{a_{3z}}{2} \\ 0 & a_{3y} & 0 & \frac{a_{3x}}{2} & \frac{a_{3z}}{2} & 0 \\ 0 & 0 & a_{3z} & 0 & \frac{a_{3y}}{2} & \frac{a_{3x}}{2} \end{bmatrix} \begin{bmatrix} \epsilon_x \\ \epsilon_y \\ \epsilon_z \\ \gamma_{yz} \\ \gamma_{zx} \\ \gamma_{xy} \end{bmatrix} \quad (2.23)$$

where  $B_\epsilon$  is the macroscopic strain. Substituting (2.23) into Eqs. (2.21) and (2.20) we get

$$\mathbf{d} = \mathbf{D}_a \mathbf{B}_\epsilon \epsilon_M = \mathbf{D}_\epsilon \epsilon_M \quad (2.24)$$

$$W = \frac{1}{2} \epsilon_M^T \mathbf{B}_\epsilon^T \mathbf{K}_{\Delta a} \mathbf{B}_\epsilon \epsilon_M. \quad (2.25)$$

Since the material stiffness is equal to the Hessian of the strain energy with respect to the deformation components, then

$$\mathbf{K}_\epsilon = \frac{1}{V} \mathbf{B}_\epsilon^T \mathbf{K}_{\Delta a} \mathbf{B}_\epsilon \quad (2.26)$$

where  $V$  is the volume of a unit cell. The elastic modulus can be extracted by inverting of the stiffness matrix.

### Internal forces and buckling

It is possible to model the single elements using Euler-Bernoulli theory. Following [53] we can write:

(i) the edge stretching  $s$

$$s = \frac{u_2 - u_1}{L} \quad (2.27)$$

where  $u_1$  and  $u_2$  are the displacements of the ends along the element axis;

(ii) the curvatures ( $\chi_y$ ,  $\chi_z$ ) around the axes perpendicular to the element axis  $x$

$$\chi_y = x \left( 12 \frac{w_1 - w_2}{L^3} - 6 \frac{\theta_{y1} - \theta_{y2}}{L^2} \right) + 6 \frac{w_2 - w_1}{L^2} + 2 \frac{2\theta_{y1} - \theta_{y2}}{L} \quad (2.28)$$

$$\chi_z = x \left( 12 \frac{v_1 - v_2}{L^3} + 6 \frac{\theta_{z1} - \theta_{z2}}{L^2} \right) + 6 \frac{v_2 - v_1}{L^2} - 2 \frac{2\theta_{z1} - \theta_{z2}}{L} \quad (2.29)$$

where  $v_1$  and  $v_2$  are the displacements of the ends in  $y$  direction and  $w_1$  and  $w_2$  in  $z$  direction;  $\theta_{y1}$  and  $\theta_{y2}$  are the rotations of the ends around  $y$ -axis and  $\theta_{z1}$  and  $\theta_{z2}$  are

the rotations of the ends around  $z$ -axis;  $x$  can vary from 0 to  $L$ ;

(iii) the angle of twist  $\phi$

$$\phi = \theta_{x2} - \theta_{x1} \quad (2.30)$$

where  $\theta_{x2}$  and  $\theta_{x1}$  are the rotations around  $x$ -axis.

Then, we can calculate:

(i) the normal force

$$N = E_s A s \quad (2.31)$$

(ii) the bending moments

$$M_y = E_s I_{zz} \chi_y \quad M_z = E_s I_{yy} \chi_z \quad (2.32)$$

(iii) the torsion moment

$$T = \frac{G_s J_p \phi}{L} \quad (2.33)$$

where  $E_s$  is the elastic modulus of solid material,  $G_s$  is the shear modulus of solid material,  $A$  is the cross sectional area,  $I_{ii}$  are the moment of inertia and  $J_p$  is the polar moment of inertia.

If we want to know when the buckling occurs, we have to resolve

$$(\mathbf{K} + \lambda \mathbf{K}_\sigma) \mathbf{x} = 0 \quad (2.34)$$

where  $\mathbf{K}$  and  $\mathbf{K}_\sigma$  are the stiffness matrix and the stress stiffness matrix of the structure [54]. The smallest eigenvalue is the multiplying factor of the applied stress which provokes buckling of the cell elements.

## 2.5 Manufacturing of cellular materials

Due to the required intricate internal geometry, manufacturing a component with cellular structure is nearly impossible with traditional subtractive process. That is why the researchers have turned to other technologies such as additive manufacturing, forming, molding and joining as means of producing this class of material.

### 2.5.1 Stochastic cellular structures

Having a random distribution of pores throughout, foams are produced by introducing a bubbling agent to the metal during the solidification transition. Foam manufacturing methods are classified into three groups: sinterization, direct foaming and indirect foaming via a precursor.

The first method consists in sintering powders which are either loosely compacted or have a filler material that disintegrates during sintering operation [Fig. 2.23]. These foams can be net-shaped and can be created from a wide variety of materials. The remaining methods are used especially to manufacture metallic foams. Direct foaming [Fig. 2.24] of metallic melts can be accomplished in one way among these three:

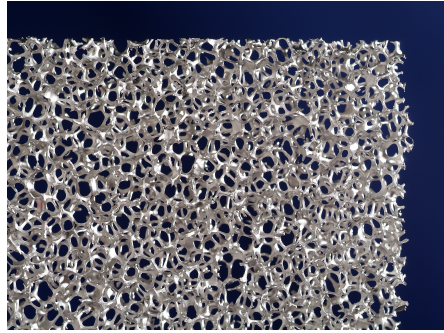


Figure 2.23: Foam made by sinterization. Figure taken from [92].

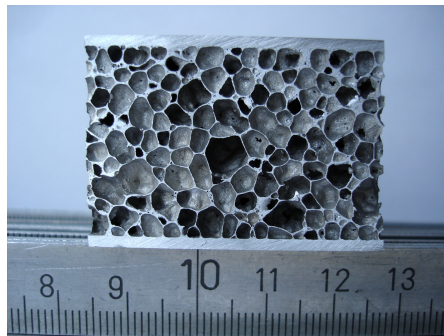


Figure 2.24: Foam made by direct foaming. Figure taken from [93].

- Injection of gas into the liquid metal from an external source.
- Injection of gas blowing agents into the molten metal to cause the formation of gas.
- Preparation of supersaturated metal-gas systems under high pressure.

While direct foaming techniques can only create foams in bulk, net-shaped parts can be molded using indirect techniques. Indirect foaming of metals is accomplished by mixing metal powders with a blowing agent, by compacting the mix and by foaming the compact by melting. A very comprehensive book which deals with the issue is undoubtedly [16].

### 2.5.2 Ordered cellular structures

Though ordered cellular structures are more difficult and expensive to manufacture than stochastic structures, this class of structures offers a repeatable part quality through careful (and often tedious) construction of the cellular structure.

#### **Honeycombs via crimping or stamping**

This process involves stamping or crimping thin sheets of metal into a corrugated shape and then joining them to create ordered cellular structures [Fig. 2.25]. Very frequently, these structures consist of periodically repeating hexagonal cells, even if the possibility of having different topologies of the cell is being studied. Typically, thin but strong skins are bonded to the lightweight honeycomb core to create sandwiches that should address to structural applications. Although this cost-effective process creates strong and lightweight structure, a significant issue is the inability for the designer to project the macrostructure. Moreover, the process of crimping and stamping is limited to uniform, hexagonal, cellular structures. Frequently, other cell shapes offer superior strength and stiffness and it may be desirable to manufacture cellular structures with variable cell sizes and topologies for specific applications. Furthermore, there are difficulties with manufacturing the cellular sandwiches into complex, non-planar shapes due to induced anticlastic property.

#### **Lattice materials**

These truss structures are created by specialized casting techniques. Jamcorp [62] produces their lattice block materials using sand casting techniques. Chiras and al. have employed rapid prototyping to create truss structure patterns for an investment casting process with Beryllium copper alloy [63]. This process is considered costlier and has poor results in structures that contain significant casting porosity (partly a consequence of the complex topology, which makes difficult continuous fluid access to the solidification interface). The use of a ductile Beryllium copper casting alloy compensates for these faults, but not for the high cost and weight.

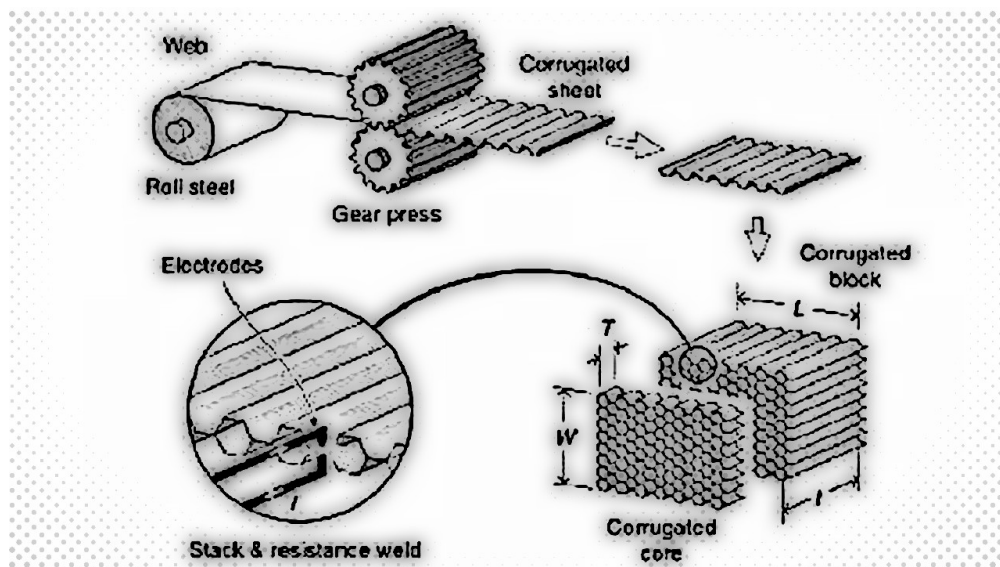


Figure 2.25: Process of crimping and stamping. Wang (2005).

### 2.5.3 Problem of the current cellular material manufacturing

From a high level of abstraction, four severe limitations are predominant in the cellular material manufacturing processes just mentioned:

- *non-repeatable results* some procedures create cellular structures where voids are distributed randomly (foams); as a result, part quality is not consistent;
- *limited materials* current techniques can draw from a limited selection of working materials;
- *limited topology of structure* many cellular manufacturing techniques cannot predict the morphology of the pores, or can only produce one certain pore size or shape;
- *limited part geometry* current techniques are unable to produce cellular structures for any three dimensional geometry.

The capabilities of the individual processes are presented in [Tab. 2.2].

As can be observed in [Tab. 2.2], no single process satisfies all the requirements of an ideal cellular material manufacturing process. These limitations are representative of the overall lack of designer freedom offered by these different manufacturing techniques. The largest limitation of stochastic cellular structures is the complete lack of control that a designer has over the topology, the size and the shape of the unit cell. Although these techniques offer a cost-effective way of lowering density, they do not provide repeatable and predictable results. Generally it can be noted that these processes are extremely difficult to control and therefore cannot be improved through process optimization. By

Table 2.2: Designer freedom offered by various cellular material production techniques.

Type	Process	Repeatable	Material Freedom	Cell structure Freedom	Macrostructure Freedom
Foams	Sinterization		✓		✓
	Direct foaming				
	Indirect foaming				✓
Lattice	Crimping & Stamping	✓	✓		
	Casting techniques	✓			

comparing the two classes of cellular materials, we can notice that foams are inexpensive, but place material in locations where it contributes little to the achievement of material properties. Lattice materials, on the other hand, can be produced through several, for the most part, costly techniques. They can be designed to optimize multifunctionality by placing material at locations where mechanical and other favorable characteristics are simultaneously maximized. While it is true that ordered cellular materials offer a designer more control over material placement, the existing manufacturing techniques constrain the designer to a predetermined cell structure, material type, and macrostructure. Such limitations prevent a designer from creating an ideal cell structure for the multiple design. Between the four limitations listed, the inability to create unlimited cell structure is, perhaps, the most debilitating. If the key benefit of using cellular materials is increased part strength maintaining a low mass (or another parameter), a designer will desire to have complete control over the placement of material and the determination of proper cell topology for the specific product intent.

#### 2.5.4 3D printing for lattice materials

Before starting this part you should read chapter 3. As mentioned before, the design of lattices is the subject of optimization techniques (often topological), whereas foams are hard to optimize. Our goal is to present a way to manufacture a cellular material previously optimized so we consider only lattice material. For this purpose, we seek a way to overcome the limitations seen in 2.5.3.

#### Overcoming limitations

Contrary to traditional manufacturing technologies which create objects through the subtraction of material from a work piece, 3D printing creates parts through the successive addition of material layer-by-layer. Due to this approach, 3D printing processes offer the utmost geometrical freedom in the design and manufacture of an artifact. As such, some researchers have looked into using 3D printing techniques for the production of cellular materials.

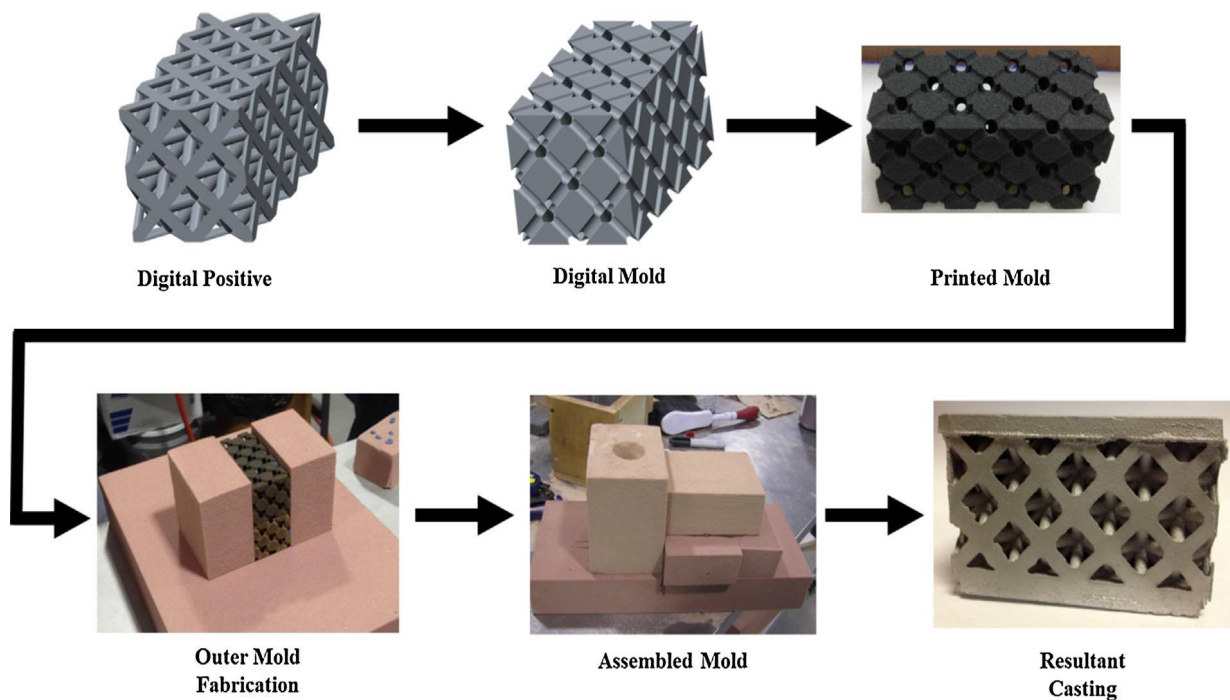


Figure 2.26: Manufacturing process for creating cellular castings - from digital mold to resultant casting. Figure taken from [9].

There are many commercial 3D printing technologies, each having their own principal solution (from the use UV laser and photopolymer resin to precisely extruding a heated plastic filament), but each has a goal in common: the manufacturing of a part through successive deposition of material one cross-sectional layer at a time.

3D printing techniques have been employed in the past for the creation of truss structure patterns for the investment casting process used to make lattice block materials [Fig. 2.26]. This indirect process is not only expensive, but it limits as well the sizes of cells and trusses which can be created. The resulting structures are typically plagued by porosity due to the inability of the fluid to access all parts of the truss structure [63]. Furthermore, indirect processing places a constraint on the cell topologies which can be made, indeed only materials with interconnected cells are feasible. Consequently, the interest has moved on direct processes.

### Direct processes

Literature about 3D printing is fairly recent and mostly characterized by argumentative descriptions of various print jobs. If we add to 3D printing the theme of cellular materials, literature becomes quite limited. Nevertheless, there are some interesting papers. In general, observing the most cited papers, some very common techniques for 3D printing

Table 2.3: Designer freedom offered by various cellular material production techniques. Introduction of 3D printing.

Type	Process	Repeatable	Material Freedom	Cell structure Freedom	Macrostructure Freedom
Foams	Sinterization		✓		✓
	Direct foaming				
	Indirect foaming				✓
Lattice	Crimping & Stamping	✓	✓		
	Casting techniques	✓			
	3D printing (direct process)	✓	✓	✓	✓

of lattice materials are:

- Electron beam melting (EBM)
- Selective Laser Melting (SLM)
- Fused Deposition Modeling (FDM)
- Self-propagating Photopolymer Waveguides (SPPW)

In table [Tab. 2.3], similar to the first [Tab. 2.2], the improvement due to 3D printing is clear. In the following text, we will outline the techniques listed above, focusing particularly on critical aspects.

**Electron Beam Melting (EBM)** Electron Beam Melting uses an electron beam to join powder particles. The parts created by this process do not require additional thermal treatments and do not present porosity. The exclusive use of metal powder is a remarkable technical restriction of this process. Interestingly, building takes place in a vacuum, so a clear path for the electrons towards the power bed is created. The procedure is not cheap, but thanks to that, the parts do not suffer from impurities and have high strength properties. *Arcam*, the company which placed EBM technology on the market, states that a wide variety of metal powders can be processed with the EBM process, although they “initially chose to concentrate on the use of H13 tool steel alloys for tooling applications.”

When it comes to building an object through 3D printing, a significant issue arises: how to introduce an analytical model that interprets, in the best way, the behavior of the printed object [Fig. 2.27]. We analyze the case of a lattice materials produced through 3D printing, using [64] as a reference. The analytical model is linked to the study of a basic structure which makes up the cellular material, i.e. the unit cell.

A question which causes the divergence in behavior between the analytical model and

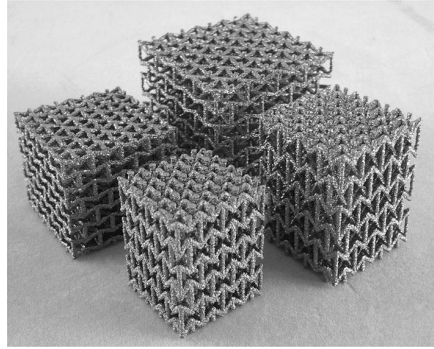


Figure 2.27: Example of printed lattice material made of Ti6Al4V. Figure taken from [64].

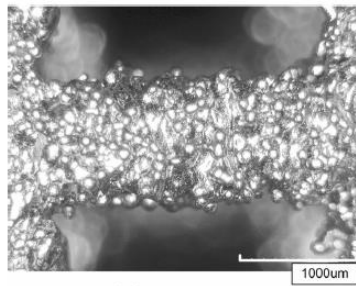


Figure 2.28: Surface sintering seen under the microscope. Figure taken from [64].

the real object is linked to the thermal dissipation during the fabrication process. This causes an important surface sintering of fabricated parts, which reduces the geometrical accuracy of the structures and creates microfractures. The surface roughness affects the precise determination of effective strut dimensions. In order to obtain a mechanically equivalent dimension, which could be employed in the mechanical property predictions in the analytical model, the minimum fully solid-sectional dimension was frequently used as the dimension of the struts [Fig. 2.28].

There is also an issue related to the realization of the cellular designs. Once the structure has been fabricated it can be noted that the thickness of the strut is greater than projected, while the length of the strut is lower than projected. [Fig. 2.29].

Another difficulty derives from *overheating*. [Fig. 2.30] shows an example of overheating. All three struts in [Fig. 2.30] were fabricated with the same process, i. e. with same

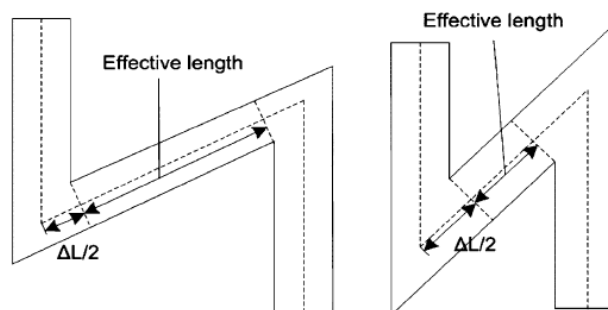


Figure 2.29: Problem linked to effective length of the strut. Figure taken from [64].

parameters and settings. However, since the diameter of the beam was around 0.1 mm, significant overheating occurred when, for instance, one decides to realize a strut with a diameter of 0.2 mm under the designed scanning strategy, thus leading to the deformation of the resulting structure. Certain thin features might not be manufacturable under certain process settings and an accurate thermal-mechanical analysis is necessary to characterize the effect of dimensions and scanning strategies on the quality of the parts.

Furthermore, in geometric modeling the material properties of cellular structures were assumed to be homogeneous, which is a very rough approximation. Indeed, we know that 3D printing processes introduce intrinsic anisotropy into the structure due, mainly, to the layered process. After all the correction factors for the problems cited above were considered and inserted in the analytical model, we can make a comparison between the analytical model predictions (made through the finite-element simulation) and the experimental results. In general, as shown in [64], the simulation results agree very well with the experimental results, which implies that the material properties of the cellular structure are consistent and predictable.

**Fused Deposition Modeling (FDM)** Fused Deposition Modeling uses a heating chamber to liquefy polymers. A polymeric filament is pushed into the chamber by a tractor wheel arrangement and, after the process of liquefaction, a new, partially-melted filament is pushed out. The main drawback in using this technology is the build speed. As mentioned earlier, the inertia of the plotting heads means that the maximum speeds and accelerations which can be obtained are certainly smaller than other systems (EBM,

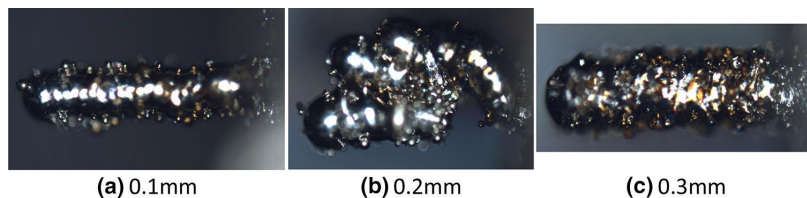


Figure 2.30: Overheating problem. Figure taken from [64].

SLM, SPPW). Furthermore, FDM requires material to be plotted in a point-wise way that involves many changes in direction.

We can use the FDM technology in three different ways in order to obtain lattice materials. The first way is undoubtedly the most common and also the one which was first studied. It consists in the realization of the so-called *structure woodpile* [Fig. 2.30]. Each strut corresponds to the deposition of the single filament, whereby the mechanical characterization of the printed object is strongly connected to the mechanical behavior of the filament itself and the mutual accession between the filaments. [65] includes a discussion on this matter.

The second way is to create 2D lattice material extruded in the third direction as we see in [Fig. 2.32] taken from [66], whereas the third method is definitely the one that arouses most interest for the construction of lattice optimized. Important in this regard is [67] which provides specimens of lattice materials [Fig. 2.33].

As the paper shows, some cellular lattices, fabricated by FDM, are tested in compression to obtain the elastic modulus and the collapse stress of the lattice. The strut diameter is measured in several points of each strut in order to compute the probability of the diameters. Then, finite element models based on a single beam and on the whole lattice specimen are developed to predict the elastic modulus and the collapse stress of the lattice. To do so, different models with variable and constant cross sections are generated using both beam and whole lattice models. The results show that, to obtain a good accuracy, it is necessary to model the cross section variations along the strut's length. It is also proved that the whole lattice model predicts a lower mechanical stress-strain curve than that by the beam model. It might be because of stress concentration at some regions. Finally, the stress-strain curves and deformed configurations obtained using beam and whole finite element models are compared with experimental findings. The

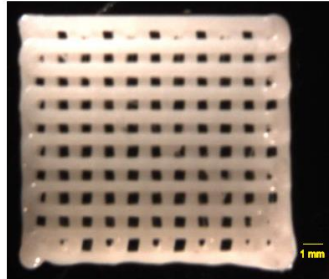


Figure 2.31: 3D Printed lattice material as structure woodpile. Figure taken from [65].

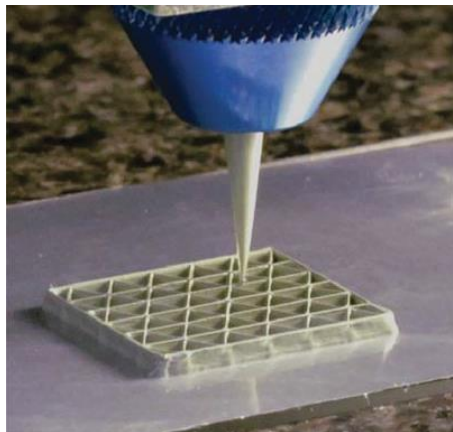


Figure 2.32: Optical image of 3D printing of a triangular honeycomb. Figure taken from [66].

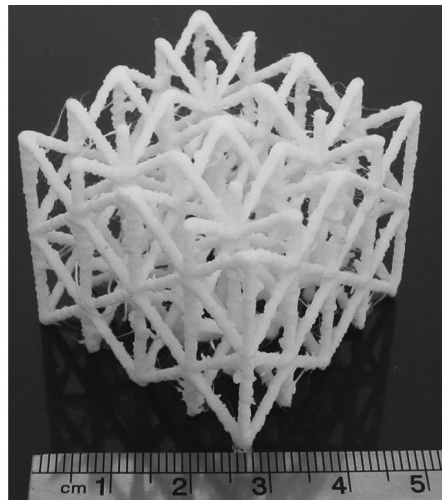


Figure 2.33: A PLA cellular lattice structure fabricated by FDM. Figure taken from [67].

results demonstrate that the whole lattice model is more accurate when each strut has a constant diameter along the length. However, the beam models are more computationally efficient, but require more intervals of different diameter along the length.

The techniques of fused deposition modeling are characterized by the use of plastic materials as low-melting. This is definitely a disadvantage; a possible remedy derives from developing new techniques using various types of plastic materials.

**Selective Laser Melting (SLM)** In Selective Laser Melting process, each layer of powder is molten by a high-energy laser beam. The laser can operate in both continuous and pulse mode. The continuous mode is characterized by a laser spot diameter of about 0.2 mm, while the diameter of the laser spot in the pulse mode is about 0.07 mm. The laser beam is directed onto the powder surface by means of scanning mirrors in order to define each layer of the powder. The powder deposition system consisted of a powder platform, and a coater, a tool which serves to deposit powder layers with thickness of about 0.03 mm in only one direction.

SLM is probably the most rapidly growing technique in 3D printing technologies; this is due to the possibility to create metal parts with complex shapes and intrinsic engineered characteristics. Furthermore, SLM can produce parts whose mechanical properties are comparable with those of components made with traditional processes. Most SLM literature focuses on the optimization of the technological process to obtain almost full density of parts and good mechanical properties of the bulk materials. More recently, the use of SLM has been extended to the fabrication of lattice structures ([68],[69],[70]). Technical literature does not present a lot of systematic investigations on properties of lattice structures in relation to different cell topologies, characterized by certain relative density, thermal dissipation and mechanical strength.

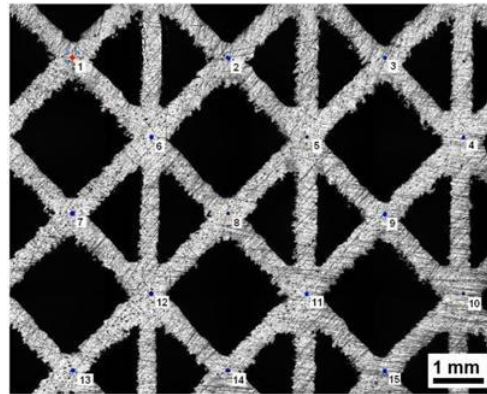


Figure 2.34: Truss thickness measured via microscope. Figure taken from [72].

An exception is represented by [72]. Said paper studies the feasibility of manufacturing lattice structures [Fig. 2.35] adopting SLM process and their properties has been studied. A Ti6Al4V powder was employed, because of its biocompatibility (very useful in medical field) and corrosion resistance. The results of the microscopic analysis demonstrate the great accuracy of the manufacturing process with a gap in model dimensions less than 0.05 mm (the different specimens have a side between 1.6 cm and 2.4 cm)[Fig. 2.34]. The layer fabrication leads to a certain dimensional variation at the level of the single cell, which can affect the effective relative density of the lattice structures in comparison with the designed porosity.

The roughness of the surface varying between a value of 0.006 - 0.015 mm is a difficulty that we encounter in the printed material; this is not negligible when you want to create a finite element model. The compression tests that were performed in order to evaluate the mechanical behavior under compression of the micro-lattice topology variants found that the carrying-load capability of the structure is affected by strut edge size and cell size and also that peak and collapse stress values increase almost linearly with relative density.

A similar paper, [71], considers another type of powder: 18Ni Marage 300 powder. The Selective Laser Melting (SLM) has evolved from the Selective Laser Sintering (SLM), from which it differs in two fundamental aspects: the type of powder employed and the mechanism by which alloy powder particles. In fact, the powder used by the SLM process is generally metallic, whereas in SLS process can also be plastic. The term *melting* is linked to the fact that the powder particles are fused to form the solid part, while *sintering* means that the particles do not melt, but they reach a temperature such that the outer part soften and burst sticking to the adjacent particles. Literature neglects the process mainly because of its poor mechanical properties compared to those found for the SLM.

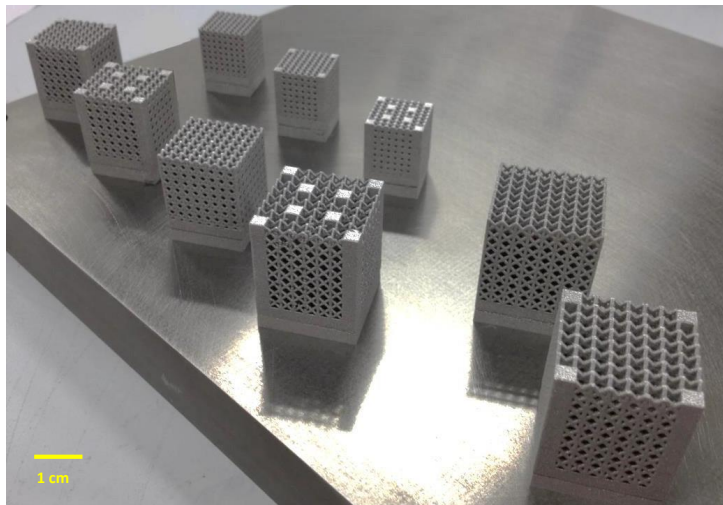


Figure 2.35: Samples on the building platform. Figure taken from [72].

**Self-Propagating Photopolymer Waveguides (SPPW)** This technology was created with the intent to overcome the shortcomings of more established 3D printing techniques. The major difficulties in traditional 3D printing process are related to the poor scalability and to the time necessary for printing.

The materials created by SPPW are formed by to ultraviolet rays a two dimensional mask with a pattern of holes covering a reservoir containing a particular photomonomer [Fig. 2.36]. UV rays, filtering through the openings, create thin beams which, at certain points, join beams generated by other rays. The chemical process that turns photomonomer in polymer, using the energy released by ultraviolet rays, is called *polymerization*. The post-processing step consists in the removal trough solvent-based or physically of the remaining resin. By simultaneously forming an interconnected array of these fibers in three dimensions and removing the uncured monomer 3D lattices open-cell are realized [Fig. 2.37]. In order to obtain certain architectural features, it is possible to control the fiber angle, diameter and three dimensional spatial location during fabrication.

In [74] and [73] strengths and weakness of this process are investigated. It is possible to fabricate open-cellular materials with lattice member diameters ranging from 0.01 mm to 1 mm with a relative density between 5% up to 30%. The overall material thicknesses can range from 0.01 mm to over 25 mm [Fig. 2.38]. The lattice member angle with respect to the exposure plane can be controlled between 50°-65° for intersecting waveguides; vertical members are also possible. When lattice member angles are greater than 70°, intersecting waveguides can pair off together to form a single propagating element. These variations in the lattice feature dimensions are made possible by changing mask features. In addition to the unit cell architectures, non-symmetric architectures, such as functionally graded materials, or hierarchical structures are also possible. This process is the only known fabrication approach that enables such flexibility and precision

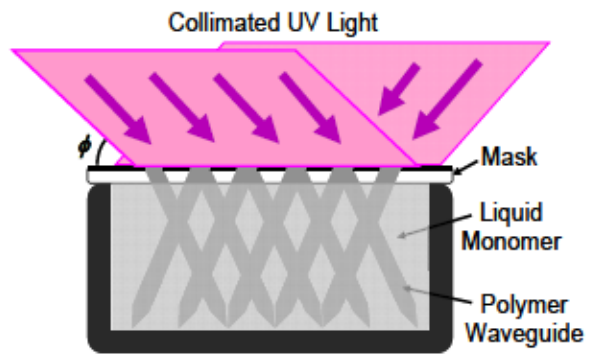


Figure 2.36: Schematic representation of the process used to form micro-lattice structure from a self-propagating polymer waveguides. Figure taken from [74].

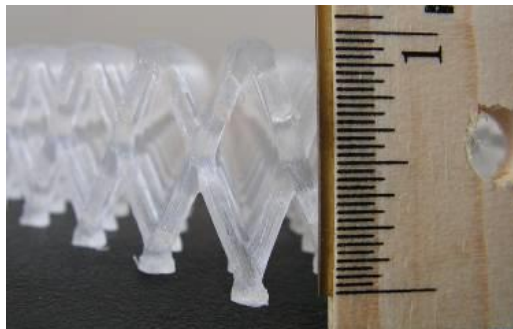


Figure 2.37: Example structure formed by this process. Figure taken from [74].

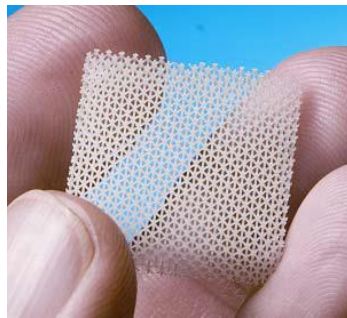


Figure 2.38: Demonstration of a significantly reduced size that can be achieved. Figure taken from [74].

of the material micro-architecture in combination with the potential for scalable, cost-effective manufacturing. The key distinction of this approach is its ability to fabricate a three-dimensional material from a single, two-dimensional exposure plane.

SPPW process is very similar to stereolithography. Unfortunately, unlike stereolithography, SPPW does not allow arbitrary shapes to be formed within the starting resin bath, but it has the potential to form a wide range of 3D polymer structures based on linear rod-type elements. The major advantage is in the speed with which polymerization can form the resulting 3D structure. For stereolithography, the elements within the structure are formed in a serial fashion (frequently stereolithography process can take many hours or days), while the optical waveguide process can form all rod-type or linear elements in the structure in parallel with a single exposure step (typically  $< 1$  minute). As already mentioned, another important feature characterizing SPPW is the scalability, that is the possibility to create lattice material with different dimensions.

Interestingly, the polymer is not fully cross-linked and can be shaped into complex curvatures. Even after curving the material in the desired manner and subjecting it to thermal post-cure procedure the micro-lattice structure will maintain this shape. The [Fig. 2.39] shows an anticlastic curvature which is not possible with conventional honeycomb cellular materials and difficult to achieve with stochastic foams.

The technique shown can be used to realize and control a wide variety of polymeric micro-truss structures. These micro-truss structures can also be used as templates to form other cellular materials. For example, the micro-truss structures can be converted to ceramic or metallic cellular materials using processes commonly applied to convert polymer foams. The ability to fabricate micro-truss structures of different materials together with the geometric flexibility of the process allow the engineers considerable flexibility in designing cellular structures with a wide range of mechanical and physical



Figure 2.39: Example of a micro-lattice structure with anticlastic curvature. Figure taken from [74].

properties.

## Chapter 3

# 3D printing

### 3.1 Introduction

The first experiments date back to the 1960s, but it was not until the mid-1980s that pioneers such as Scott Crump (who founded Stratasys) and Charles Hull (who founded 3D Systems) developed a range of technologies now known as *3D printing*. Their work was based on additive processes which created solid objects layer by layer. As these processes evolved, they became known as *Additive Manufacturing (AM)*. Because many AM methods were based on ink-jet printing technology, the term *3D printing* has been widely adopted by the industry and mass media to refer to any AM process. While the term Additive Manufacturing is very explanatory of the production process, we choose to use the term 3D printing because of its greater impact in conveying the image of an object built in three dimensions.

As many business experts say, 3D printing technology is *disruptive* because it seems to be cheaper, simpler and more convenient to use than traditional manufacturing technology. It is possible to say that current technology is good enough to serve markets that previously did not have manufacturing capability (e.g. small factories, hospitals, schools).

Obviously, a disruptive technology starts as inferior to the dominant technology of the time. When the first experimental 3D printers emerged about 30 years ago, the product quality was very far from that of the traditional production techniques. However, new techniques can find a niche in a market neglected by current technology. Therefore, 3D printing was placed at the service of rapid prototyping, which was an expensive process using traditional manufacturing techniques. Therefore it became possible to create cheap and high-quality prototypes, which in turn sped up product development. Afterwards, 3D printing started to be used to directly manufacture customized goods.

This new technique evolves rapidly, with practical examples in several industries including aerospace, automotive and health care. Although it has been applied mainly to small volume production, the products may be far superior — which means lighter, stronger,

custom-made, already assembled and cheaper — to those created with traditional manufacturing processes. That is because 3D printing can control exactly how materials are deposited, making it possible to create structures which could not be produced using conventional means.

Another disruptive element is certainly the fact that a single 3D printer can create different products. This is an advantage over traditional manufacturing methods, where the production line must be modified and tailored if the product is changed, requiring expensive investment in tooling and considerable downtime in the manufacturing process. It would be great to imagine a future factory that can manufacture automotive components or medical products all in the same facility via 3D printers.

The ability to build a wide range of products, coupled with the fact that 3D printing can be done closed to the point of consumption (amount of product required by consumers), will generate serious changes to supply chains and economic models. Many steps in the supply chain, like distribution, storage and retail, could potentially be eliminated. The economics of manufacturing will also change. Manufacturing is less labor-intensive, employs less material, produces less waste and can use new materials which are light and strong. Customization becomes very easy, starting new product strategies and customer relationships through collaboration with customers to create products.

Currently, and for the near future, 3D printing cannot produce finished products on an industrial scale. However, to dismiss the impact of 3D printing would be like ignoring the impending revolution (just as the minicomputer makers did when personal computers appeared).

## 3.2 Overview

### 3.2.1 Definition

3D printing or Additive Manufacturing is a process of making three dimensional solid objects from a digital file. The creation of a 3D printed object is attained using additive processes. In an additive process an object is created by laying down successive layers of material until the whole object is built. Each of these layers can be seen as a thin horizontal cross-section of the eventual object.

### 3.2.2 Printing process in 8 steps

Most 3D printing processes involve the following eight steps [20]:

**Step 1: Virtual model** It is necessary to start from a 3D model which describes the external geometry of the object. We can use professional CAD (Computer Aided Design as computer graphics software) or reverse engineering equipment (e.g. laser and optical scanning).

**Step 2: Conversion to .STL file** This format describes the external surfaces of the original CAD model and forms the basis for calculation of the slices.

**Step 3: Transfer of .STL file to the machine** This step may require some general manipulation of the file in order to set the correct size, position, and orientation for building.

**Step 4: Machine setup** We have to set up the machine before the beginning of the build process. For instance, we would set build parameters like material constraints, energy source, layer thickness, timings or other.

**Step 5: Printing** Printing the object is an automated process and the machine can mostly carry on without user control. Only superficial monitoring of the machine needs to take place in order to ensure the absence of macroscopic errors.

**Step 6: Removal** After the printing process is completed, we have to remove the object from the machine. The machine has safety interlocks to ensure, for example, that the operating temperatures are sufficiently low or that there are no moving parts.

**Step 7: Post processing** The printed objects often require an amount of additional cleaning up before they are ready to be use. Parts may be weak at this stage or they may have supporting features that must be removed. Time and careful, experienced manual manipulation are paramount.

**Step 8: Finishing** Many objects require, before being ready to be used, some finishing. For instance, it may be necessary to paint their surface to give it an acceptable texture. Treatments may be laborious if the finishing requirements are very exacting. Frequently, the printed object must be assembled with other mechanical or electronic components to form a final product.

### 3.2.3 Techniques of printing

Not all 3D printers use the same technology. All the several available way to print in 3D are additive; they differ mainly in the way the layers are built to create the final object. Since 2012 the *American Society for Testing and Materials (ASTM)* developed a set of standards to classify the Additive Manufacturing processes into 7 categories. According to Standard Terminology for Additive Manufacturing Technologies, these seven processes are:

1. Vat Photopolymerization
2. Material Jetting

3. Binder Jetting
4. Material Extrusion
5. Powder Bed Fusion
6. Sheet Lamination
7. Directed Energy Deposition

We provide below a short description of the above-mentioned techniques:

### **Vat Photopolymerization**

The fundamental process that characterizes *Vat Photopolymerization* [Fig. 3.1] method is the hardening of photopolymer resin contained in vat through ultraviolet rays(UV). The most commonly used technology in this processes is *Stereolithography (SLA)*. This technology uses a vat of photopolymer resin hardening in contact with the ultraviolet rays and a UV laser to build the object, one layer at a time. For each layer, the laser beam creates a cross-section of the part pattern on the surface of the resin. The exposure to ultraviolet rays solidifies the resin and makes sure that the new layer is joined to the previous one.

After the pattern has been outlined, the elevator platform descends by a distance equal to the thickness of a layer (0.06 mm to 0.14 mm). Afterwards, a new layer of resin is injected on top of the platform by covering the material previously hardened. On this new liquid surface, the subsequent layer pattern is traced, joining the previous layer. The finite three dimensional object is formed this way. Stereolithography requires the use of supporting structures which serve to link the object to the platform and to hold the object since otherwise it would float in the basin filled with liquid resin. These reinforcements are removed manually after the object is completed.

This technique was invented in 1986 by an engineer named Charles Hull, who also invented the STL file format and founded the company 3D Systems.

### **Material Jetting**

In this process, the material is deposited on a build platform in droplets through a nozzle of small diameter, similarly to how a 2D printed inkjet works, but it is applied layer-by-layer in order to define a 3D object, and then hardened by UV light [Fig. 3.2].

### **Binder Jetting**

In *Binder Jetting* we use two materials: powder base material and a liquid binder [Fig. 3.3]. The procedure consists in spreading the powder (contained in a build chamber) in equal layers and then in the application of the binder through jet nozzles. This

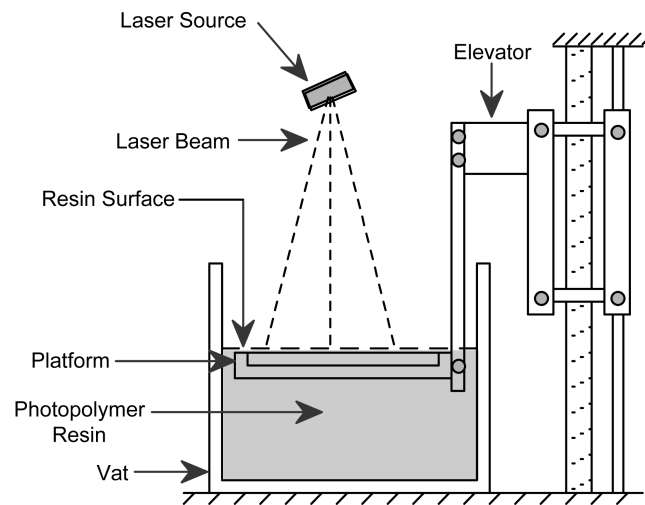


Figure 3.1: Vat photopolymerisation schematics. Figure taken from [80].

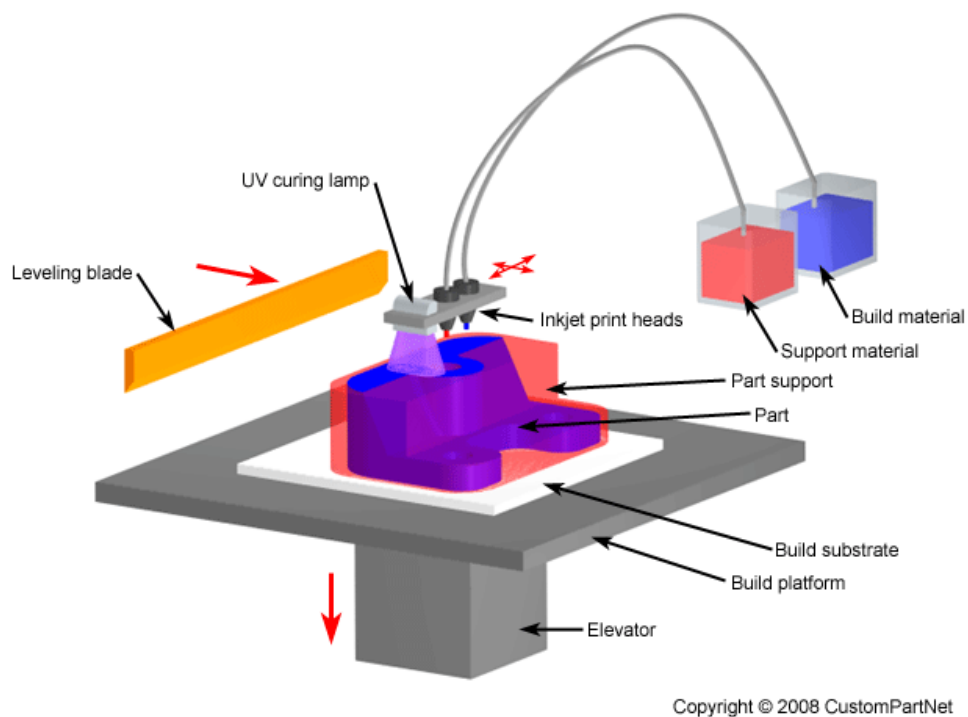


Figure 3.2: Material Jetting schematics. Figure taken from [81].

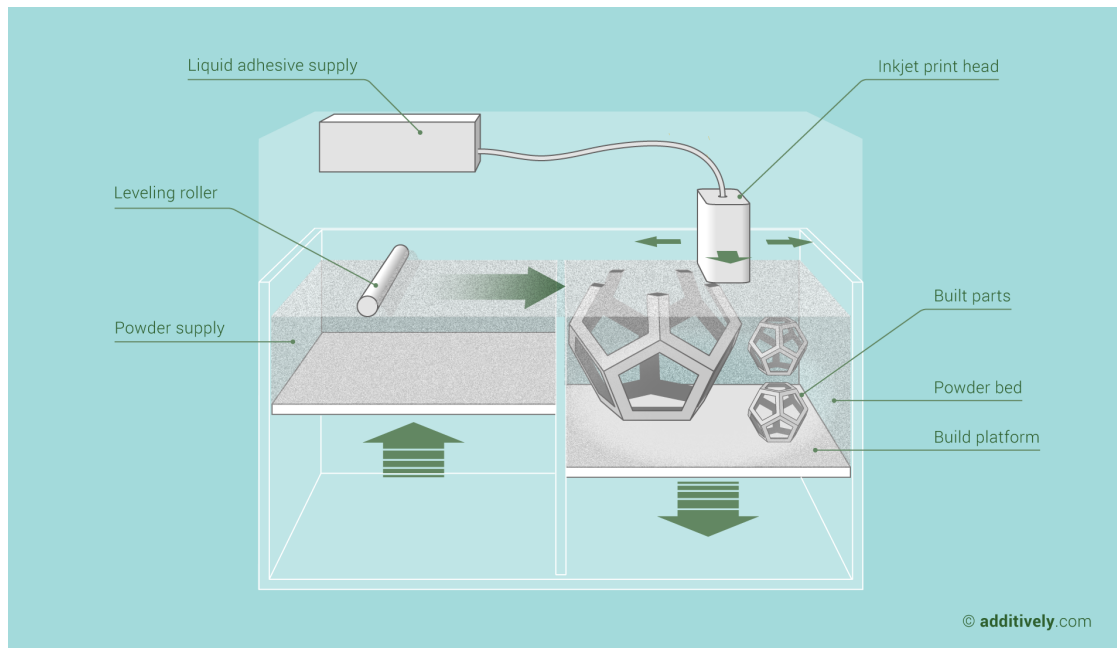


Figure 3.3: Binder Jetting schematics. Figure taken from [82].

liquid binder glues the powder particles in the shape determined by 3D model of the object. The finished object is glued together by binder remains in the container with the powder base material. When 3D printing is complete, the residual powder is removed and is possible to use that powder to 3D print the next object.

This technology was first developed at the Massachusetts Institute of Technology (MIT) in 1993; in 1995 Z Corporation obtained an exclusive license.

### Material extrusion as Fused Deposition Modeling

The term *Fused Deposition Modeling* and its acronym *FDM* was introduced for the first time by Stratasys Inc., which owns the patent. An equivalent denomination, *Fused Filament Fabrication (FFF)*, was introduced by the members of the RepRap project, in order to use a similar technique, but without the legal limits the old name implies [Fig. 3.4].

The FDM technology uses a plastic or metal wire, wound into a reel, which is carried towards the nozzles. Then, the nozzle is heated to melt the material and can be moved in both horizontal and vertical directions by a numerically-controlled mechanism, directly governed by a computer-aided manufacturing (CAM) software package. A specific file called *G-code* contains the coordinates for moving the nozzles. The object is created by extruding melted material to form layers. The material hardens immediately after extrusion from the nozzle. The plastic filaments used consist of two main materials: *ABS*

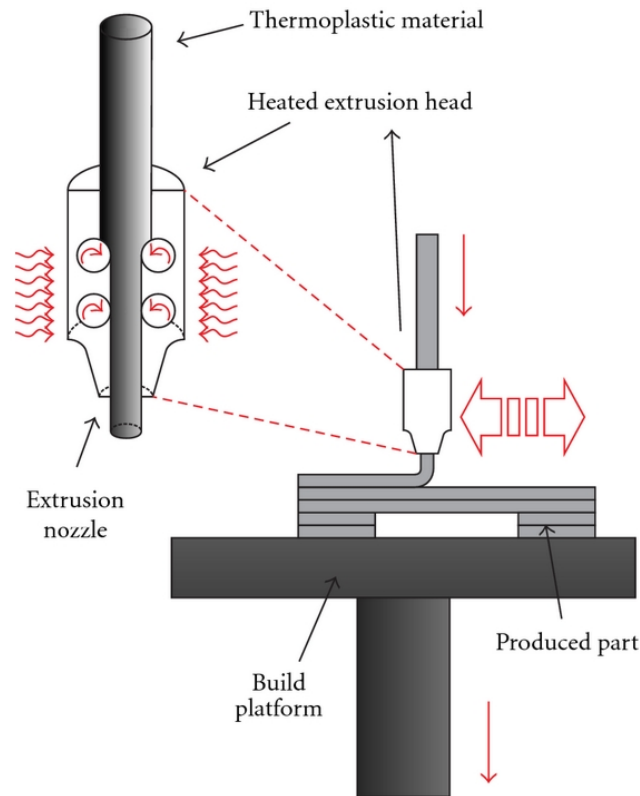


Figure 3.4: FDM schematics. Figure taken from [83].

(*Acrylonitrile Butadiene Styrene*) and *PLA (Polylactic acid)*, but many other materials are available, for instance, (*PC*) *Polycarbonate*, (*PA*) *Polyamide*, (*PS*) *Polystyrene*, *lignin*, *rubber* etc. . Typically, printers have two nozzles, one for the building material and the other to achieve the supports.

FDM was invented by Scott Crump in the late '80s. After patenting this technology, he founded with his wife the company *Stratasys* in 1988. The software that comes with this technology automatically generates support structures if required.

### Powder Bed Fusion

The *Powder Bed Fusion* process includes the following commonly used printing techniques:

- Selective Laser Sintering (SLS),
- Selective Laser Melting (SLM),
- Direct Metal Laser Sintering (DMLS),

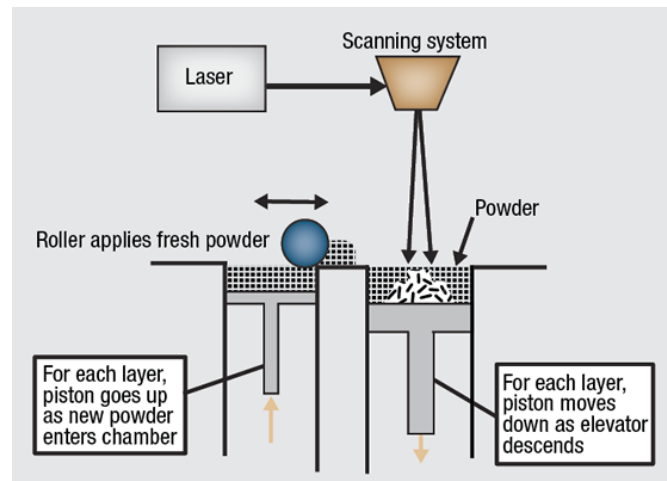


Figure 3.5: SLS schematics. Figure taken from [84].

- Electron Beam Melting (EBM),
- Selective Heat Sintering (SHS).

Powder Bed Fusion (PBF) methods employ either a laser or electron beam to melt and sinter material powder.

The most commonly used technology in this processes is Selective Laser Sintering (SLS) [Fig. 3.5]. This technique employs a high power laser to sinter particles of plastic, metal, ceramic or glass powders into a mass which has a determined three dimensional shape. The laser selectively sinters the powdered material by scanning the layers generated by the 3D modeling program on the surface of a powder bed. After each cross-section is scanned, the powder bed is lowered and a new layer of powder is placed and the process is repeated until the object is finished. Part of the residual powder will become a support structure for the object. Therefore, there is no need for any support structure generated by the printers, which is a good advantage over FDM and SLA. All unused powder can be employed again for the next print. Selective Laser Sintering was developed and patented by Carl Deckard and Joseph Beaman at the University of Texas at Austin in the mid-1980s, under sponsorship of DARPA. A similar process was patented without being commercialized by R. F. Housholder in 1979.

The other techniques mentioned before are quite similar, differing in few aspects. For instance, in the SLM the powder is not sintered, but is melted; in EBM, laser is substituted by an electron beam.

### Sheet Lamination

The process of *Sheet Lamination* consists in joining of the sheets through the use of an external force [Fig. 3.6]. The sheets can be made of metallic, papery or polymeric ma-

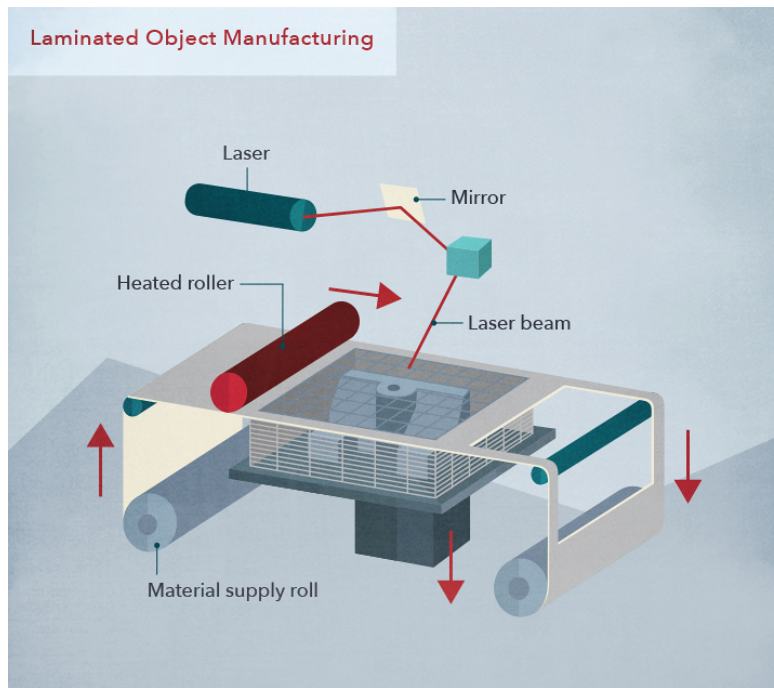


Figure 3.6: Sheet Lamination schematics. Figure taken from [99].

material. The best known and most used processes are: *Ultrasonic Additive Manufacturing (UAM)* and *Laminated Object Manufacturing (LOM)*.

The Ultrasonic Additive Manufacturing process uses sheets and ribbons of metal, which are bound together by using ultrasonic welding. The procedure requires additional computer numerical control and removal of the unbound metal during the welding process. UAM uses metals as aluminum, copper, stainless steel and titanium. The process is low temperature and allows the creation of internal geometries; it can bond different materials and requires relatively little energy, as the metal is not melted.

Laminated Object Manufacturing uses a similar layer by layer approach but employs only paper as material and adhesive glue instead of welding. The LOM process uses a cross-hatching method during the printing process to allow for easy removal post build. Laminated objects are, often used for aesthetic and visual models, are not suitable for structural use.

### Directed Energy Deposition

This process is mostly used in the high-tech metal industry and in rapid manufacturing applications [Fig. 3.7]. The 3D printing apparatus is usually attached to a multi-axis robotic arm; consists of a nozzle that deposits metal powder or wire on a surface and an

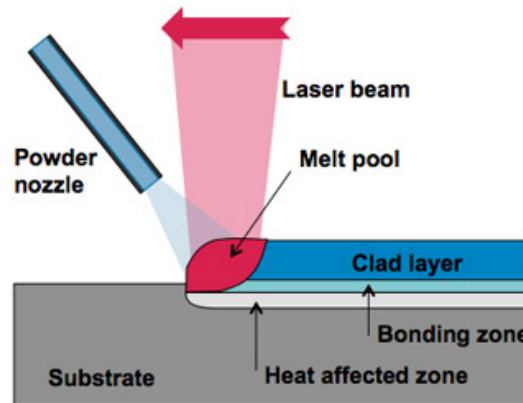


Figure 3.7: Directed Energy Deposition schematics. Figure taken from [84].

energy source (laser, electron beam or plasma arc) which melts it, therefore creating a solid object.

The processes of Addictive Manufacturing are in continuous development, so new technologies of fabrication will be soon available.

### 3.2.4 Types of printable materials

3D printing started with plastics, but today there is a surprising and growing variety of printable materials which includes ceramics, food, glass and even human tissue [19].

Researchers, organizations and hobbyists from all over the world have modified the underlying methods of printing to dramatically widen the scope of possibilities. For example, researchers at the University of Exeter (England, U.K.) have modified a 3D printer to print chocolate; Cornell University (New York, U.S.A), working with the French Culinary Institute (New York, U.S.A), drew inspiration from that idea and created a range of 3D printed food items such as miniature space shuttles made of ground scallops and cheese.

The principles have even been applied to biological tissue, opening the door to research on a range of health applications:

- Washington State University (Oregon, U.S.A.) has developed a bone-like material that provides support for new bone to grow.
- Researchers from the University of Glasgow (Scotland, U.K.) have perfected a system that creates organic and inorganic compounds, which they believe could have long term potential for creating customized medicines.

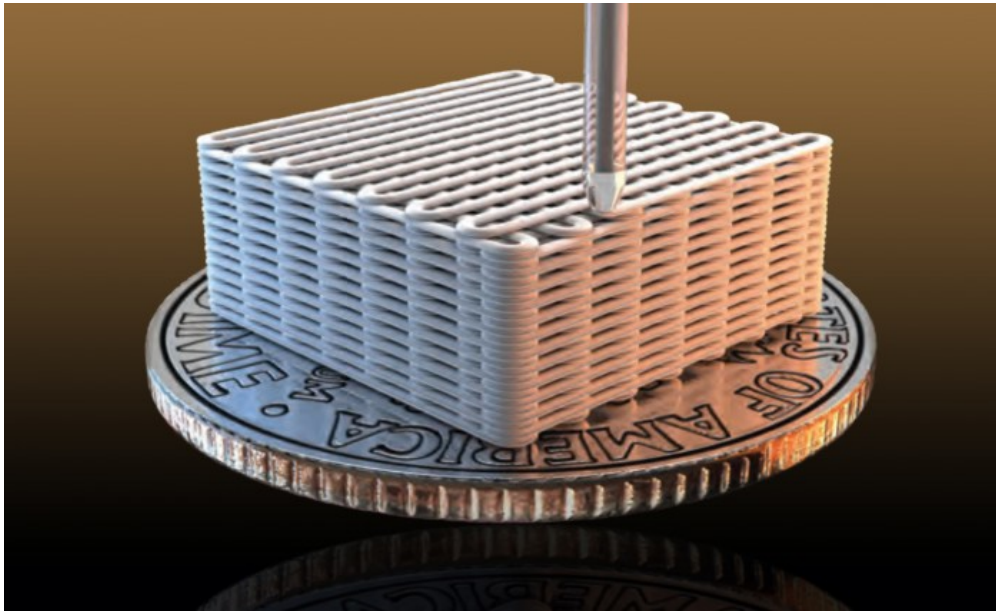


Figure 3.8: Example of accuracy of 3D printing. Figure taken from [93]

- Organovo (U.S.A.) has created some human tissues using human cells as material and has also printed a human vein.

Scholars in the field are working on several different techniques that can control the exact material properties of printed components, even down to the microscopic crystalline structures of metals, changing the bonds between the atoms and the arrangement of the molecules. For example, 3D printing of metal can result in more uniform microstructures due to rapid solidification, in contrast to the traditional metal casting or forging, which require metal to cool from the outer surface to the core. 3D printing would allow engineers to control the object's strength, hardness, flexibility and ability to support stress. The result of this research will be products exhibiting combinations of physical, electrical and mechanical properties that are only dreamed about today.

The University of Illinois Lewis Research Group (U.S.A.) has created a number of custom *inks* (printing materials) with very small feature sizes [Fig. 3.8].

Also the Massachusetts Institute of Technology (MIT) Media Lab (Massachusetts, U.S.A.) is conducting research about 3D printing and available materials as well. For instance, it is experimenting with printing large molds for concrete structures using a spray polyurethane foam. Printing with polyurethane offers advantages in weight, time, control and stability compared to concrete. It also useful for thermal insulation. Once printed, the mold can be filled with concrete or another castable building material. MIT has printed several prototype wall molds which are 1.5-2 m tall as they are exploring the benefits of large-scale 3D printed molds including design, cost, efficiency and safety.

*Contour Crafting* is a 3D printing technology invented by Prof. Behrokh Khoshnevis of



Figure 3.9: 3D printed wall. From University of Naples Federico II.

the University of Southern California (California, U.S.A.). He proposes 3D printing an entire house using specially formulated concrete outgoing from a large nozzle, targeting low-cost and emergency housing. One of the objectives is to build an entire 240 m<sup>2</sup> in 20 hours (fixtures will be placed at the end) with extremely large 3D printers. The social implications of using automated construction to replace dilapidated or destroyed dwellings can be considered significant. The Italian company *WASP* is working on building a printer to produce houses walls as well.

*Sinterhab project* is studying a lunar base constructed by 3D printing using lunar powder as a base material. Similar researches and projects could allow faster construction for lower costs; the possibility to build off-Earth habitats has been investigated [Fig. 3.9].

### 3.3 Current applications

The following quotes give a good introduction to the current state of the applications of 3D printing:

Engineers and designers have been using 3D printers for more than a decade, but mostly to make prototypes rapidly and cheaply. [...] the majority are used as functional models, prototypes, and casting patterns, or for presentation models. [...] as the technology is getting better more things are being printed as finished goods. [...] around 28% of the output of 3D printers is now final products rather than prototypes, and this is expected to rise to 50% by 2016 and 80% by 2020. [Technopolis Group 2013]



Figure 3.10: Local Motors car 3D printed during the International Manufacturing Technology Show (2014). Figure taken from *Wikipedia*.

The compound annual growth rate (CAGR) of additive manufacturing was 29.4% in 2011 [...]. The CAGR for the industry's 24 year history is 26.4%. The AM industry is expected to continue strong double-digit growth over the next several years. By 2015, Wohlers Associates believes that the sale of AM products and services will reach 3.7 billion of dollars worldwide, and by 2019, surpass the 6.5 billion of dollars mark. [Wohlers Associates 2012]

In the following pages, typical examples for applications of 3D printing are presented:

### Automobile components

The Swedish supercar manufacturer *Koenigsegg* produces *One*, a supercar with side mirror internals, air ducts, titanium exhaust components, and even complete turbocharger assemblies that have been 3D printed as part of the manufacturing process.

An American company *Local Motors*, has developed large-scale additive manufacturing processes suitable for printing the body of an entire car. The first car was printed during a motor show in front of thousand people.

*Urbee* is the name of the first car in the world car mounted using the technology 3D printing (its bodywork and its windows were printed). It was created in 2010 through the partnership between the US engineering group *Kor Ecologic* and the company *Stratasys* (manufacturer of printers Stratasys 3D).

*BMW* produces prototypes of engine parts for motor sports racing cars that have been

fabricated using Selective Laser Sintering.

Some luxury car manufacturers, like *Bentley* and *Rolls-Royce*, produce some parts more economically by using 3D printing instead of conventional manufacturing.

Also *Tesla*, a producer of electric cars, builds automobile components by using 3D printers.

### Aircraft components

*Airbus Group* has developed the technology with the intent to manipulate metals, nylon and carbon-reinforced plastics at a molecular level, which allows the application for high-stress scenario, typical of critical aviation uses. Compared to a traditional machined part, those produced by 3D printing are up to 65% lighter, but equally strong. The development of 3D printing is an activity that involves the entire Airbus Group, with applications in the production of fixtures and tooling for Airbus, *Eurocopter* (manufacturer of helicopters) and *Astrium* (aerospace company). In 2011, Airbus Group also produced a door bracket through using 3D printing.

*Boeing* and other companies in the aerospace sector have also developed large internal 3D printing research groups. The Boeing company has been utilizing Selective Laser Sintering for flight hardware in regular production since 2002, for both military and commercial programs.

### Health care

For the first time the lower jaw of a patient was completely replaced by an artificial jaw which was 3D printed. Titanium powder was used to print that implant.

Future applications are 3D printed organs [Fig. 3.11]. Parts of bones have been produced by using 3D printing. Some of these artificial bones are even degradable and after some time will be replaced by the body's own bone tissue. Parts from faces or ears as well are often produced by 3D printers. Silicon is used as a material instead of titanium because of its better suitability in medical fields.

However, research in this area is still far away from practical applications applications, that is to say transplantation. Scientists developed an artificial ear with the help of 3D printing; the ear was purposely different from the natural human ear: an antenna which is part of the artificial ear registers frequencies that a person would not be able to perceive. Many applications of 3D printing are now available also for dentistry and hearing aids.

### Architectural models

Architects are often forced to show their clients drawings of their projects and clients usually need to see the product from all possible view-points in space to get a clear picture of the design. In order to get these scale models to clients in less time, architecture firm



Figure 3.11: 3D printed heart. Figure taken from [85]

tend to choose 3D printing. Using 3D printing, it is possible to reduce long times of production, producing lighter models.

### Other applications

In 2013, the world's first handgun made almost entirely by a 3D printer was printed. 15 of 16 pieces were printed by a 3D printer using ABS (Acrylonitrile Butadiene Styrene) as a material. The pictures of 3D printed handgun, which was only a prototype, went viral all over the world. The company which built the gun planned to publish the digital file for the gun production online, which drew a lot of criticism.

For the first time *Nike* produced a part of a shoe, the plate, by using 3D printing technique.

A huge range of different products can be purchased online. This includes jewelry, games, clothes, furniture, gadgets, design articles and more.

Private consumers constitute an important market for 3D printing that is in constant growth. Consumer interest derives from the affordable price of the new generation of printers but also from the popularity that 3D printing has gained in the last few years. Some of the information on 3D printing we included comes from Wikipedia [18], but the web is saturated with it.

## 3.4 Ten reasons for choosing 3D printing

**Reason one: Different types of objects.** 3D printers are able to create objects of very different shapes, a feature that makes them similar to human artisans. Traditional machines can produce a limited range of objects, i.e. they are not very versatile. Indeed,

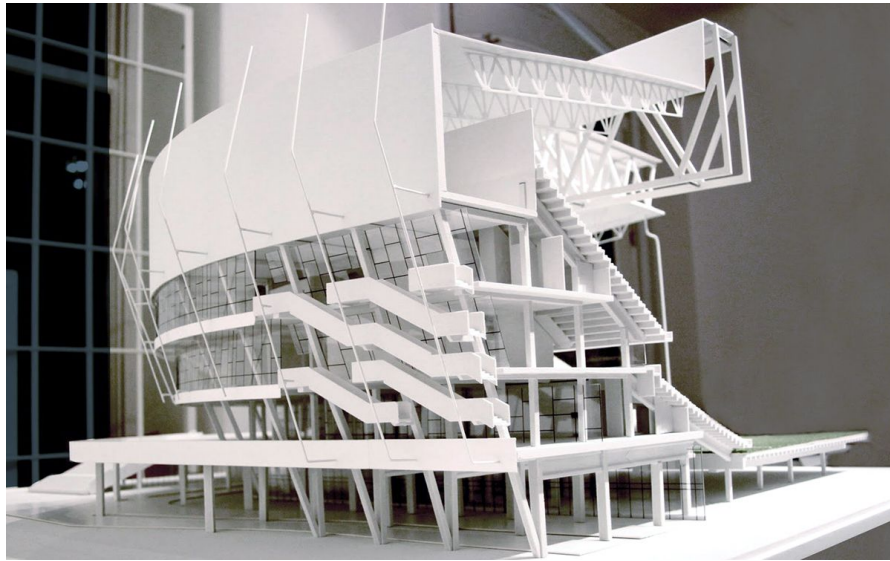


Figure 3.12: Example of architectural 3D model depicting a stadium. Figure taken from [86].

if you wanted to change the type of object to be produced, it would be necessary to retrain or even change the machinery. A 3D printer only needs a digital design and new material.

**Reason two: More complicated = more expensive?** In the manufacture of an object, traditionally, the more complicated the object's shape, the more expensive its realization. Generally, the process of 3D printing a complex object does not require more time, more ability or higher costs than a simpler product. This will change the way in which the cost of objects is attributed.

**Reason three: No limit in shape.** The main limitation of a human artisan is represented by the tools at his disposal. For example, a traditional wood lathe can only make round objects, a molding machine can only make an established shape set by the mold. A 3D printer can create an infinite number of shapes. Human imagination is the only constraint.

**Reason four: No assembly required.** Traditional production is strongly linked to the assembly line. In modern factories, products are made of pieces which are assembled by human workers or by a machine in order to build the final object. Assembling and mounting require high costs, especially when considering the possibility of a product made up by a large number of pieces. In the 3D printing process, the product is manufactured and assembled entirely by printer itself, solving this age-old problem.

**Principle five: Print on demand.** A 3D printer is capable of producing objects when they are actually required. This reduces the need for inventory and the problem of unsold products. Another advantageous aspect could be the minimization of the cost of transportation by creating objects in a place close to where they are needed.

**Reason six: No particular skills.** Artisans have to train a lot before acquiring all the necessary skills. The introduction of computers in mass production has resulted in a decrease of these skills; however, the presence of an expert who understands how to operate the production machines is still necessary. In a production by 3D printing, the most onerous work is related to the creation of the object's virtual model. Achieving an object of equal complexity with an injection molding machine requires many more skills. The ease of use and implementation could offer new ways of production in remote and extreme conditions.

**Reason seven: Portable manufacturing.** The production capacity of a 3D printer is much greater than the production capacity of a traditional machine. For instance, the injection molding machine can build objects much smaller than itself. A 3D printer is capable of producing objects as large as its platform to print. Once we invent a way to move the printing apparatus independently, we would be able to build directly very big and complex objects, like an entire house.

**Reason eight: Little waste material.** 3D printers working with metal produce less waste by-product than traditional manufacturing techniques. Generally machining metal is very wasteful and more than 80% percent of the original metal gets ground off and ends up on the floor. 3D printing is less wasteful for metal manufacturing.

**Reason nine: Perfect copies.** When a digital music file is copied there is no loss of audio quality. In a near future, 3D printing process would extend digital precision to the world of physical objects. 3D scanning technology and 3D printing are the keys to combine the physical world with the digital. We will scan, modify, and duplicate physical objects to create perfect replicas.

**Reason ten: Infinite shades of materials.** The combination of different materials in a single product is difficult for existing machinery. Since machines work according to traditional production methods (which are very different: some cut, some merge, some drip), the concurrent use of a large assortment of materials is hard to put in practice. 3D printing has the ability to melt and mix different raw materials. New mixtures of raw materials could offer a wide range of unexplored materials with new properties or useful behaviors.

Lipson and Kurman's book [17] includes a very detailed explanation about the convenience of 3D printing.

## Chapter 4

# Lightweight structure: design and production

This chapter presents two codes whose ultimate goal is to outline structures with better features than those they would have without the use of a topology optimization algorithm. The first code considers the optimization of a beam subject to a determined static load according to the density-based approach. The second code, instead, arises from the necessity to obtain a 2D lattice material that is characterized by light weight without affecting the necessary shear stiffness and axial stiffness. The optimization process is made possible by the software *Matlab*, well-known in the scientific community and characterized by a high-level language which allows to group commands using simple single strings. The last part of the chapter refers to two 3D printed objects.

### 4.1 Realization of a beam

#### 4.1.1 Approach to the problem

In this section we will show the functioning of the code implemented in order to obtain a beam optimized according to the density-based approach. Since the problem we are facing is two-dimensional, unlike traditional problems, we consider the area and not the volume. As in the case of volume,  $\rho$  is a relative density which indicates the filling percentage of the mesh element (cube, square, etc.) in which the structure is discretized. We are referring to the problem of minimization of the mass subject to stress constraints. For the generic problem, already seen in [1.3.2](#), it is possible to write:

$$\left\{ \begin{array}{l} \min_{\rho_e} m(\rho) = \sum_{e=1}^n \rho_e \\ \text{s.t.} \quad F(\sigma_e)/\sigma_y \leq 1 \quad e = 1, \dots, n. \\ \mathbf{K}\mathbf{u} = \mathbf{F} \\ 0 < \rho_{min} \leq \rho_e \leq \rho_{max} \end{array} \right. \quad (4.1)$$

Though the structure of the problem remains the same, we add displacement constraints, so the problem becomes:

$$\left\{ \begin{array}{l} \min_{\rho_e} m(\rho) = \sum_{e=1}^n \rho_e + \alpha \rho_e (1 - \rho_e) \\ \text{s.t.} \left( \frac{\sigma_{vm_e}}{\sigma_y} \right) - 1 - \frac{\epsilon}{\rho_e} + \epsilon \leq 0 \quad e = 1, \dots, n. \\ \mathbf{U} \leq \mathbf{U}_{lim} \\ \mathbf{K}\mathbf{u} = \mathbf{F} \\ 0 < \rho_{min} \leq \rho_e \leq \rho_{max} \end{array} \right. \quad (4.2)$$

In the previous system (4.2) we have noted the introduction of the mass penalty and the relaxation of stress constraints. The method we are going to use, i. e. SIMP, is based on a heuristic relation between element density  $\rho_e$  and element Young's modulus  $E_e$  given by:

$$E_e = E_e(\rho_e) = \rho_e^p E_0 \quad \rho_e \in (0, 1] \quad (4.3)$$

A modified SIMP approach is given by

$$E_e = E_e(\rho_e) = E_{min} + \rho_e^p (E_0 - E_{min}) \quad \rho_e \in (0, 1] \quad (4.4)$$

where  $E_{min}$  is the elastic modulus of the void material, which is non-zero to avoid singularity of the finite element stiffness matrix, and  $E_0$  is the elastic modulus of solid material. This new formulation of SIMP offers several advantages, like the independency between the minimum value of the material's elastic modulus and the penalization power [26].

Frequently, in the implementation of codes we meet problems that are not identified in the general theory and that therefore lead to numerical difficulties. These numerical difficulties are *mesh-dependency*, *checkerboard patterns* and *local minima*. In particular, the problem of the checkerboards consists of alternating areas with void and solid spaces in the optimized configuration. Originally that type of effect was believed to be part of the optimal solution. Later it was discovered that the problem is related to poor modeling of the stiffness of the checkerboard (thanks to studies conducted in the mid 1990s by Sigmund and Diaz, and, almost simultaneously, by Jog and Haber). Mesh-dependency pertains to the problem of not obtaining qualitatively the same solution for different mesh-sizes or discretization. [28] is a truly enlightening paper on the problems just mentioned. In order to mitigate mesh-dependency and checkerboard patterns, researchers have proposed the use of regularization techniques. One of the most common approaches is the use of *density filters*. A basic filter density function is defined as

$$\tilde{\rho}_e = \frac{\sum_{j \in N_e} H_{ej} a_j \rho_j}{\sum_{j \in N_e} H_{ej} a_j} \quad (4.5)$$

where  $N_e$  is the neighborhood of an element  $\rho_e$  with area  $a_e$ , and  $H_{ej}$  is a weight factor [26]. The neighborhood is defined as

$$N_e = \{j : \text{dist}(e, j) \leq R\}, \quad (4.6)$$

where the operator  $\text{dist}(e, j)$  is the distance between the center of element  $e$  and the center of element  $j$ , and  $R$  is the size of the neighborhood or filter size. The weight factor  $H_{ej}$  is defined as a function of the distance between elements in the neighborhood, for example

$$H_{ej} = R - \text{dist}(e, j), \quad (4.7)$$

where  $j \in N_e$ . In this way, the filtered density  $\tilde{\rho}_e$  defines a modified density that is incorporated in the topology optimization formulation and the SIMP model becomes

$$E_e(\tilde{\rho}_e) = E_{\min} + \tilde{\rho}_e^p (E_0 - E_{\min}) \quad \tilde{\rho}_e \in (0, 1]. \quad (4.8)$$

This regularized SIMP interpolation formula is employed in this work. To counter the possibility of local minima we use the continuation method seen in 1.3.2.

#### 4.1.2 Finite Element Analysis

Following the regularized SIMP method given by (4.8) and the generalized Hooke's law, the bidimensional constitutive matrix for an isotropic element  $e$  is interpolated from void to solid as

$$\mathbf{C}_e(\tilde{\rho}_e) = E_e(\tilde{\rho}_e) \mathbf{C}_e^0, \quad \tilde{\rho}_e \in (0, 1] \quad (4.9)$$

where  $\mathbf{C}_e^0$  is the constitutive matrix with unit Young's modulus. Using the finite element method, the elastic solid element stiffness matrix is the area integral of the elements constitutive matrix  $\mathbf{C}_e(\tilde{\rho}_e)$  and the strain-displacement matrix  $\mathbf{B}$  in the form of

$$\mathbf{k}_e(\tilde{\rho}_e) = \int_{-1}^{+1} \int_{-1}^{+1} \mathbf{B}^T \mathbf{C}_e(\tilde{\rho}_e) \mathbf{B}^T d\xi d\eta \quad (4.10)$$

where  $\xi$  and  $\eta$  are the natural coordinates as sketched in [Fig. 4.1], and the square coordinates of the corners are illustrated in [Tab. 4.1]. The strain-displacement matrix  $\mathbf{B}$  relates the strain  $\epsilon_e$  and the nodal displacement  $\mathbf{u}_e$  as  $\epsilon_e = \mathbf{B} \mathbf{u}_e$ . Using the SIMP method, the element stiffness matrix is interpolated as

$$\mathbf{k}_e(\tilde{\rho}_e) = E_e(\tilde{\rho}_e) \mathbf{k}_e^0 \quad (4.11)$$

where

$$\mathbf{k}_e^0 = \int_{-1}^{+1} \int_{-1}^{+1} \mathbf{B}^T \mathbf{C}_e^0 \mathbf{B}^T d\xi d\eta \quad (4.12)$$

where  $\mathbf{k}_e^0$  is the elastic solid element stiffness matrix with unitary elastic modulus.

The global stiffness matrix  $\mathbf{K}$  is obtained by the assembly of elementary matrix  $\mathbf{k}_e$ ,

$$\mathbf{K}(\tilde{\rho}) = A_{e=1}^n \mathbf{k}_e(\tilde{\rho}_e) = A_{e=1}^n E_e(\tilde{\rho}_e) \mathbf{k}_e^0, \quad (4.13)$$

Node	$\eta$	$\xi$
1	-1	-1
2	1	-1
3	1	1
4	-1	1

Table 4.1: Square element with node numbering conventions.

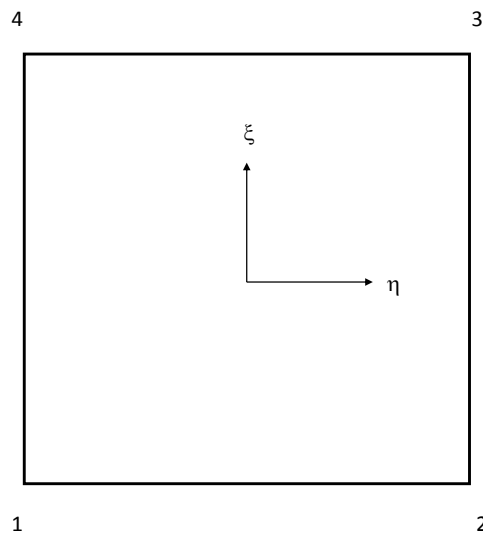


Figure 4.1: Natural coordinates.

where  $n$  is the total number of elements.

The nodal displacements vector  $\mathbf{U}(\tilde{\rho})$  is the solution of the equilibrium equation

$$\mathbf{K}(\tilde{\rho})\mathbf{U}(\tilde{\rho}) = \mathbf{F} \quad (4.14)$$

where  $\mathbf{F}$  is the vector of nodal forces and it is independent from physical densities  $\tilde{\rho}$ . Now it is possible to calculate the strain  $\epsilon_e$

$$\epsilon_e = \begin{bmatrix} \epsilon_{xx} \\ \epsilon_{yy} \\ \gamma_{xy} \end{bmatrix} \quad (4.15)$$

the strain  $\epsilon_e$  as

$$\epsilon_e = \mathbf{B}\mathbf{u}_e \quad (4.16)$$

and then the stress  $\sigma_e$

$$\sigma_e = \begin{bmatrix} \sigma_{xx} \\ \sigma_{yy} \\ \sigma_{xy} \end{bmatrix} \quad (4.17)$$

as

$$\sigma_e = \mathbf{C}_e(\tilde{\rho}_e)\epsilon_e. \quad (4.18)$$

The values obtained with (4.18) are inserted in the Von Mises formulation already seen in (1.115). For brevity of notation, we omitted the dependence of physical densities  $\tilde{\rho}$  on the design variables  $\rho$ ,  $\tilde{\rho} = \tilde{\rho}(\rho)$ . To write this paragraph we drew inspiration from [42].

### 4.1.3 Sensitivity analysis

The derivative of the objective function can be easily obtained as

$$\frac{\partial m(\tilde{\rho})}{\partial \tilde{\rho}_e} = \sum_{e=1}^n 1 + \alpha(1 - \tilde{\rho}_e) - \alpha\tilde{\rho}_e = \sum_{e=1}^n 1 + \alpha(1 - 2\tilde{\rho}_e). \quad (4.19)$$

Instead, in the case of the derivatives of the constraint functions, it is a priority to find the displacement's derivative with respect to the density. Once we have done this, it is trivial to find the derivative of strain and therefore the derivative of stress.

The starting point is

$$\mathbf{K}(\tilde{\rho})\mathbf{U}(\tilde{\rho}) = \mathbf{F} \quad (4.20)$$

and differentiating with respect to  $\tilde{\rho}_e$

$$\frac{\partial \mathbf{K}(\tilde{\rho})}{\partial \tilde{\rho}_e} \mathbf{U}(\tilde{\rho}) + \mathbf{K}(\tilde{\rho}) \frac{\partial \mathbf{U}(\tilde{\rho})}{\partial \tilde{\rho}_e} = \mathbf{0} \quad (4.21)$$

which yields

$$\frac{\partial \mathbf{U}(\tilde{\rho})}{\partial \tilde{\rho}_e} = -\mathbf{K}^{-1}(\tilde{\rho}) \frac{\partial \mathbf{K}(\tilde{\rho})}{\partial \tilde{\rho}_e} \mathbf{U}(\tilde{\rho}) \quad (4.22)$$

and the derivative of the stress can be written as

$$\frac{\partial \sigma_e(\tilde{\rho}_e)}{\partial \tilde{\rho}_e} = \frac{\partial E_e(\tilde{\rho}_e)}{\partial \tilde{\rho}_e} \mathbf{C}_e^0 \mathbf{B} \mathbf{u}_e + E_e(\tilde{\rho}_e) \mathbf{C}_e^0 \mathbf{B} \frac{\partial \mathbf{u}_e(\tilde{\rho}_e)}{\partial \tilde{\rho}_e} \quad (4.23)$$

Hence it is simple to replace the values obtained in the derivative of Von Mises criterion.

#### 4.1.4 Functioning of the algorithm

Here is a summary for the operation of the optimization algorithm:

1. Choose the initial values of design variables  $\rho$  and the size of the neighborhood  $R$  (generally 1.5-2).
2. Global stiffness matrices are assembled for the calculation of elementary displacements  $\mathbf{u}_e$ , elementary strains  $\epsilon_e$  and elementary stresses  $\sigma_e$ .
3. Calculation of the sensitivity of the objective function and the constraint functions with respect to the design variables.
4. Effective use of the Sequential Quadratic Programming by which upgrades the design variables.
5. If the penalization factor  $p$  has not reached its maximum, increase it. The initial  $p$  is equal to the unit, whereas the final one is equal to 4.
6. Check whether the algorithm converges, that is to say if the thresholds, imposed on design variables and on the value of the objective function, are exceeded and if the maximum number of iteration has been reached. If the above-mentioned does not happen, go back to Step 2.

#### 4.1.5 Matlab optimization

Matlab provides three types of algorithms to solve optimization problems:

- Gradient-based algorithms,
- Heuristic algorithms,
- Direct-search algorithms.

**Gradient-based algorithms** The *gradient-based algorithms* are frequently called *classic algorithms*. This type of algorithms employs the gradient of objective function and constraint functions to check the direction in order to position at a point closer to the optimum point. The functioning of these algorithms is explained in [1.2](#).

Classic algorithms provided by Matlab are:

- Interior-point,
- Sequential Quadratic Programming,
- Active-set,
- Trust region.

**Heuristic algorithms** The term *heuristic* suggests a technique designed to solve an optimization problem quicker when classic methods are too slow, or to find an approximate solution when classic methods fail to find any exact solution. This is achieved by trading optimality, completeness, accuracy, or precision for speed. In a way, it can be considered a shortcut. The heuristic optimization's goal is to produce a solution in a reasonable period of time that is good enough to solve the problem at hand. This solution may not be the best of all the actual solutions to this problem, or it may simply approximate the exact solution. However, it is still valuable because finding it does not require a prohibitively long time. Heuristics may produce results by themselves, or they may be used in conjunction with classic optimization algorithms to improve their efficiency (e.g., they may be used to generate good seed values). Fundamental questions that must be asked to decide whether to use a heuristic algorithm are:

- When several solutions exist for a given problem, does the heuristic guarantee that the best solution will be found? Is it necessary to find the best solution?
- When several solutions exist for a given problem, can the heuristic find them all? Do we actually need all solutions?
- Can the heuristic provide a confidence interval for the purported solution? Is the error bar on the solution unreasonably large?
- Is this the best-known heuristic for solving this type of problem?

In some cases, it may be difficult to decide whether the solution found by the heuristic is good enough, because the theory underlying that heuristic is not very elaborate. The heuristic algorithms Matlab provides are:

- Genetic algorithm,
- Simulated annealing,
- Particle swarm.

**Direct-search algorithms** *Direct-search algorithms* is a family of numerical optimization algorithms that do not require the gradient of the problem to be optimized. Hence, direct-search algorithms can be employed on functions that are not continuous or differentiable. Such optimization methods are also known as pattern-search, derivative-free, or black-box algorithms. Matlab provides a generic solver called Pattern search method.

Paper [78] examines these methods more in depth. In the proposed code, we decide to use a gradient-based algorithm (Sequential Quadratic Programming) since the objective function is known and also the constraint functions. In addition, the first derivatives of the functions can be easily found (see 4.2.4), whereby the second derivatives are quickly approximated by the solver. Given the explicit formulation of the problem it is not necessary to consider other types of algorithms (heuristic algorithms and direct-search algorithms), which are mainly used when there is a difficulty in defining the function especially of their derivatives. For well-defined problems like the one discussed, the use of algorithms not based on the gradient leads to good results, but not comparable with those of classic algorithms.

#### 4.1.6 Use of the code

In this problem, a rectangular domain is constrained at the two ends and a point load is applied at the center [Fig. 4.2]. Due to symmetry, only the right half of the beam is modeled, as sketched in [Fig. 4.3]. Thence, the optimization of the MBB (Messerschmitt-Bolkow-Bolhm) beam was performed to check if the code worked.

The half-beam is 50 mm in length ( $l$ ) and 25 mm in height ( $h$ ), modeled with 1250 quadrangular elements, 1326 nodes, and 2652 degrees of freedom. The material parameters are  $E_0 = 2100$  MPa,  $\nu = 0.3$  with a force of  $P = 10$  N in the vertical direction. The limits are:

- $\sigma_{max} = 40$  MPa,
- $\delta_{max} = 1$  mm.

For completeness, we report the results of the beam considered as full, i. e. the relative densities of each element of which is composed the mesh is equal to 1: the maximum stress of Von Mises (extrados of the center line) is equal to 10.5 MPa, and the maximum displacement (at the center line) is equal to 0.18 mm.

The figures in [Fig. 4.4] show how the iterative process, produced by Matlab, leads to the optimal solution. The images reported are the most significant for the phase of figure formation. For the latest iterations (from iteration 41) there are no big differences, it is easy to see that the final image and the previous running deck are almost identical. It is important to note that the starting point has been chosen with a density equal to 1 for all quadrangular elements; this assumption is not relevant in the prosecution of the

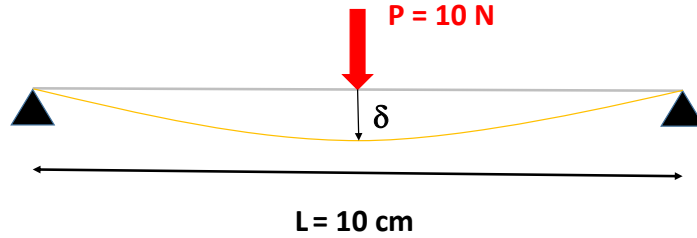


Figure 4.2: Structure to be analyzed [1].

optimization, but it is relevant that, starting from this density, the process requires a smaller number of iterations.

The iterations produced by Matlab are 49. The thresholds chosen to block the process are applied to the design variables ( $10^{-3}$ ) and to the objective function ( $10^{-6}$ ). For more information about stopping criteria see [78]. With a simple personal computer, the optimization thus presented has a duration of about 120 minutes. The figures [Fig. 4.5] and [Fig. 4.6] show the final structure optimized in terms of density and stress. The maximum stress recorded is 40.0004 MPa whereas the maximum vertical displacement is equal to 0.9522 mm. The maximum mass function is 2500 (initial domain as full), whereby that optimized is 763.

What would happen if we changed the limits of Von Mises stress and vertical displacement? Suppose we take as limits 10.5 MPa and 0.22 mm, which is the maximum stress recorded in the full beam and the displacement of the full beam increased by 20% (of 0.18 mm + 0.2 0.18 mm). The final maps of density are displayed in [Fig. 4.8] and Von Mises stress is shown in [Fig. 4.9]. Maximum Von Mises stress is 10.53 MPa, maximum vertical displacement is 0.218 mm and the final mass function is 2094.

If the beam was constrained in some other way, keeping 40 MPa and 1 mm as limits of Von Mises stress and vertical displacement? For instance, consider the structure in [Fig. 4.7]. As done previously, we will model only half of the beam, simply by fixing the part in [Fig. 4.3] which was just supported. We observe that the result of the opti-

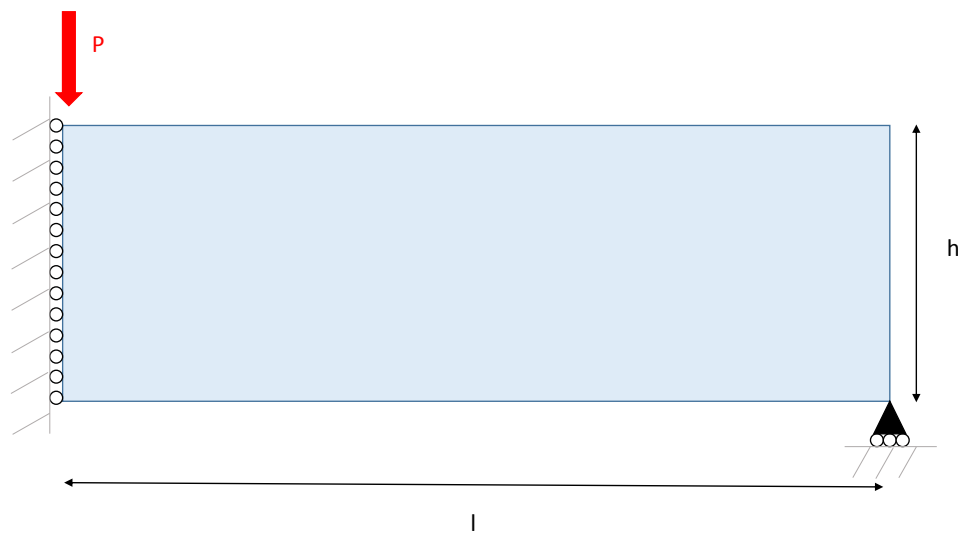


Figure 4.3: MBB beam: geometry and loading.



(a) iteration 0



(b) iteration 6



(c) iteration 13



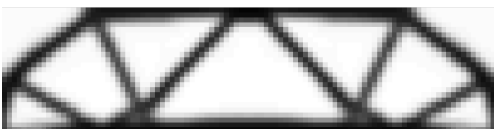
(d) iteration 19



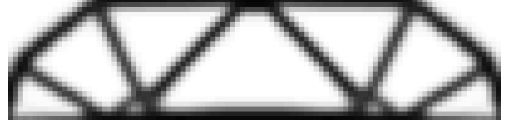
(e) iteration 25



(f) iteration 35



(g) iteration 41



(h) iteration 49

Figure 4.4: Progressive optimization.

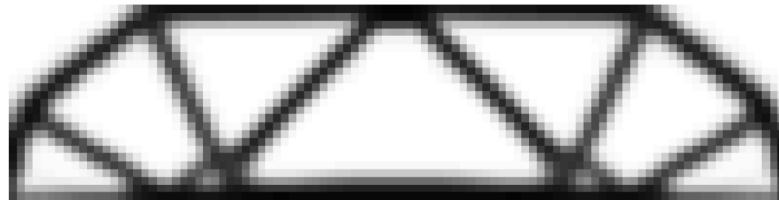


Figure 4.5: Final result [1].

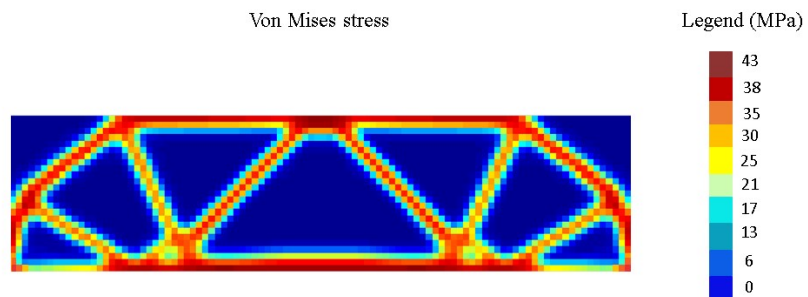


Figure 4.6: Von Mises stress [1].

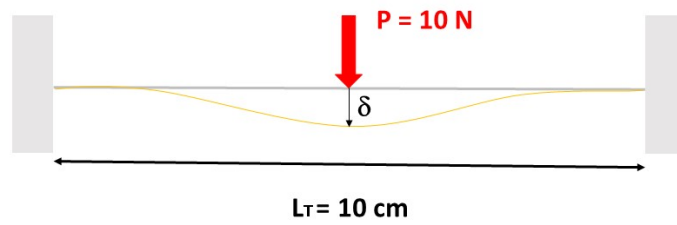


Figure 4.7: Structure to be analyzed [2].

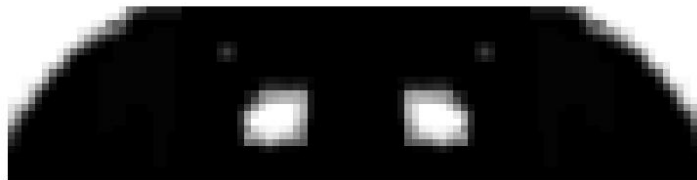


Figure 4.8: Final result [2].

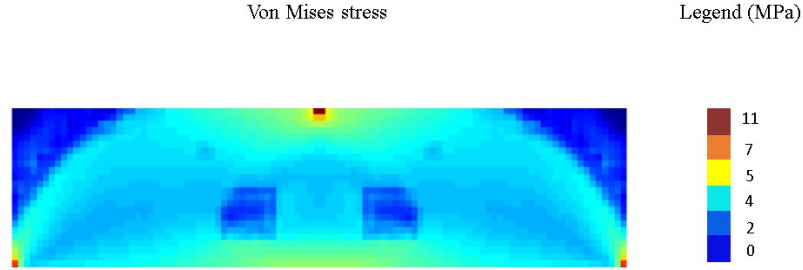


Figure 4.9: Von Mises stress [2].

mized beam provides a maximum Von Mises stress equal to 31.7 MPa [Fig. 4.11], and a maximum vertical displacement (at the center of the beam) of 0.55 mm. The final mass function is of 496 [Fig. 4.10].

## 4.2 Realization of 2D lattice material

### 4.2.1 Approach to the problem

The code we have achieved has the aim of demonstrating how it is possible to connect the themes of the (topological) optimization and lattice materials. The code is intended for two-dimensional periodic materials, but can be implemented for three-dimensional problems. In doing so, the processing time and memory required by the computer would increase.

The objective of the optimization is to find the minimum weight of a two-dimensional periodic lattice material under simultaneous axial and shear stiffness constraints or more simply means that the optimized lattice maintains a minimum axial stiffness as well as a minimum shear stiffness.

We use as guideline paper [37]. The theory is similar (obviously not identical), but the implementation of the code is different. The optimization algorithm starts with a complete mesh finite element. In order to maintain greater generality, it was decided to use beam elements rather than truss elements. This is because the beam elements support



Figure 4.10: Final result [3].

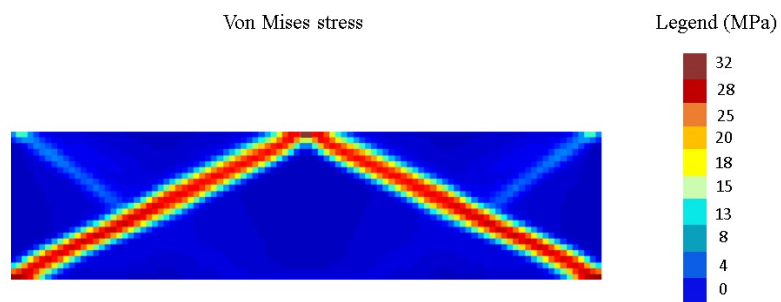


Figure 4.11: Von Mises stress [3].

the load not only axially (as truss elements), but also flexurally; said assumption is very important when treating anisotropic materials for which the request of axial and bending stiffness can be very different. However, observe that lattice materials are frequently statically determined and hence carry the load axially.

The principle on which the algorithm is based, is explained in removing the inefficient elements and resizing the remaining ones until the algorithm does converge to a solution of minimum weight. The problem can be expressed mathematically:

$$\begin{cases} \min_{\mathbf{x}} \bar{\rho}(\mathbf{x}) = \sum_{\forall e \in \Omega} \frac{v_e(\mathbf{x})}{V^\Omega} \\ \text{s.t.} \quad C_E^\Omega(\mathbf{x}) \leq C_E^* \\ \quad \quad C_G^\Omega(\mathbf{x}) \leq C_G^* \end{cases} \quad (4.24)$$

where:

- $\mathbf{x}$  is the vector of design variables, i.e. the cross section of each element;
- $\Omega$  is a discretized domain representing a unit cell or fraction;
- $\bar{\rho}$  is the relative density of the lattice;
- $v_e$  is the volume of the element  $e$ ;
- $V^\Omega$  is the volume of design domain;
- $C_E^\Omega$  and  $C_G^\Omega$  are the compliances of the design domain under uniaxial compressive and shear states of stress, respectively;
- $C_E^*$  and  $C_G^*$  are the upper bounds on the compliances.

Even if the approach we present can be employed for any kind of section of the element, in this case we will use a circular section, so that the radius of the section becomes our design variable  $\mathbf{x}$ . In order to keep all the design variables between 0 and 1, the radius of element  $e$  can be represented by

$$r^e(x^e) = r_{max} x^e \quad (4.25)$$

where  $r_{max}$  is the maximum radius and  $x^e$  is the design variable for the radius of element  $e$ . The algorithm that we propose to create must allow the achievement of the minimum weight while succumbing to certain restrictions, and must be able to obtain a structure with the least number of elements possible. For this reason, we add a *penalty function* to the relative density  $\bar{\rho}$ , so (4.24) can be rewritten as

$$\begin{cases} \min_{\mathbf{x}} (1 + \omega_p \eta_{el}(\mathbf{x})) \bar{\rho}(\mathbf{x}) = (1 + \omega_p \eta_{el}(\mathbf{x})) \sum_{\forall e \in \Omega} \frac{v_e(\mathbf{x})}{V^\Omega} \\ \text{s.t.} \quad C_E^\Omega(\mathbf{x}) \leq \alpha_E \tilde{C}_E \\ \quad \quad C_G^\Omega(\mathbf{x}) \leq \alpha_G \tilde{C}_G \\ \quad \quad 0 \leq x_{min} \leq x^e \leq 1 \end{cases} \quad (4.26)$$

where:

- $\omega_p$  is a penalizing weight for existence of each element;
- $\eta_{el}$  is the number of existing elements;
- $\alpha_E$  and  $\alpha_G$  express the prescribed minimum relative axial and shear stiffness in non-dimensional form, respectively;
- $\bar{C}_E$  and  $\bar{C}_G$  are the compliances of the design domain entirely filled with the constituent material and subjected to uniaxial compressive and uniaxial shear states of stress, respectively;
- $x_{min}$  is a small number to keep the stiffness matrix positive definite.

Since the most used optimization algorithms are the well-known gradient-based, i.e. algorithms that use the derivatives of objective functions and constraint functions, is necessary to express  $\eta_{el}$  as a differentiable function, which is why we write:

$$\eta_{el} = \sum_{\forall e \in \Omega} H_p(x^e) \quad (4.27)$$

where  $H$  is the regularized Heaviside step function [77] as

$$H(x^e) = 1 - \exp(-\beta x^e) + x^e \exp(-\beta) \quad (4.28)$$

When  $\beta$  approaches infinity, the above function approximates the Heaviside function more and more accurately.

### 4.2.2 Finite Element Analysis

The definition of global stiffness matrix is the most important issue for the finite element analysis, which is aimed at the solution of mechanical problems. Then, the displacements of free degrees of freedom and the reaction forces of the constrained degrees of freedom can be deduced. Each element is associated with a matrix of elementary stiffness obtained through the theory of Timoshenko, which is adopted because the initial mesh is frequently constituted by thick elements whose deformation in shear is not negligible. When calculating axial compliance, it is possible to use an elementary matrix obtained by the theory of Euler-Bernoulli, since the deviation in terms of values with that of Timoshenko is insignificant. Assembling the stiffness matrices of each element we achieve the global stiffness, written as

$$\mathbf{Kd} = \begin{bmatrix} \mathbf{K}_{ff}(\mathbf{x}) & \mathbf{K}_{fc}(\mathbf{x}) \\ \mathbf{K}_{cf}(\mathbf{x}) & \mathbf{K}_{cc}(\mathbf{x}) \end{bmatrix} \begin{bmatrix} \mathbf{d}_f(\mathbf{x}) \\ \mathbf{d}_c \end{bmatrix} = \begin{bmatrix} \mathbf{f}_f(\mathbf{x}) \\ \mathbf{f}_c(\mathbf{x}) \end{bmatrix} = \mathbf{f} \quad (4.29)$$

where  $\mathbf{K}$  is the global stiffness,  $\mathbf{d}$  is the displacement vector and  $\mathbf{f}$  is the force vector. The unknowns of the system are the free displacements  $\mathbf{d}_f$  and the reaction forces  $\mathbf{f}_c$ . First we calculate the free displacements

$$\mathbf{d}_f(\mathbf{x}) = \mathbf{K}_{ff}(\mathbf{x})^{-1}(\mathbf{f}_f(\mathbf{x}) - \mathbf{K}_{fc}(\mathbf{x})\mathbf{d}_c) \quad (4.30)$$

subsequently, we can obtain the reaction forces  $\mathbf{f}_c$

$$\mathbf{f}_c(\mathbf{x}) = \mathbf{K}_{cf}\mathbf{d}_f(\mathbf{x}) + \mathbf{K}_{cc}(\mathbf{x})\mathbf{d}_c. \quad (4.31)$$

#### 4.2.3 Calculation of the compliance

The explicitation of axial and shear compliance is necessary. A generic formulation is given by [76]:

$$\mathbf{C}^\Omega(\mathbf{x}) = \mathbf{f}_f^T(\mathbf{x})\mathbf{d}_f(\mathbf{x}) - \mathbf{f}_c^T(\mathbf{x})\mathbf{d}_c. \quad (4.32)$$

Given the generality of (4.32) it can be employed for both compliances mentioned above.

**Boundary condition for the calculation of axial compliance** The introduction of a unit cell is usually based on certain assumptions, such as a regular pattern in the microstructure, which is sometimes a reasonable approximation or an idealization otherwise. A regular pattern offers certain symmetries, which can then be employed to define the unit cell and to derive the boundary conditions for micromechanical analysis. In the literature, there are many accounts where simplistic boundary conditions have been imposed to unit cells in an intuitive manner, sometimes, rather casually and without much justification. Such simplistic boundary conditions are correct only in a few special cases. Another very confusing issue is how many boundary conditions need to be prescribed at any given part of the boundary of a unit cell. Sometimes, only one displacement has been prescribed but in other cases, more than one are prescribed. In order to avoid the use of mere intuition, we use [75] as reference in which the mode of constraint of the unit cell is explained in depth.

Consider a rectangular unit cell with dimensions  $L_X$  and  $L_Y$  along the  $X$  and  $Y$  directions, respectively. Often it is assumed that the desired unit cell has reflectional symmetry [Fig. 4.12] about the  $X$  and  $Y$  so that the design domain  $\Omega$  can be chosen as one quarter of the lattice unit cell. The compliance of the design domain under uniaxial loading along the  $Y$  direction can be calculated with the following prescribed displacements and boundary conditions [Fig. 4.13]

$$u_{X|X=0} = 0 \quad u_{X|X=L_X^\Omega} = \epsilon_{XX}L_X^\Omega \quad (4.33)$$

$$u_{Y|Y=0} = 0 \quad u_{Y|Y=L_Y^\Omega} = \epsilon_{YY}L_Y^\Omega \quad (4.34)$$

where:

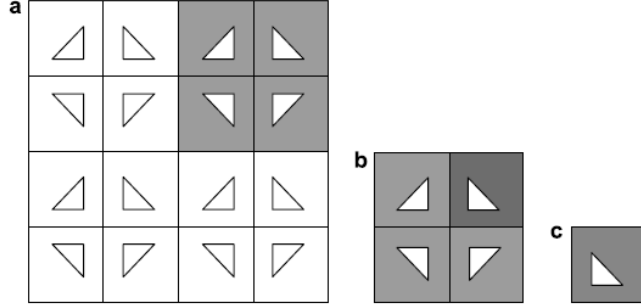


Figure 4.12: Square packing with further reflectional symmetries.

- $u_X$  and  $u_Y$  are translational degrees of freedom along  $X$  and  $Y$ ;
- $L_X^\Omega$  and  $L_Y^\Omega$  are the dimensions of the design domain  $\Omega$ ;
- $\epsilon_{XX}$  and  $\epsilon_{YY}$  are the normal strains along  $X$  and  $Y$ .

Only  $\epsilon_{YY}$  is the applied uniform strain along the  $Y$  axis, whereas  $\epsilon_{XX}$  are the resulting uniform strain along the  $X$  axis required to ensure a one-dimensional state of stress along the  $Y$  direction.

The rotational degrees of freedom are chosen to be compatible with the translational degrees of freedom for axial stiffness at these boundaries and are as follows:

$$\theta_{Z|X=0} = 0 \quad \theta_{Z|X=L_X^\Omega} = 0 \quad (4.35)$$

$$\theta_{Z|Y=0} = 0 \quad \theta_{Z|Y=L_Y^\Omega} = 0 \quad (4.36)$$

where  $\theta_Z$  is rotational degree of freedom about  $Z$  axis, which is the axis coming out of the Cartesian plane  $XY$ . This choice of constraint conditions is equivalent to imposing the minimum for the Young's modulus of the lattice  $E_{lattice}$  that is

$$\alpha_E = \frac{E_{lattice}}{E} \quad (4.37)$$

where  $E$  is Young's modulus of constituent material.

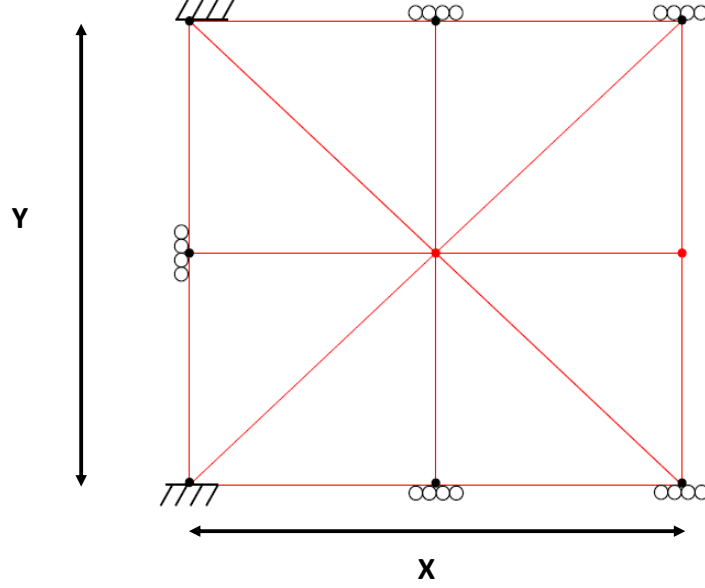


Figure 4.13: Constraints of a quarter of a unit cell used for the calculation of the axial compliance; the uniform translation is applied along the  $Y$  direction in  $Y = L_Y^\Omega$ .

**Boundary condition for the calculation of shear compliance** Like for the calculation of the axial compliance, we proceed to the calculation of the shear compliance, i.e. the compliance of the design domain under uniaxial shear in the  $XY$  plane. It can be calculated with the following prescribed displacements and boundary conditions [Fig. 4.14]:

$$u_{Y|X=0} = 0 \quad u_{Y|X=L_X^\Omega} = 0 \quad (4.38)$$

$$u_{X|Y=0} = 0 \quad u_{X|Y=L_Y^\Omega} = \gamma_{YX} L_Y^\Omega \quad (4.39)$$

The rotational degrees of freedom are not constrained. This choice of constraint conditions is equivalent to imposing the minimum for the shear modulus of the lattice  $G_{lattice}$  i.e.

$$\alpha_G = \frac{G_{lattice}}{G} \quad (4.40)$$

where  $E$  is the shear modulus of constituent material.

Of course, by suitably modifying the constraints it is possible to find stiffness (and therefore also compliance) in other directions. Boundary conditions presented for axial compliance and for shear compliance are individually applied to the lattice to evaluate  $C_E^\Omega$  and  $C_G^\Omega$  respectively. It is worth mentioning that the proposed approach for the

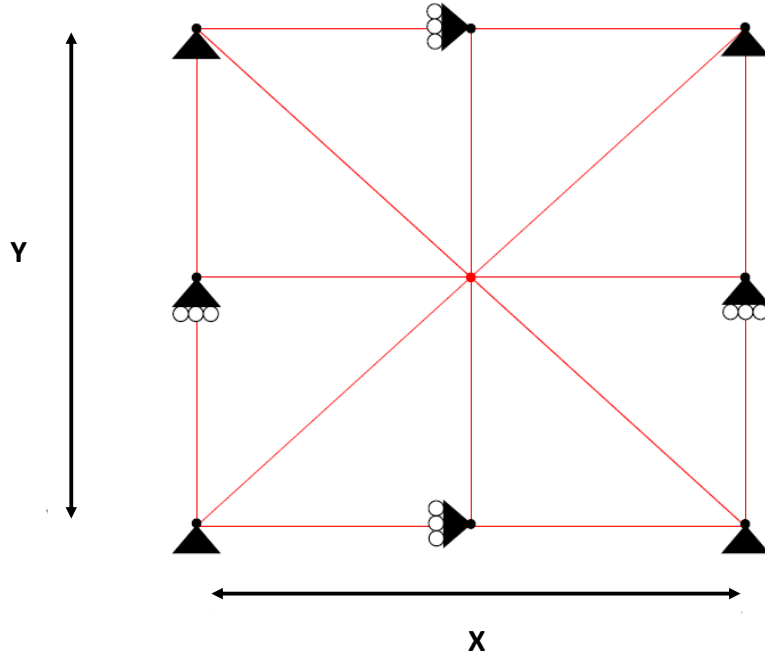


Figure 4.14: Constraints of a quarter of a unit cell used for the calculation of the shear compliance; the uniform translation is applied along the  $X$  direction in  $Y = L_Y^\Omega$ .

extraction of axial and shear moduli only requires two analyses, while the conventional approach requires 3 and 6 distinct analyses in 2D and 3D respectively, to fully characterize the unit cell elastic properties. Furthermore, the proposed approach allows us to model one quarter of unit cell; given that the cost of inverting the stiffness matrix is cubic in the number of degrees of freedom, this reduces the computational cost.

#### 4.2.4 Sensitivity analysis

The key step in the optimization process is efficiently computing derivatives of the objective functions and constraint functions. Topology optimization problems are often large-scale and the use of traditional numerical methods such as the finite difference method is not efficient. Thus, we employ an analytical method to compute derivatives efficiently. In deriving the derivatives of functions with respect to design variables, two groups of functions can be recognized. One group is explicitly a function of design variables, for which derivatives are simple to compute. In objective function,  $\eta_{el}$  and  $\bar{\rho}_{el}$  are explicitly functions of design variables, i.e.  $\mathbf{x}$ , and their derivatives with respect to  $\mathbf{x}^e$  are:

$$\frac{\eta_{el}}{dx^e} = \beta \exp(-\beta x^e) + \exp(-\beta), \quad (4.41)$$

$$\frac{d\bar{\rho}}{dx^e} = \frac{1}{V^\Omega} \frac{dv^e}{dx^e}. \quad (4.42)$$

The second group contains functions that are not explicitly dependent on the design variables. For instance  $C^\Omega$  is a function of  $\mathbf{d}_f$ , which, in turn, is a function of the inverse of  $\mathbf{K}_{ff}$ . Now, if you were to use a method of numerical calculation, the computation of the derivative would be very cumbersome. This is why the best choice is to use an analytical method. To solve our problem, we use the *adjoint method* and consequently we take the derivative of the function with the addition of the equilibrium equation with an arbitrary constant vector  $\chi$ :

$$\frac{dC^\Omega}{dx^e} = \frac{d}{dx^e} (C^\Omega + \chi(\mathbf{K}_{ff}\mathbf{d}_f + \mathbf{K}_{fc}\mathbf{d}_c - \mathbf{f}_f)). \quad (4.43)$$

From equation (4.29) we get

$$\mathbf{f}_c = \mathbf{K}_{cf}\mathbf{d}_f + \mathbf{K}_{cc}\mathbf{d}_c \quad (4.44)$$

And substituting this equation in (4.32) and then in (4.43) we obtain

$$\frac{dC^\Omega}{dx^e} = \left( \frac{d\mathbf{f}_f^T}{dx^e} - \mathbf{d}_c^T \frac{d\mathbf{K}_{fc}}{dx^e} \right) (\mathbf{d}_f - \chi) + \chi^T \frac{d\mathbf{K}_{ff}}{dx^e} \mathbf{d}_f - \mathbf{d}_c^T \frac{d\mathbf{K}_{cc}}{dx^e} \mathbf{d}_c + \frac{d\mathbf{d}_f^T}{dx^e} (\mathbf{K}_{ff}\chi - (\mathbf{f}_f - \mathbf{K}_{fc}\mathbf{d}_c)). \quad (4.45)$$

Because we do not want to calculate  $d\mathbf{d}_f^T/dx^e$ , then we do an assumption on  $\chi$  i.e.

$$\chi = -\mathbf{K}_{ff}^{-1}(\mathbf{f}_f - \mathbf{K}_{fc}\mathbf{d}_c) = -\mathbf{d}_f \quad (4.46)$$

so the equation (4.45) can be written as

$$\frac{dC^\Omega}{dx^e} = 2 \frac{d\mathbf{f}_f^T}{dx^e} \mathbf{d}_f - \mathbf{d}^T \frac{d\mathbf{K}}{dx^e} \mathbf{d} \quad (4.47)$$

since they are not applied forces, the first term of the second member in (4.47) is canceled and therefore

$$\frac{dC^\Omega}{dx^e} = -\mathbf{d}^T \frac{d\mathbf{K}}{dx^e} \mathbf{d} \quad (4.48)$$

#### 4.2.5 Functioning of the algorithm

Here is a summary for the operation of the optimization algorithm:

1. You must choose the initial values of design variables  $\mathbf{x}$ ; in general, each variable is assigned the maximum value.
2. The global stiffness matrices are assembled for the calculation of the axial compliance  $C_E^\Omega$ , and the shear compliance  $C_G^\Omega$ .
3. You must calculate free displacements  $\mathbf{d}_f$  and reaction forces  $\mathbf{f}_c$  for the two systems of constraint seen in figure [Fig. 4.13] and [Fig. 4.14].

4. Calculation of the objective function's sensitivity and of the constraint functions with respect to the design variables.
5. Effective use of the Sequential Quadratic Programming by which the design variables are upgraded.
6. Check whether the algorithm converges, that is to say if the threshold imposed on design variables is exceeded or if it has reached the maximum number of iterations. If the above does not happen, go back to Step 2.
7. Check whether  $\eta_{el}$  (in its values modified  $\beta$  and  $\omega_p$ ) has reached its maximum value, and if the resulting solution is satisfactory, though this does not happen  $\eta_{el}$  is changed (in its values modified  $\beta$  and  $\omega_p$ ) and you go back to Step 2.
8. If there is any item that is  $x^e \leq x_{lim}$ , then you must remove it and go back to Step 1.

In Step 8  $x_{lim}$  might be 1% - 0.1% of  $r_{max}$ . As in 4.1 we employ the Sequential Quadratic Programming. The threshold is imposed on  $\mathbf{x}$  and is equal to  $10^{-6}$ . For more information about stopping criteria see [78].

#### 4.2.6 Comparison

In order to investigate the efficiency of the results obtained, the code can compare the results obtained, with Hashin–Shtrikman (H–S) bounds for isotropic two-phase (solid-void) composites, that can be obtained as follows:

$$\alpha_E^{HS} \leq \frac{\bar{\rho}}{3 - 2\bar{\rho}} \quad (4.49)$$

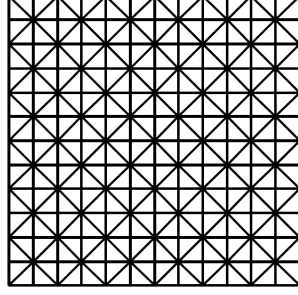
$$\alpha_G^{HS} \leq \frac{K\bar{\rho}}{(1 - \bar{\rho})(K + 2G) + K} \quad (4.50)$$

where  $\alpha_E^{HS}$  and  $\alpha_G^{HS}$  are the relative axial and shear moduli of the cellular material at the H-S bounds, respectively,  $G$  and  $K$  are the shear and the bulk moduli of the constituent material, respectively, and  $\bar{\rho}$  represent the relative density of the composite material. This comparison helps quantifying the effect of anisotropy on the mechanical efficiency of the lattices.

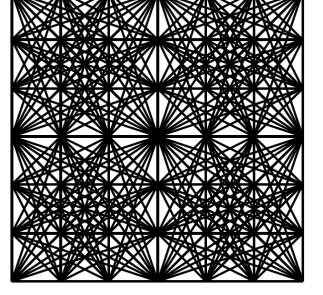
It is instructive to compare the performance of our optimized lattices with that of classic 2D lattice designs, in particular hexagonal, fully triangular, and Kagome designs. The values of  $\alpha_E$  and  $\alpha_G$  for hexagonal have been obtained by

$$\alpha_E^H = \frac{3}{2}\bar{\rho}^3 \quad (4.51)$$

$$\alpha_G^H = \frac{3(1 + \nu)}{4}\bar{\rho}^3 \quad (4.52)$$



(a) Locally connected mesh



(b) Fully connected mesh

Figure 4.15: Initial meshes used to model a square unit cell.

and fully triangular

$$\alpha_E^{FT} = \frac{1}{3} \bar{\rho} \quad (4.53)$$

$$\alpha_G^{FT} = \frac{(1 + \nu)}{4} \bar{\rho} \quad (4.54)$$

where  $\alpha_E^H$  and  $\alpha_E^H$  are relative axial and shear moduli of hexagonal design and  $\alpha_E^{FT}$  and  $\alpha_G^{FT}$  are relative axial and shear moduli of fully triangular design, respectively. We remember that the elastic properties of a Kagome design are identical to those of a fully triangular lattice. It is simple to note as hexagonal design is always less stiff than fully triangular and Kagome.

#### 4.2.7 Use of the code

There are two different initial mesh topologies:

- meshes with local connections, where the nodes are connected those closest to them with horizontal, vertical and diagonal elements.
- meshes with full connections, where each pair of nodes is connected by an element (the elements that overlap are removed, if necessary).

The two types of initial meshes are shown in [Fig. 4.15].

Consider the following values of  $\alpha_E$  and  $\alpha_G$  equal to  $10^{-1}$ ,  $10^{-2}$ ,  $10^{-3}$  and  $10^{-4}$ . The combinations we need to examine are 16 as it is evident in [Tab. 4.2]. For each iteration we perform two FEM analysis: one to calculate the axial compliance and the other for the shear compliance. Knowing that, when  $\beta$  tends to infinity,  $H$  tends to the number of the elements actually present in the cell, we assume a value of  $\beta = 100$ . The value of penalty  $\omega_p$  generally is varied from 0.1 to 0.001, hence it is assumed  $\omega_p = 0.01$ . The

Table 4.2: Combinations of  $\alpha_E$  and  $\alpha_G$ .

combo	$\alpha_E$	$\alpha_G$
1	$10^{-1}$	$10^{-1}$
2	$10^{-1}$	$10^{-2}$
3	$10^{-1}$	$10^{-3}$
4	$10^{-1}$	$10^{-4}$
5	$10^{-2}$	$10^{-1}$
6	$10^{-2}$	$10^{-2}$
7	$10^{-2}$	$10^{-3}$
8	$10^{-2}$	$10^{-4}$
9	$10^{-3}$	$10^{-1}$
10	$10^{-3}$	$10^{-2}$
11	$10^{-3}$	$10^{-3}$
12	$10^{-3}$	$10^{-4}$
13	$10^{-4}$	$10^{-1}$
14	$10^{-4}$	$10^{-2}$
15	$10^{-4}$	$10^{-3}$
16	$10^{-4}$	$10^{-4}$

maximum radius,  $r_{max}$ , is set to  $L_{min}/5$  and kept fixed during the optimization, where  $L_{min}$  is the length of shortest element in the mesh, to ensure that the Timoshenko beam theory can be applied. For simplicity, only crossings that occur at the square lattice grid points are assumed to be lattice nodes. This simplification is conservative, indeed, introducing lattice nodes at each crossing would result in a stiffer structure. Finally, we have chosen a mesh of 7x7 nodes (120 elements) to model a quarter of unit cell, for locally connected mesh, and a mesh of 4x4 nodes (120 elements) for fully connected mesh.

Graphical results for fully connected meshes and for locally connected mesh are reported in appendix 4.3, from whose optimal designs we can draw some general observations. These conclusions hold for both mesh connectivities:

- Most topologies include two groups of bars: vertical and diagonal members; the former are efficient in compression, whereas the latter in shear. In situations where  $\alpha_G \gg \alpha_E$ , the bending stiffness of diagonal members is sufficient to support the axial stiffness, and no vertical elements generally appear.
- About 50% of the optimized designs all elements have the same cross-sectional area, about 40% have two groups of elements and for the remaining cases three groups of elements emerge.

- Notice that the existence of non-strong elements in the optimal solution (particularly at high stiffness), in spite of the penalization they receive from  $\omega_p$ , is proof of the structural benefit of hierarchy and complexity.
- Although the actual lattice topologies are significantly different for the local and full mesh connectivities, the relative densities are very similar in both cases.
- For all combinations the shear constraint is active, while for specific combinations, the axial stiffness constraint can be inactive. Frequently the structure we obtain has an unwanted axial overstiffness, so we can find axial resistances thousands of times higher than initially established.
- Observe that optimized lattices with high shear stiffness and low axial stiffness have cubic symmetry. This is due to the fact that these lattices possess strong diagonal elements, which provide equal axial stiffness in the X and Y direction by bending. On the contrary, optimized lattices with low shear stiffness and high axial stiffness, have weak diagonal members and their effect on axial stiffness becomes negligible compared to that of the axial members.

When  $\alpha_G \geq \alpha_E$ , that is when it is required that the shear stiffness is greater than the axial one, the structure of the optimized cell presents better characteristics than conventional cellular materials such as hexagonal or fully triangular and Kagome. It is also remarkable that they have characteristics far superior to the limits of Hashin–Shtrickman bounds. When  $\alpha_G < \alpha_E$ , instead, it is evident that the optimized material, from the point of view of the shear stiffness, has worse characteristics than those of fully triangular and Kagome. The author notes also that once the relative density has exceeded 12% the optimized material is always better (and in the case that  $\alpha_G \geq \alpha_E$  that  $\alpha_G < \alpha_E$ ) of existing lattice materials and the limits of Hashin–Shtrickman bounds. Tables [Tab. 4.3] and [Tab. 4.3] show the results for the aforementioned combinations of  $\alpha_E$  and  $\alpha_G$  where Fully triangular lattice, Kagome lattice and Hexagonal lattice are considered with the same relative density  $\bar{\rho}$  as the optimized lattice.

Many of the optimal topologies obtained are hierarchical; indeed, they contain sublattices with elements of different sections. It is true that manufacturing of hierarchical designs presents challenges in comparison with simpler geometries, but it useful to study hierarchy in achieving lightweight lattices with prescribed elastic properties. This is why we repeat the optimization taking into account the combinations of  $\alpha_E$  and  $\alpha_G$  we have just illustrated [Tab. 4.2] and imposing the conditions that all elements in the lattice must have the same cross-sections (a sort of simplified size optimization). For each combination, we see an increase of relative density compared to topology optimization. The percentage increases is depicted in [Tab. 4.5]. For locally connected meshes, percentage increases between 15% and 57%; these numbers change to 41% and 88% in the case of fully connected meshes.

Table 4.3: Results for locally connected mesh. HSa for Hashin–Shtrickman axial bound, HSs for Hashin–Shtrickman shear bound; TKa for Fully triangular lattice and Kagome lattice axial bound, TKs for Fully triangular lattice and Kagome lattice shear bound; Ha for Hexagonal lattice axial bound, Hs for Hexagonal lattice shear bound.

$\alpha_E$	$\alpha_G$	HSa	HSs	TKa	TKs	Ha	Hs	$\bar{\rho}(\%)$
$10^{-1}$	$10^{-1}$	✓	✓	✓	✓	✓	✓	9.80
$10^{-1}$	$10^{-2}$	✓	✓	✓		✓	✓	5.39
$10^{-1}$	$10^{-3}$	✓	✓	✓		✓	✓	4.97
$10^{-1}$	$10^{-4}$	✓		✓		✓	✓	4.92
$10^{-2}$	$10^{-1}$	✓	✓	✓	✓	✓	✓	6.75
$10^{-2}$	$10^{-2}$	✓	✓	✓	✓	✓	✓	0.98
$10^{-2}$	$10^{-3}$	✓	✓	✓		✓	✓	0.54
$10^{-2}$	$10^{-4}$	✓		✓		✓	✓	0.50
$10^{-3}$	$10^{-1}$	✓	✓	✓	✓	✓	✓	6.75
$10^{-3}$	$10^{-2}$	✓	✓	✓	✓	✓	✓	0.68
$10^{-3}$	$10^{-3}$	✓	✓	✓	✓	✓	✓	0.10
$10^{-3}$	$10^{-4}$	✓	✓	✓		✓	✓	0.05
$10^{-4}$	$10^{-1}$	✓	✓	✓	✓	✓	✓	6.75
$10^{-4}$	$10^{-2}$	✓	✓	✓	✓	✓	✓	0.68
$10^{-4}$	$10^{-3}$	✓	✓	✓	✓	✓	✓	0.07
$10^{-4}$	$10^{-4}$	✓	✓	✓	✓	✓	✓	0.01

Table 4.4: Results for fully connected mesh. HSa for Hashin–Shtrickman axial bound, HSs for Hashin–Shtrickman shear bound; TKa for Fully triangular lattice and Kagome lattice axial bound, TKs for Fully triangular lattice and Kagome lattice shear bound; Ha for Hexagonal lattice axial bound, Hs for Hexagonal lattice shear bound.

$\alpha_E$	$\alpha_G$	HSa	HSs	TKa	TKs	Ha	Hs	$\bar{\rho}(\%)$
$10^{-1}$	$10^{-1}$	✓	✓	✓	✓	✓	✓	7.49
$10^{-1}$	$10^{-2}$	✓	✓	✓		✓	✓	4.96
$10^{-1}$	$10^{-3}$	✓	✓	✓		✓	✓	4.84
$10^{-1}$	$10^{-4}$	✓	✓	✓		✓	✓	4.83
$10^{-2}$	$10^{-1}$	✓	✓	✓	✓	✓	✓	5.70
$10^{-2}$	$10^{-2}$	✓	✓	✓	✓	✓	✓	0.75
$10^{-2}$	$10^{-3}$	✓	✓	✓		✓	✓	0.48
$10^{-2}$	$10^{-4}$	✓	✓	✓		✓	✓	0.48
$10^{-3}$	$10^{-1}$	✓	✓	✓	✓	✓	✓	5.70
$10^{-3}$	$10^{-2}$	✓	✓	✓	✓	✓	✓	0.57
$10^{-3}$	$10^{-3}$	✓	✓	✓	✓	✓	✓	0.04
$10^{-3}$	$10^{-4}$	✓	✓	✓		✓	✓	0.05
$10^{-4}$	$10^{-1}$	✓	✓	✓	✓	✓	✓	5.70
$10^{-4}$	$10^{-2}$	✓	✓	✓	✓	✓	✓	0.57
$10^{-4}$	$10^{-3}$	✓	✓	✓	✓	✓	✓	0.06
$10^{-4}$	$10^{-4}$	✓	✓	✓	✓	✓	✓	0.01

Table 4.5: Percentage increase for locally connected mesh and fully connected mesh.

$\alpha_E$	locally	Fully	
$10^{-1}$	$10^{-1}$	15.8	24.4
$10^{-1}$	$10^{-2}$	52.9	49.9
$10^{-1}$	$10^{-3}$	56.6	51.1
$10^{-1}$	$10^{-4}$	57.1	51.2
$10^{-2}$	$10^{-1}$	41.7	41.8
$10^{-2}$	$10^{-2}$	15.5	24.2
$10^{-2}$	$10^{-3}$	52.6	51.5
$10^{-2}$	$10^{-4}$	56.14	51.8
$10^{-3}$	$10^{-1}$	41.7	41.8
$10^{-3}$	$10^{-2}$	41.8	41.5
$10^{-3}$	$10^{-3}$	41.4	69.2
$10^{-3}$	$10^{-4}$	18.3	62.8
$10^{-4}$	$10^{-1}$	51.1	41.8
$10^{-4}$	$10^{-2}$	41.7	41.8
$10^{-4}$	$10^{-3}$	41.4	56.1
$10^{-4}$	$10^{-4}$	37.7	87.7

### 4.3 Use of 3D printing

3D printing has been carried out by the technique of Fused Deposition Modeling (FDM). The 3D printer used is fabricated by *Leapfrog* [Fig. 4.16]. More information about this 3D printers manufacturer and technical specifications on its 3D printers can be found at the website <http://www.lpfrg.com>.

In this section we are going to show the objects printed. We have printed two objects through the use of the first code described 4.1.

The first object is sketched in [Fig. 4.5]. It is possible to print the structure just as it is presented in 4.1.6, but size does not allow the viewer to grasp the details of the optimization. This is why the size of the beam has been doubled and has been set an adequate thickness:

- length = 200 mm
- height = 50 mm
- thickness = 4 mm

The material used is PLA. The procedure used for the realization of the object can be read in 3.2.2. In [Fig. 4.17] the process is shown schematically; see [Fig. 4.18] for a picture of the printed objects.

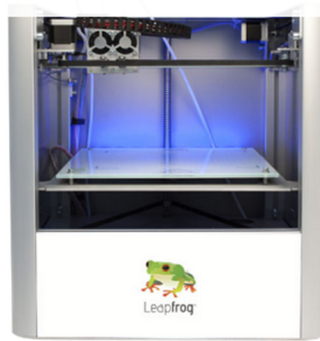


Figure 4.16: 3D printer used. Figure taken by Leapfrog website.

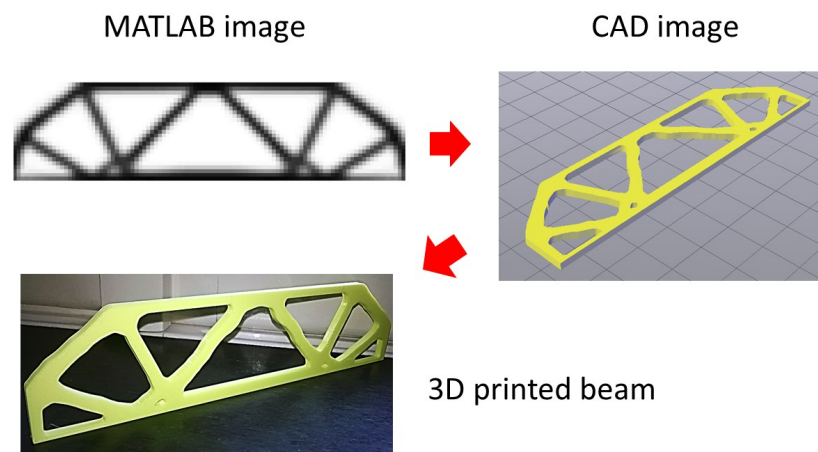


Figure 4.17: Main steps in 3D printing.

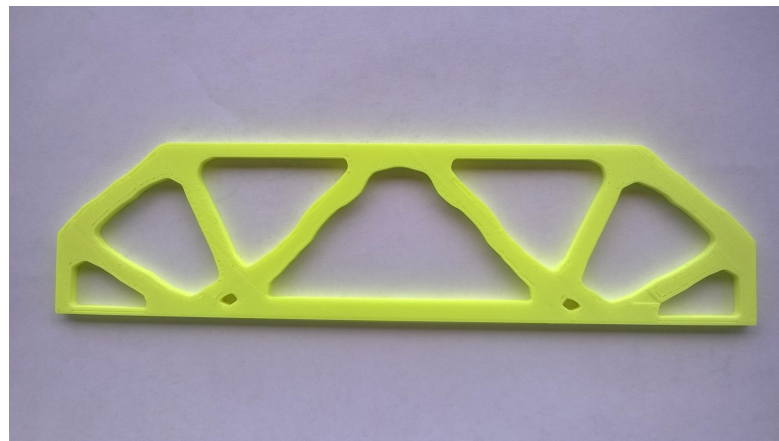


Figure 4.18: First 3D printed object.

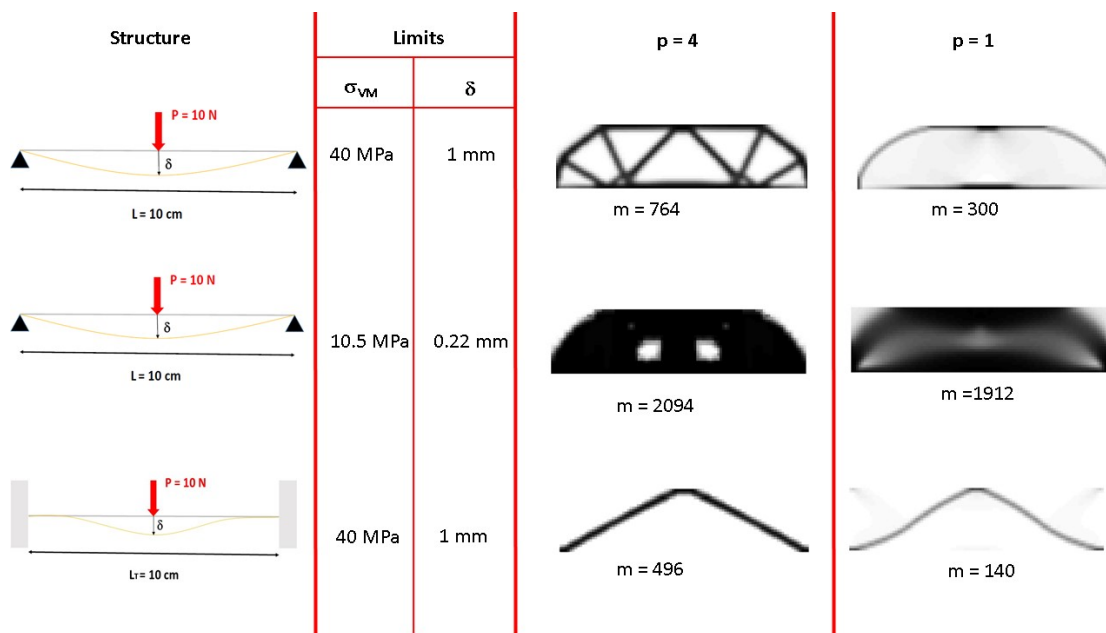


Figure 4.19: Solutions penalized (already seen) and solutions not penalized.

In the cases just analyzed in 4.1.6, the coefficient of penalization is assumed to be equal to 4. This choice is dictated by the desire to have a white-black solution type, where black represents the presence of mass and white represents the absence of mass. What would happen if we optimize it with a coefficient of penalization equal to 1, i. e. in the absence of penalization? Intuitively we can speculate the presence of intermediate density (gray areas), as indeed happens looking at [Fig. 4.19].

[Fig. 4.19] shows the results of maximum Von Mises stress, maximum vertical displacement and mass for penalized and not penalized solutions. It can be noted that the solutions without penalization are advantageous in terms of mass function. But can we realize them with 3D printing?

It is possible by exploiting the concept of cellular materials. These particular materials allow variable relative densities as seen in 2.3. In addition, a 3D printer's default option is the possibility between structures such as honeycomb, square, triangular lattice and many others to fill of the structure [Fig. 4.20]. The filling of the printed object is called, in technical terms, *infill*. In [Fig. 4.21] is sketched the relative density map related to the case 1 without penalization shown in [Fig. 4.19]. The ranges of relative density considered are 10. If relative density falls in the range  $[0, 0.1)$  then it assumes a value of 0.1, if it falls in the range  $[0.1, 0.2)$  then it is assumed the value of 0.2 and so on until the last interval  $(0.9, 1]$ . [Fig. 4.22] portrays the printed second object.

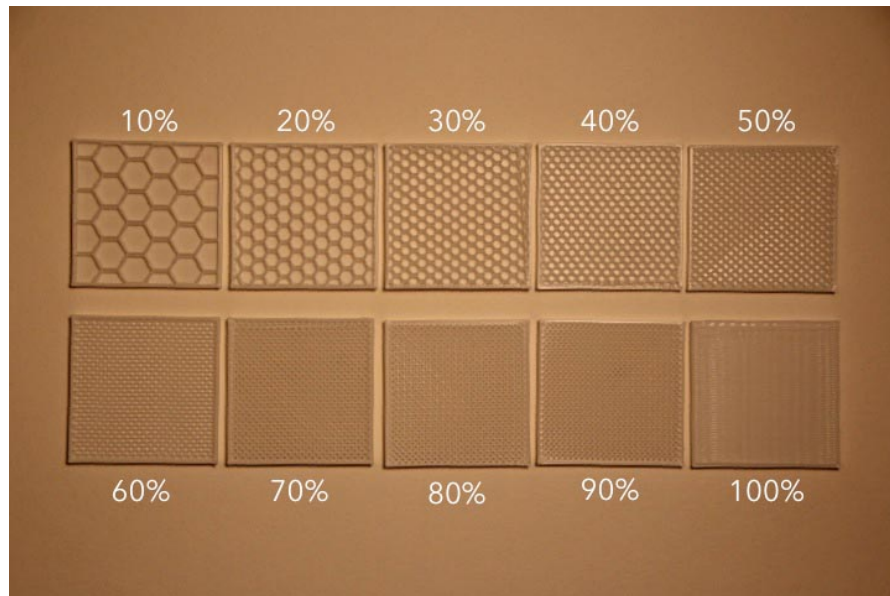


Figure 4.20: Example of percentage increase of infill. Figure taken from [98].

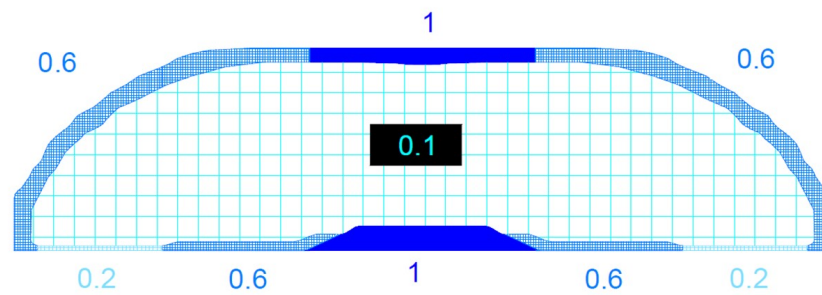


Figure 4.21: Relative density map.

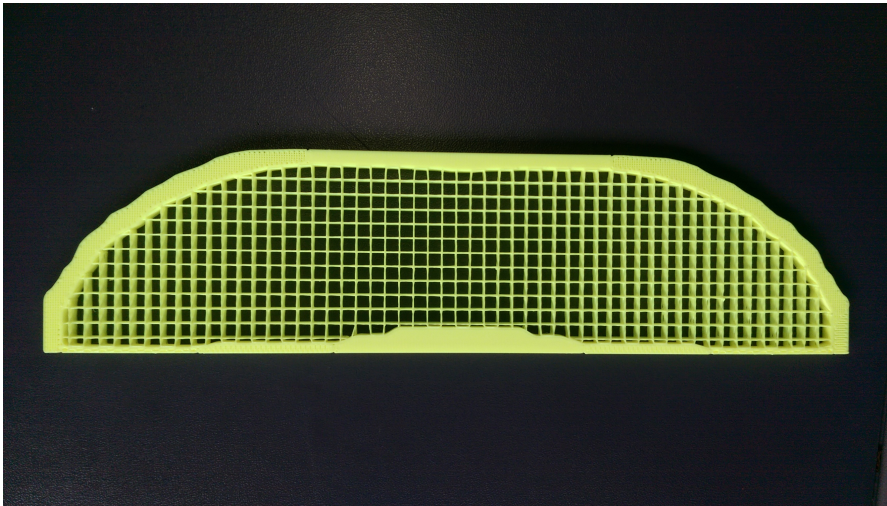


Figure 4.22: Second 3D printed object.



# Concluding Remarks

Structural optimization is well-established from the academic point of view, as the massive amount of papers on the theme proves. In particular, topology optimization is being deeply investigated as fundamental step of the *complete optimization process*. By “complete optimization process”, we mean the consecutive use of topology optimization and shape optimization; the former helps us to understand what is the best distribution of the material in the space allowed, the latter allows us to modify in detail the previous result.

Many companies usually use optimization techniques and dedicated softwares to boost the performances of their products, requiring highly specialized professionals. Nevertheless, the theme of optimization is often overlooked in the training of future engineers. More time should be devote to the subject. As well as bringing undoubted positive characteristics to the designed structures, the optimization process allows the engineers to be aware of how the distribution of mass, shape and density of materials could affect the potential of a structure.

In this thesis, we were faced with one of the major issues concerning optimization, the high variability in terms of shape and size of the optimized structures even though there is a slight variation of the constraints or loads. Traditional production machinery is often able to produce only one type of shape. This a significant problem. The solution provided by 3D printing will enable us to overcome this limitation thanks to 3D printing’s ability to create completely different shapes in an efficient and inexpensive way.

Obviously, given the relative novelty of 3D printing techniques, there are many possible improvements. For instance, there is often a request to use a wider range of printable materials or build objects in large scale (house walls, columns, beams, etc.). Another question which remains unanswered regards the mechanical model can be associated to a printed object. As we have discussed in detail previously, these issues are being studied and are already providing interesting ideas.

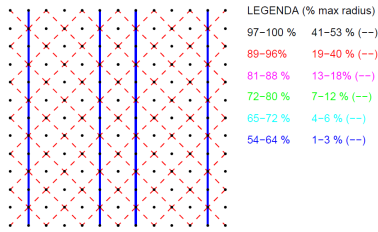
Earlier we have seen how to apply topology optimization to a cell of lattice material. Lattice materials suffer from a lack of consideration by professionals working in industrial and architectural fields. It is enough to note that the term cellular materials is often declined only for one type of material: foams. In fact, foams find wide usages in the sector of thermal and acoustic insulation, but also in the protection from impacts. However, the

growing demand for lightweight structures, which maintain adequate levels of stiffness and strength at the same time, changed the perception towards lattice materials that, albeit slowly, are being rediscovered.

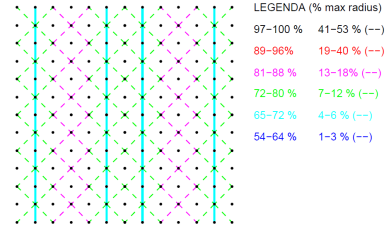
Using topology optimization to improve the characteristics of lattice materials may be the starting point to rethink the concept of lightweight structure from the design standpoint. In the same way, the current limits of 3D printing may represent a starting point to consider new ways of building with less manpower, fewer cost and less waste in terms of time and material used.

# Graphical results

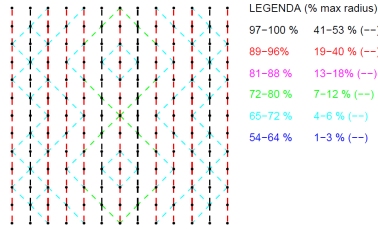
Below, we show the results of the optimizations for locally connected mesh (LCM) and fully connected mesh (FCM).



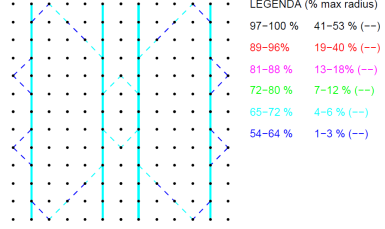
(a) (LCM)  $\alpha_E = 10^{-1}$ ,  $\alpha_G = 10^{-1}$



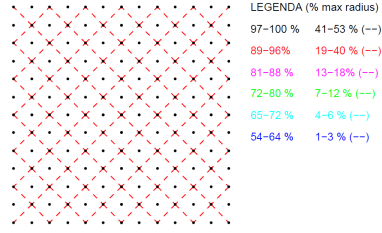
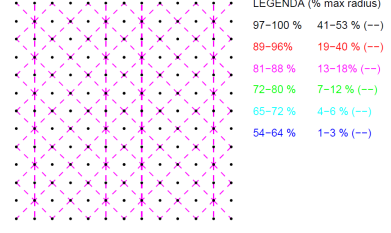
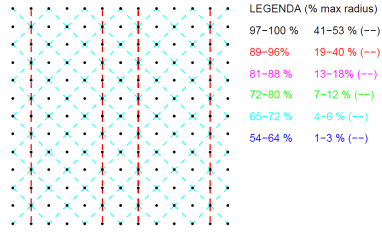
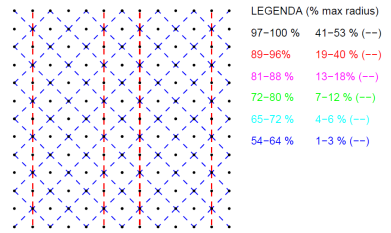
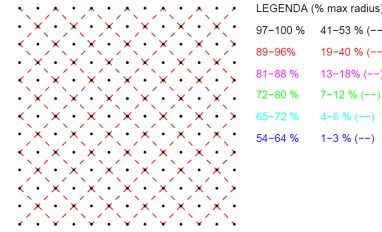
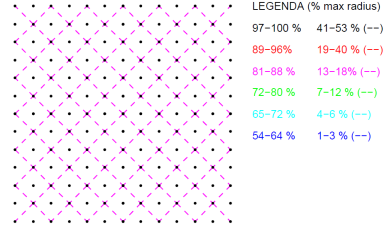
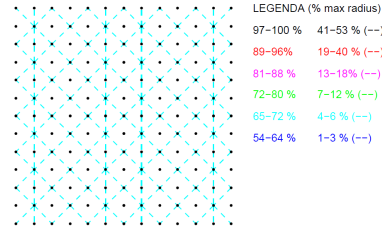
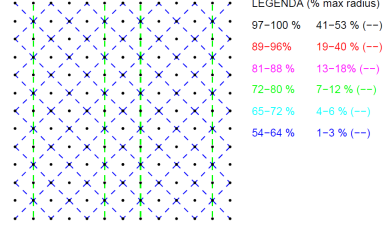
(b) (LCM)  $\alpha_E = 10^{-1}$ ,  $\alpha_G = 10^{-2}$

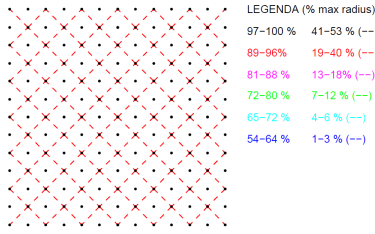
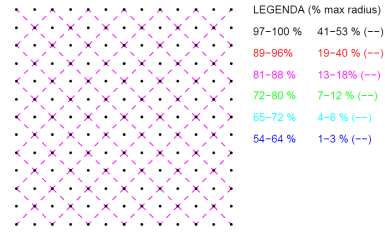
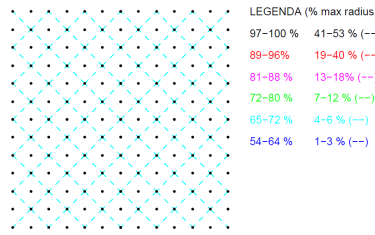
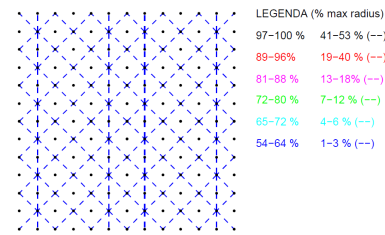
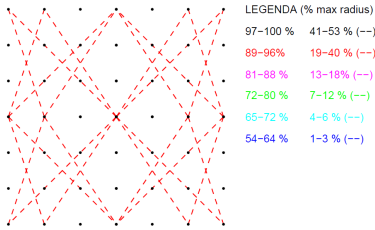
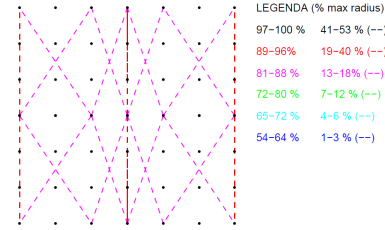
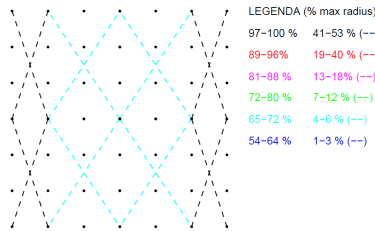
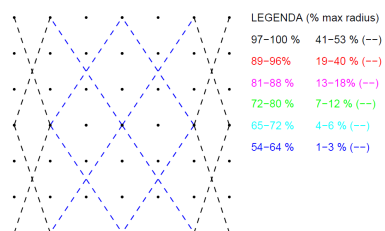


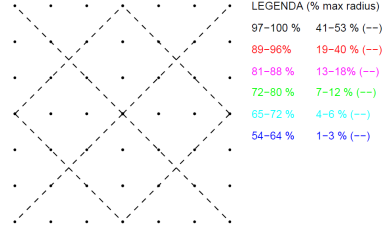
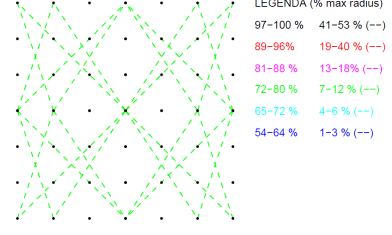
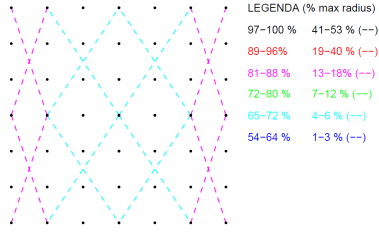
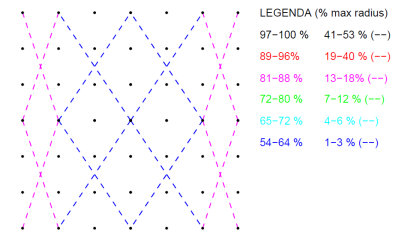
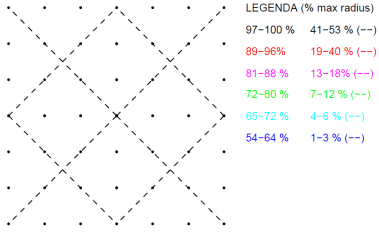
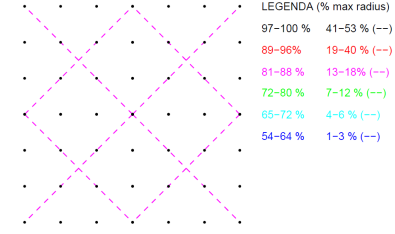
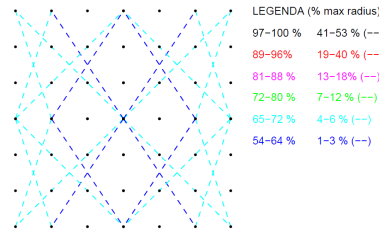
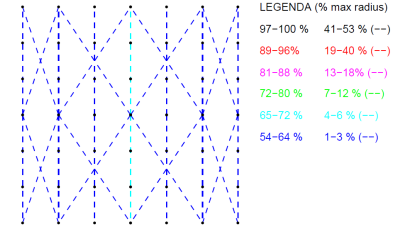
(c) (LCM)  $\alpha_E = 10^{-1}$ ,  $\alpha_G = 10^{-3}$

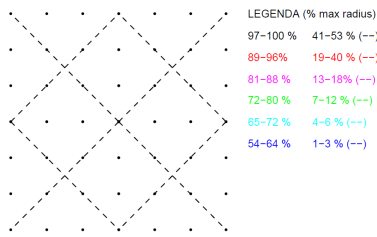
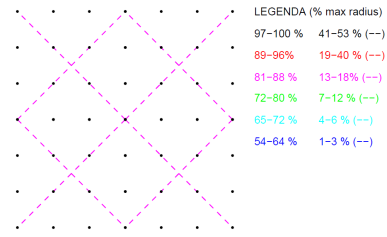
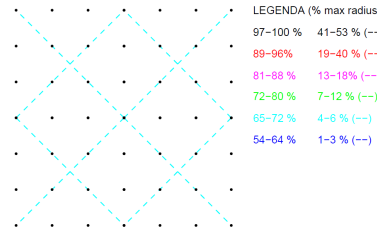
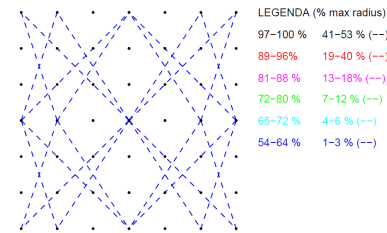


(d) (LCM)  $\alpha_E = 10^{-1}$ ,  $\alpha_G = 10^{-4}$

(a) (LCM)  $\alpha_E = 10^{-2}$ ,  $\alpha_G = 10^{-1}$ (b) (LCM)  $\alpha_E = 10^{-2}$ ,  $\alpha_G = 10^{-2}$ (c) (LCM)  $\alpha_E = 10^{-2}$ ,  $\alpha_G = 10^{-3}$ (d) (LCM)  $\alpha_E = 10^{-2}$ ,  $\alpha_G = 10^{-4}$ (a) (LCM)  $\alpha_E = 10^{-3}$ ,  $\alpha_G = 10^{-1}$ (b) (LCM)  $\alpha_E = 10^{-3}$ ,  $\alpha_G = 10^{-2}$ (c) (LCM)  $\alpha_E = 10^{-3}$ ,  $\alpha_G = 10^{-3}$ (d) (LCM)  $\alpha_E = 10^{-3}$ ,  $\alpha_G = 10^{-4}$

(a) (LCM)  $\alpha_E = 10^{-4}$ ,  $\alpha_G = 10^{-1}$ (b) (LCM)  $\alpha_E = 10^{-4}$ ,  $\alpha_G = 10^{-2}$ (c) (LCM)  $\alpha_E = 10^{-4}$ ,  $\alpha_G = 10^{-3}$ (d) (LCM)  $\alpha_E = 10^{-4}$ ,  $\alpha_G = 10^{-4}$ (a) (FCM)  $\alpha_E = 10^{-1}$ ,  $\alpha_G = 10^{-1}$ (b) (FCM)  $\alpha_E = 10^{-1}$ ,  $\alpha_G = 10^{-2}$ (c) (FCM)  $\alpha_E = 10^{-1}$ ,  $\alpha_G = 10^{-3}$ (d) (FCM)  $\alpha_E = 10^{-1}$ ,  $\alpha_G = 10^{-4}$

(a) (FCM)  $\alpha_E = 10^{-2}$ ,  $\alpha_G = 10^{-1}$ (b) (FCM)  $\alpha_E = 10^{-2}$ ,  $\alpha_G = 10^{-2}$ (c) (FCM)  $\alpha_E = 10^{-2}$ ,  $\alpha_G = 10^{-3}$ (d) (FCM)  $\alpha_E = 10^{-2}$ ,  $\alpha_G = 10^{-4}$ (a) (FCM)  $\alpha_E = 10^{-3}$ ,  $\alpha_G = 10^{-1}$ (b) (FCM)  $\alpha_E = 10^{-3}$ ,  $\alpha_G = 10^{-2}$ (c) (FCM)  $\alpha_E = 10^{-3}$ ,  $\alpha_G = 10^{-3}$ (d) (FCM)  $\alpha_E = 10^{-3}$ ,  $\alpha_G = 10^{-4}$

(a) (FCM)  $\alpha_E = 10^{-4}$ ,  $\alpha_G = 10^{-1}$ (b) (FCM)  $\alpha_E = 10^{-4}$ ,  $\alpha_G = 10^{-2}$ (c) (FCM)  $\alpha_E = 10^{-4}$ ,  $\alpha_G = 10^{-3}$ (d) (FCM)  $\alpha_E = 10^{-4}$ ,  $\alpha_G = 10^{-4}$



# Bibliography

- [1] J. G. Gordon, *Structures or Why Things Don't Fall Down*, Baltimore (1978), Penguin.
- [2] U. Kirsch, *Structural Optimization—Fundamentals and Applications*, Berlin (1993), Springer.
- [3] M. Ehrgott, *Multicriteria Optimization*, Berlin (2005), Springer.
- [4] A. Verbart, M. Langelaar, F. van Keulen, *A new approach for stress-based topology optimization: Internal stress penalization*, 10th World Congress on Structural and Multidisciplinary Optimization (2013).
- [5] E. Lee, *Stress-constrained structural topology optimization with design-dependent loads*, Structural and Multidisciplinary Optimization. 46, 647 - 661 (2012), (<http://dx.doi.org/doi:10.1007/s00158-012-0780-x>).
- [6] N. A. Fleck, V. S. Deshpande, M. F. Ashby, *Micro-architected materials: past, present and future*, Proc. R. Soc. A 466, 2495–2516 (2010), (<http://dx.doi.org/doi:10.1098/rspa.2010.0215>).
- [7] M. F. Ashby, *The properties of foams and lattices*, Proc. R. Soc. A 316, 15–30 (2006), (<http://dx.doi.org/doi:10.1098/rsta.2005.1678>).
- [8] M. F. Ashby, *Designing architected materials*, Scripta Materialia 68(1), 4–7 (2013), (<http://dx.doi.org/doi:10.1016/j.scriptamat.2012.04.033>).
- [9] D. Snelling, Q. Li, N. Meisel, C. B. Williams, R. C. Batra, A. P. Druschitz, *Lightweight metal cellular structures fabricated via 3D printing of sand cast molds*, Advanced Engineering Materials 17(7), 923 - 932 (2015), (<http://dx.doi.org/doi:10.1002/adem.201400524>).
- [10] C. R. Scullard, R. M. Ziff, *Critical surfaces for general inhomogeneous bond percolation problems*, Journal of Statistical Mechanics: Theory and Experiment 3, 3-21 (2010).
- [11] A. Amendola, *On the use of mechanical metamaterials for innovative seismic isolation system*, Tesi di dottorato, Università degli Studi di Salerno, A.A. 2014-2015.

- [12] N. A. Fleck, V. S. Deshpande, M. F. Ashby, *Foam topology: bending versus stretching dominated architectures*, Acta mater. 49, 1035–1040 (2001), ([http://dx.doi.org/doi:10.1016/S1359-6454\(00\)00379-7](http://dx.doi.org/doi:10.1016/S1359-6454(00)00379-7)).
- [13] L. J. Gibson, M. F. Ashby, *Cellular solids. Structure and properties*, Cambridge(1997), Cambridge University Press.
- [14] H. N. G. Wadley, *Multifunctional periodic cellular metals*, Acta mater. 49, 1035–1040 (2001), (<http://dx.doi.org/doi:10.1098/rsta.2005.1697>).
- [15] V. S. Deshpande, N. A. Fleck, M. F. Ashby, *Effective properties of the octet-truss lattice material*, Journal of the Mechanics and Physics of Solids. 49, 1747 – 1769 (2001), ([http://dx.doi.org/10.1016/S0022-5096\(01\)00010-2](http://dx.doi.org/10.1016/S0022-5096(01)00010-2)).
- [16] M. F. Ashby, A. G. Evans, N. A. Fleck, L. J. Gibson, J. W. Hutchinson, H. N. G. Wadley *Metal Foams: A Design Guide*, (2000), Butterworth-Heinemann.
- [17] H. Lipson, M. Kurman, *Fabricated: The New World of 3D Printing*, Indianapolis (2013), John Wiley and Sons Inc.
- [18] Wikipedia, the free encyclopedia, *3D printing*, [https://en.wikipedia.org/wiki/3D\\_printing](https://en.wikipedia.org/wiki/3D_printing), last modify on 29 July 2015.
- [19] CSC leading edge forum, *3D printing and the future of manufacturing*, (2012), Computer Sciences Corporation.
- [20] I. Gibson, D. Rosen, B. Stucker, *Additive Manufacturing Technologies. 3D Printing, Rapid Prototyping, and Direct Digital Manufacturing*, New York (2015), Springer.
- [21] UK Intellectual Property Office Patent Informatics Team, *3D printing. A patent overview*, Newport (2013), Intellectual Property Office.
- [22] K. Svanberg, *The methods of moving asymptotes—A new method for structural optimization*, Internat. J. Numer. Methods Eng. 24, 359–373 (1987).
- [23] C. Fleury, *CONLIN: an efficient dual optimizer based on convex approximation concepts*, Structural Optimization 1, 81-89 (1989).
- [24] P. W. Christensen, A. Klarbring, *An Introduction to Structural Optimization*, Berlin (2003), Springer.
- [25] M. P. Bendsøe, O. Sigmund, *Topology Optimization: Theory, Methods and Applications*, Berlin (2009), Springer.
- [26] O. Sigmund, *Morphology-based black and white filters for topology optimization*, Struct. Multidiscip. Optim. 33, 401–424 (2007), (<http://dx.doi.org/10.1007/s00158-006-0087-x>).

- [27] D. C. Guth, M. A. Luersen, P. A. Muñoz-Rojas, *Optimization of three-dimensional truss-like periodic materials considering isotropy constraints*, Berlin (2015), Springer, (<http://dx.doi.org/10.1007/s00158-015-1282-4>).
- [28] O. Sigmund, J. Petersson, *Numerical instabilities in topology optimization: A survey on procedures dealing with checkerboards, mesh-dependencies and local minima*, Structural Optimization 16, 68-75 (1998).
- [29] M. P. Bendsøe, A. Ben-Tal, J. Zowe, *Optimization methods for truss geometry and topology design*, Structural Optimization 7, 141-159 (1994).
- [30] G. Cheng, *Some aspects of truss topology optimization*, Structural Optimization 10, 173-179 (1995).
- [31] J. Nocedal, S. J. Wright, *Numerical Optimization*, Berlin (2006), Springer.
- [32] J. C. Wallach, L. J. Gibson, *Mechanical behavior of a three-dimensional truss material*, International Journal of Solids and Structures, 38(40-41), 7181 – 7196 (2001), ([http://dx.doi:10.1016/S0020-7683\(00\)00400-5](http://dx.doi:10.1016/S0020-7683(00)00400-5)).
- [33] D. H. Chen, L. Yang, *Analysis of equivalent elastic modulus of asymmetrical honeycomb*, Composite Structures 93, 767–773 (2011), (<http://dx.doi.org/10.1016/j.compstruct.2010.07.014>).
- [34] J. C. Maxwell, *On the calculation of the equilibrium and stiffness of frames*, Philosophical Magazine, 27 (182), 294–299 (1864).
- [35] N. Fleck, X. Qiu, *The damage tolerance of elastic–brittle, two-dimensional isotropic lattices*, Journal of the Mechanics and Physics of Solids 55, 562-588 (2007), (<http://dx.doi.org/10.1016/j.jmps.2006.08.004>).
- [36] G.D. Cheng, X. Guo,  *$\epsilon$ -relaxed approach in structural topology optimization*, Structural and Multidisciplinary Optimization 13(4), 258-266 (1993), (<http://dx.doi.org/10.1007/BF01197454>).
- [37] A. Asadpoure, L. Valdevit, *Topology optimization of lightweight periodic lattices under simultaneous compressive and shear stiffness constraint*, International Journal of Solids and Structures 60–61, 1–16 (2015), (<http://dx.doi.org/10.1016/j.ijsolstr.2015.01.016>).
- [38] P. Duysinx, P. Bendsøe, *Topology optimization of continuum structures with local stress constraints*, International Journal for Numerical Methods in Engineering 43, 1453-1478 (1998).

- [39] M. Bruggi, *On an alternative approach to stress constraints relaxation in topology optimization*, Structural and Multidisciplinary Optimization 36, 125-141 (2008), (<http://dx.doi.org/10.1007/s00158-007-0203-6>).
- [40] C. Le, J. Norato, T. Bruns, C. Ha, D. Tortorelli, *Stress-based topology optimization for continua.*, Structural and Multidisciplinary Optimization 41(4), 605-620 (2010), (<http://dx.doi.org/10.1007/s00158-009-0440-y>).
- [41] E. Lee, K. A. James, J.R.R.A. Martins, *Stress-Constrained Topology Optimization with Design-Dependent Loading.*, Structural and Multidisciplinary Optimization 46(5), 647-661 (2012), (<http://dx.doi.org/10.1007/s00158-012-0780-x>).
- [42] K. Liu, A. Tovar, *An efficient 3D topology optimization code written in Matlab.*, Structural and Multidisciplinary Optimization 50, 1175-1196 (2014), (<http://dx.doi.org/10.1007/s00158-014-1107-x>).
- [43] G. Sved, Z. Ginos, *Structural optimization under multiple loading*, International Journal of Mechanical Sciences 10, 803-805 (1968), ([http://dx.doi.org/10.1016/0020-7403\(68\)90021-0](http://dx.doi.org/10.1016/0020-7403(68)90021-0)).
- [44] G. Allaire, G. Francfort, *A numerical algorithm for topology and shape optimization*, NATO ASI Series 227, 239-248 (1993).
- [45] U. Kirsch, *On singular topologies in optimum structural design. Structural and Multidisciplinary Optimization*, Journal of the Mechanics and Physics of Solids 2, 133-142 (1990), (<http://dx.doi.org/10.1007/BF01836562>).
- [46] R. S. Kumar, D. L. McDowell, *Generalized continuum modeling of 2D periodic cellular solids*, International Journal of Solids and Structures 41 (26), 7399 – 7422 (2004).
- [47] S. Gonella, M. Ruzzene, *Homogenization and equivalent in-plane properties of two-dimensional periodic lattices*, International Journal of Solids and Structures 45(10), 2897–2915 (2008), (<http://dx.doi.org/10.1016/j.ijsolstr.2008.01.002>).
- [48] A. S. Phani, J. Woodhouse, N. A. Fleck, *Wave propagation in two-dimensional periodic lattices*, The Journal of the Acoustical Society of America, 119(4), 1995–2005 (2006), (<http://dx.doi.org/10.1121/1.2179748>).
- [49] A. Vigliotti, S. Pasini, *Stiffness and strength of tridimensional periodic lattices*, Comput. Methods Appl. Mech. Engrg. 229–232, 27–43 (2012), (<http://dx.doi.org/10.1016/j.cma.2012.03.018>).
- [50] H. G. Allen, *Analysis and Design of Structural Sandwich Panels*, (1969), Pergamon Press.

- [51] H. J. Rathbun, Z. Wei, M. Y. He, F. W. Zok, A. G. Evans, D. J. Sypeck, H. N. G. Wadley, *Measurement and simulation of the performance of a lightweight metallic sandwich structure with a tetrahedral truss core.*, Journal of Applied Mechanics 71 (5), 368–374 (2004).
- [52] L. Valdevit, J. W. Hutchinson, A. G. Evans, *Structurally optimized sandwich panels with prismatic cores*, International Journal of Solids and Structures 41, 5105–5124 (2004).
- [53] O. Zienkiewicz, R. L. Taylor, *The Finite Element Method for Solid and Structural Mechanics*, (2006), Elsevier.
- [54] R. D. Cook, D. S. Malkus, M. E. Plesha, *Concepts and Applications of Finite Element Analysis*, (1989), John Wiley and Sons Canada Ltd.
- [55] L. Valdevit, Z. Wei, C. Mercer, F. W. Zok, A. G. Evans, *Structural performance of near-optimal sandwich panels with corrugated cores*, International Journal of Solids and Structures 43, 4888–4905 (2006).
- [56] O. Sigmund, *Materials with prescribed constitutive parameters: an inverse homogenization problem*, Int. J. Solids Struct. 31 (17), 2313–2329 (1994), ([http://dx.doi.org/10.1016/0020-7683\(94\)90154-6](http://dx.doi.org/10.1016/0020-7683(94)90154-6)).
- [57] O. Sigmund, S. Torquato, *Design of materials with extreme thermal expansion using a three-phase topology optimization method*, J. Mech. Phys. Solids 45 (6), 1037–1067 (1995), ([http://dx.doi.org/10.1016/S0022-5096\(96\)00114-7](http://dx.doi.org/10.1016/S0022-5096(96)00114-7)).
- [58] E. C. Silva, O. Nelli, J. S. Fonseca, N. Kikuchi, *Optimal design of piezoelectric microstructures*, Comput. Mech. 19 (5), 397–410 (1997), (<http://dx.doi.org/10.1007/s004660050188>).
- [59] D. C. Dobson, S. J. Cox, *Maximizing band gaps in two-dimensional photonic crystals*, SIAM J. Appl. Math. 59 (6), 2108–2120 (1999), (<http://dx.doi.org/10.1137/S0036139998338455>).
- [60] F. Wang, O. Sigmund, J. S. Jensen, *Design of materials with prescribed nonlinear properties*, J. Mech. Phys. Solids 69, 156–174 (2014), (<http://dx.doi.org/10.1016/j.jmps.2014.05.003>).
- [61] A. Asadpoure, L. Valdevit, *Topology optimization of lightweight periodic lattices under simultaneous compressive and shear stiffness constraints*, International Journal of Solids and Structures 60–61, 1–16 (2015), (<http://dx.doi.org/10.1016/j.ijsolstr.2015.01.016>).
- [62] Jamcorp Inc., 2004, *Jonathon Aerospace Materials website*, ([www.jamcorp.com](http://www.jamcorp.com)).

- [63] S. Chiras, D. R. Mumm, A. G. Evans, N. Wicks, J. W. Hutchinson, K. Dharmasena, H. N. G. Wadley, S. Fichter, *The Structural Performance of Near-Optimized Truss Core Panels*, International Journal of Solids and Structures 39, 4093-4115 (2002).
- [64] L. Yang, O. Harrysson, D. Cormier, H. West, H. Gong, B. Stucker, *Additive Manufacturing of Metal Cellular Structures: Design and Fabrication*, International Journal of Solids and Structures 60-61, 1-16 (2015), (<http://dx.doi.org/10.1007/s11837-015-1322-y>).
- [65] E. Cuan-Urquizo, S. Yang, A. Bhaskar, *Mechanical characterisation of additively manufactured material having lattice microstructure*, IOP Conf. Series: Materials Science and Engineering 74, 1-8 (2015), (<http://dx.doi.org/10.1088/1757-899X/74/1/012004>).
- [66] B. G. Compton, J. A. Lewis, *3D-Printing of Lightweight Cellular Composites*, Adv. Mater. 26, 5930-5935 (2014), (<http://dx.doi.org/10.1002/adma.201401804>).
- [67] M. R. Karamooz Ravari, M. Kadkhodaei, M. Badrossamay, R. Rezaei, *Numerical investigation on mechanical properties of cellular lattice structures fabricated by fused deposition modeling*, International Journal of Mechanical Sciences 88, 154-161 (2014), (<http://dx.doi.org/10.1016/j.ijmecsci.2014.08.009>).
- [68] G. Reinhart, S. Teufelhart, *Load-adapted design of generative manufactured lattice structures*, Phys. Proced. 12, 385-392 (2012), (<http://dx.doi.org/10.1016/j.phpro.2011.03.049>).
- [69] M. Smith, W. J. Cantwell, Z. Guan, S. Tsopanos, M. D. Theobald, G. N. Nurick, G. S. Langdon, *The quasi-static response of steel lattice structures*, Struct. Mater. 13, 479-501 (2010), (<http://dx.doi.org/10.1177/1099636210388983>).
- [70] Y. Shen, W. J. Cantwell, R. Mines, K. Ushijima, *The properties of lattice structures manufactured using Selective Laser Melting*, Adv. Mater. Res. 445, 386-391 (2012), (<http://dx.doi.org/10.4028/www.scientific.net/AMR.445.386>).
- [71] S. L. Campanelli, N. Contuzzi, A. D. Ludovico, *Manufacturing of 18 Ni Marage 300 steel samples by selective laser melting*, Adv. Mater. Res. 83-86, 850-857 (2010), (<http://dx.doi.org/10.3390/ma6083451>).
- [72] S. L. Campanelli, N. Contuzzi, A. D. Ludovico, F. Caiazzo, F. Cardaropoli, V. Sergi, *Manufacturing and characterization of Ti6Al4V Lattice components manufactured by Selective Laser Melting*, Adv. Mater. Res. 83-86, 850-857 (2010), (<http://dx.doi.org/10.3390/ma7064803>).
- [73] A. J. Jacobsen, W. Barvosa-Carter, S. Nutt, *Micro-scale truss structures formed from self-propagating photopolymer waveguides*, Adv. Mater. Res. 19(22), 3892 - 3896 (2007), (<http://dx.doi.org/10.1002/adma.200700797>).

- [74] A. J. Jacobsen, J. A. Kolodziejska, R. Doty, K. D. Fink, C. Zhou, C. S. Roper, W. B. Carter, *Interconnected self-propagating photopolymer waveguides: an alternative to stereolithography for rapid formation of lattice-based open-cellular materials*, Twenty-First Annual International Solid Freeform (2010).
- [75] S. Li, *Boundary conditions for unit cells from periodic microstructures and their implications*, Composites Science and Technology 68, 1962–1974 (2008) , (<http://dx.doi.org/10.1016/j.compscitech.2007.03.035>).
- [76] F. Niu, S. Xu, G. Cheng, *A general formulation of structural topology optimization for maximizing structural stiffness*, Struct Multidisc Optim 43, 561–572 (2011), (<http://dx.doi.org/10.1007/s00158-010-0585-8>).
- [77] J. K. Guest, J. H. Prévost, T. Belytschko, *Achieving minimum length scale in topology optimization using nodal design variables and projection functions*, Int. J. Numer. Meth. Engng 61, 238–254 (2004), (<http://dx.doi.org/10.1002/nme.1064>).
- [78] MathWorks, *Global Optimization Toolbox. User's Guide*, 2015.



# Sitography

- [79] <http://giuseppestagnitto.it>
- [80] <https://whiteclouds.com>
- [81] <http://lboro.ac.uk>
- [82] <https://additively.com>
- [83] <http://suggestkeyword.com>
- [84] <http://3dprinting.com>
- [85] <http://wonderfulengineering.com>
- [86] <http://ngopolis.com>
- [87] <http://boeingconsult.com>
- [88] <http://mccormickdc.com>
- [89] <http://boston.com>
- [90] <http://schuetz.net>
- [91] <http://users.aber.ac.uk>
- [92] <http://ifam.fraunhofer.de>
- [93] <http://tms.org>
- [94] <http://blog.cafefoundation.org>
- [95] <http://bristol.ac.uk>
- [96] <http://silver.neep.wisc.edu>
- [97] <http://ibk.ethz.ch>
- [98] <http://enablingthefuture.org>
- [99] <http://itac.nyc>